RAPID AUTHENTICATION OF RED WINE AND CHIRAL RECOGNITION OF DRUGS BY MASS SPECTROMETRY

LIN XUEWEI

PhD

The Hong Kong Polytechnic University

2024

The Hong Kong Polytechnic University

Department of Applied Biology and Chemical Technology

Rapid Authentication of Red Wine and Chiral Recognition of Drugs by Mass Spectrometry

LIN Xuewei

A thesis submitted in partial fulfilment of the requirements for the degree of Doctor of Philosophy

August 2023

CERTIFICATE OF ORIGINALITY

I hereby declare that this thesis is my own work and that, to the best of my knowledge and belief, it reproduces no material previously published or written, nor material that has been accepted for the award of any other degree or diploma, except where due acknowledgement has been made in the text.

LIN Xuewei

Abstract

Mass spectrometry (MS) is a powerful and versatile analytical tool with advantages such as high sensitivity and high speed. The process of mass spectrometry involves the ionization of chemical compounds to produce charged molecules or fragments, followed by measuring their mass-to-charge ratios. There are various types of mass spectrometers, with different advantages and applications, including time-of-fligh, quadrupole, ion trap, orbitrap and Fourier transform ion cyclotron resonance mass spectrometers. MS has numerous applications in various fields such as chemistry, pharmacology, forensic science, environmental science and biology. In this thesis, two studies involving MS-based analytical methods are performed, including authentication of red wine and chiral recognition of drugs.

The importance of authentication of red wine as well as current analytical methods for the authentication have been introduced in Chapter 1. Red wine, among the most consumed alcoholic drinks, occupies a great market worldwide. Due to its commercial value, though considerable efforts have been made to protect both consumers and producers, counterfeiting of wine has long time been a severe problem concerning dilution, prohibited addition and mislabeling of brands or years. The authenticity of wine with regard to its origins, vintage years, grape varieties, etc., has thus become an important issue. Developing a rapid, simple and accurate method to authenticate plenty of samples with complex features is required.

Two direct mass spectrometry techniques, matrix-assisted laser desorption/ionization mass spectrometry (MALDI-MS) and direct analysis in real time mass spectrometry (DART-MS), were employed to analyze red wine in this project. The two methods were found to be complementary to each other in terms of mass ranges and detected compounds. A simple, rapid and high-throughput approach was developed for authentication of red wine for the first time, by combining spectral results from MALDI-MS and DART-MS. By coupling with orthogonal partial least squares discrimination analysis (OPLS-DA), this approach allowed the successful classification of 535 wine samples collected from 8 key wine-producing countries, with the correct classification rates of 100% on the calibration set and over 90% on the validation set for almost all countries, and 26 potential characteristic markers were selected. Compared to one single technique, this approach allowed the detection of more compound ions, and with higher fitting and predictive consequences. The satisfactory differentiation results of vintages and grape varieties further verified the robustness of the approach. This study demonstrated the feasibility of combining multiple mass spectrometric techniques for wine analysis, which can be extended to other fields or combinations of other analytical techniques.

In Chapter 2, MS was applied for chiral recognition of chiral drugs. Chirality plays an important role in various fields, including chemistry, biology, pharmaceutical science, etc. Chiral compounds such as amino acids, proteins, enzymes, and nucleosides are vital

for life. The biological activities of the drug enantiomers can vary significantly due to their structural differences, emphasizing the important role of chiral recognition of drugs. Chiral recognition by MS is typically achieved by analysis of complexes found between enantiomers and chiral selectors, and tandem mass spectrometry (MS/MS) is commonly used for such analyses due to its simplicity and high reproducibility. In this thesis, MS/MS was utilized for the discrimination of several types of chiral drugs.

Four chiral drugs, ofloxacin, clopidogrel, omeprazole and bupivacaine, were investigated first, by introducing various chiral selectors, such as amino acids and cyclodextrins. The influence of metal ions was investigated and optimized as well. For the first three drugs, various complex ions were formed by introducing chiral selectors. The results showed that using MS/MS, chiral differentiation could be obtained with all drugs studied. The MS/MS analysis of singly charged trimers $[\text{ofloxacin+2Pro+Cu}-\text{H}]^+$ with proline (Pro) as the chiral selector allowed effective analysis with a chiral recognition ratio (CR) of 1.44 ± 0.13, as well as enantiomeric excess determination of ofloxacin, the calibration curve of which gave a linear coefficient of 0.9878. The copper-bound trimers $[\text{clopidogrel+2Trp+Cu}-\text{H}]^+$ with tryptophan (Trp) as the chiral selector exhibited the highest level of chiral discrimination for clopidogrel, with a CR value of 2.16 ± 0.04. The doubly charged complex ions $[\text{omeprazole+2Trp+K+H}]^{2+}$ contributed to a significant CR value of 0.27 ± 0.15 for the effective discrimination of omeprazole enantiomers. Interestingly,

for bupivacaine, the MS/MS of its self-assembly trimers $[3\text{bupivacaine}+H]^+$ allowed differentiation of the enantiomers without any chiral selectors. However, the chiral analysis results obtained by the four chiral drugs were different, mainly due to the different sizes and chemical structures of the drugs, which had a significant impact on the formation of cluster ions and the binding strength within ions. Overall, these findings highlighted the varying chiral effects of drugs with different spatial structures, which might give instructions for the selection of selectors for chiral compounds.

In Chapter 3, a further study was performed with omeprazole as a representative chiral drug first due to its excellent discrimination results, and the use of different types of chiral selectors was studied, including one amino acid, combinations of two amino acids, and dipeptides, with or without copper-bound, and the differences of complex ions were compared and discussed. Interestingly, it was found that the chiral discrimination of omeprazole could be achieved by introducing these three types of chiral selectors with dipeptides as the best, followed by two amino acids, and one amino acid the last. Results showed that increased numbers of complex ions were observed with dipeptides as the chiral selectors, indicating stronger binding between omeprazole and dipeptides. Chiral discrimination was observed with all dipeptides chiral selectors tested, even with only one chiral center in dipeptides or different orders of amino-acid residues in dipeptides. The application of peptides as chiral selectors was also extended to the analysis of other chiral drugs, e.g., clopidogrel. The results indicated the

exceptional efficacy of peptides as the chiral selectors for the chiral MS analysis and their potential for other chiral analyses, e.g., the design of chiral columns for chiral analysis by high-performance liquid chromatography.

In Chapter 4, the results and general conclusions of the two studies were summarized, together with the prospects for them, especially for the second study, further investigations are needed.

Research publications

Journal papers

1. Lin, X. W.; Wu, H.; Huang, G.F.; Wu, Q.; Yao, Z. P. (2023). Rapid authentication of red wine by MALDI-MS combined with DART-MS. *Analytica Chimica Acta*, 1283, 341966.
2. Li, S., Lin, X., Ng, T. T., & Yao, Z. P. (2024). Quantitative Analysis of Blended Oils Based on Intensity Ratios of Marker Ions in MALDI-MS Spectra. *Journal of Agricultural and Food Chemistry*, 72, 27, 15376–15386.

Conference papers

1. Lin, X. W.; Wu, H.; Huang, G. F.; Wu, Q.; Yao, Z. P., Rapid Authentication of Red Wine by MALDI-MS and DART-MS, The 28th Symposium on Chemistry Postgraduate Research in Hong Kong, Hong Kong. 24 September **2021**. (Poster)
2. Lin, X. W.; Wu, H.; Huang, G. F.; Wu, Q.; Yao, Z. P., Rapid Authentication of Red Wine by MALDI-MS and DART-MS, The Hong Kong Society of Mass Spectrometry Symposium, Hong Kong. 11 June **2022**. (Oral)
3. Lin, X. W.; Wu, H.; Huang, G. F.; Wu, Q.; Yao, Z. P., Rapid Authentication of Red Wine by MALDI-MS Combined with DART-MS, American Society for Mass Spectrometry Conference on Mass Spectrometry and Allied Topics, The United States. 8 June **2023**. (Poster)
4. Lin, X. W.; Wu, H.; Huang, G. F.; Wu, Q.; Yao, Z. P., Rapid Authentication of Red Wine by MALDI-MS Combined with DART-MS, The Hong Kong Society of Mass

Spectrometry Symposium, Hong Kong. 17 June **2023**. (Poster, Conference Award).

Acknowledgements

First of all, I would like to express my sincere gratitude to my supervisor Prof. Zhong-Ping Yao for providing me with a well-established platform to conduct my research projects, where I gained practical experience and valuable knowledge of mass spectrometry that would definitely be a great help to my future career development. During my PhD study, Prof. Yao gave me much patient guidance, professional suggestions and strong encouragement to support me in accomplishing two projects. His serious attitude in research also has inspired me to think deeper and more scientifically.

I am grateful to people for their help. I would like to especially thank Dr. Pui Kin So for his technical supports, Dr. Qian Wu for her kind guidance at the beginning of my study, and Dr. Suying Li for the assistance in data analysis and manuscript preparation. Mr. Ho Yin Ma and Mr. Yin Zhou are acknowledged for data processing. Besides, other group members Dr. Jianying Wang, Dr. Tsz Fung Wong, Dr. Dongqi Han, Dr. Dong Zhang, Mr. Eugene Zhen Yan Li, Miss Deejay Suen Yui Mak, Mr. Jun Dai, Miss Qinyu Jia, Miss Qi Yi, Mr. Chengxi Liu, Mr. Xiuer Luo, Miss Elena Bolonova, Miss Jessie Wing Yin Wu and Dr. Cheuk Chi Ng for their precious suggestions on my research and their accompanying when I am in need of help. Thanks are given to Ms. Josephine Leung for the proofreading of this thesis.

The technical supports by The University Research Facility in Life Sciences and The University Research Facility in Chemical and Environmental Analysis of The Hong Kong Polytechnic University (PolyU) are acknowledged, as well as administrative supports from The Department of Applied Biology and Chemical Technology. Thanks are given to the Hong Kong Research Grants Council (Grant Nos. 15304020, R5013-19, R4005-18 and C4002-20WF) and the National Natural Science Foundation of China (Grant No. 31701699) for the financial supports. The Food Inspection Center of Shenzhen Entry-Exit Inspection and Quarantine Bureau is also appreciated for providing the wine samples.

Finally, I would also give thanks to my family, my parents and my elder sister, for the spiritual and emotional support, as well as their understanding and encouragement throughout my life. I also appreciate all of my friends for their constant assistance during these years, especially during the pandemic period.

Table of contents

List of figures

List of tables

List of abbreviations

Abbreviation	Full form
AA	Amino acid
Ala	Alanine
Arg	Arginine
Asp	Aspartic acid
AUC	Area under curve
ACN	Acetonitrile
CD	Cyclodextrin
CE	Capillary electrophoresis
CHCA	α-Cyano-4-hydroxycinnamic acid
CID	Collision induced dissociation
CR	Chiral recognition ratio method
CS	Chiral selector
CSPs	Chiral stationary phases
DART	Direct analysis in real time
DHB	2, 5-Dihydroxybenzoic acid
ee	Enantiomeric excess
ESZ	*S*-omeprazole
FDA	Food and Drug Administration
FN	False negative
FP	False positive
FPR	False positive rate
FT-IR	Fourier transform infrared
GC	Gas chromatography

Glu	Glutamic acid
Gly	Glysine
His	Histidine
HPLC	High-performance liquid chromatography
ICP	Inductively coupled plasma
IR	Isotopic ratio
IT	Ion trap
KM	Kinetic method
Leu	Leucine
Lys	Lysine
MALDI	Matrix-assisted laser desorption ionization
MS	Mass spectrometry
NMR	Nuclear magnetic resonance
OMZ	Omeprazole
OPLS-DA	Orthogonal partial least squares discrimination analysis
PCA	Principal component analysis
Phe	Phenylalanine
PLS	Partial least squares
Pro	Proline
ROC	Receiver-operating characteristic curve
RSD	Relative standard deviation
SDs	Standard deviations
SFC	Supercritical fluid chromatography
TFA	Trifluoroacetic acid
THAP	2 ,4 ,6 -Trihydroxy acetophenone

Thr	Threonine
TLC	Thin layer chromatography
TN	True negative
TOF	Time of flight
TP	True positive
TPR	True positive rate
Trp	Tryptophan
Tyr	Tyrosine
UV-Vis	Ultraviolet-visible
VIP	Variable importance on projection

Chapter 1. Rapid Authentication of Red Wine by MALDI-MS Combined with DART-MS

1.1 Introduction

1.1.1 Red wine

Red wine, among the most consumed alcoholic drinks, occupies a great market worldwide. For example, 679 million liters of wine were imported to China in 2018[1], and 9.05 billion Euros of bottled wine were exported from France in 2017[2]. It has become such an important part of the culture that people are more interested in tasting wines from different regions around the world.

Compared with other spirits and beers, wine is highly popular, partially due to its unique production process, which is influenced by factors such as weather, region, and variety. This irregularity in production can lead to the scarcity of certain wines, which can be of great commercial value. Even by the same winemaker, the prices for wines can vary based on factors such as year, variety and growing condition. Wines with different quality and ages have different values[3]. With the rising prices and expanding market, wine has become an investment and collectible item.

Except for its commercial values, the health effects of moderate consumption of wine have also been studied. Research has shown that light to moderate intake of wine can have a positive impact on protecting against coronary heart disease, which is attributed to the presence of active polyphenols in red wine that have properties of antioxidant and anti-inflammatory that help prevent atherosclerotic pathologies[4-6]. Bioactive compounds in wine are grouped as non-flavonoids and flavonoids[7], among which the

benefits from resveratrol and anthocyanins have been widely discussed. Resveratrol primarily presents in grape berry skins, so the concentration is much higher in red wine. Resveratrol, found primarily in grape berry skins, has been proven to regulate lipid metabolism and prevent oxidation and aggregation of low-density lipids, which helps to increase the antioxidant potential, thereby reducing the risk of cardiovascular diseases[8, 9]. Anthocyanins, responsible for the color of red wine, are key components of the human diet that possess numerous health-promoting properties, e.g., antioxidant and anti-carcinogenic activities[10, 11]. Besides, other bioactive components also have great positive effects on human health[4].

Due to its financial profitability and health effects, counterfeiting of wine has long time been a severe problem. This includes using the branding of well-known wine companies, imitating bottle designs, filling empty bottles with fake liquid, mislabeling the production year, and diluting the wine with alcohol or water[12]. Considerable efforts have been made by many countries to protect both consumers and producers from this issue. The European Union, being the major importer and exporter of wine, has the most regulated wine market[13]. Similarly, countries including Argentina, Australia, South Africa, and the United States have also implemented regulations regarding the original regions, added chemicals and additives, and proper labeling of bottles[14]. However, despite these measures, wine fraud remains a persistent problem. An annual income loss of nearly €1.3 billion because of counterfeit alcoholic beverages and wines was reported by the EU market in 2016[15]. In the past decade, the Chinese wine market has experienced significant growth, increasing more than fourfold, while it is said that less than 30% of wines sold in China were original[16]. Consequently, establishing reliable and accurate methods to ensure authenticity control of wine origin, year, variety, etc.

has become an important task.

1.1.2 Current techniques for analysis of wine

Wine is derived from grape berries, and the compositions of the berries vary widely and thus contribute differently to the overall compositions of the wine. Being a complex mixture with hundreds of components, the chemical compositions of wine change during production and storage, ultimately affecting its flavor[17, 18]. The wine production process involves berry growth, fermentation and aging[19], each of which contributes to the unique chemical fingerprint of the wine. During berry development, polyphenolic compounds undergo a series of chemical reactions that create the complex texture found in red wine. Additionally, the viticultural methods and growing environment of the grapes also affect the chemical composition. Fermentation involves various chemical reactions of sugars, amino acids, and flavor compounds, which can be influenced by temperature, humidity, and other conditions[20]. Due to the metabolic activity of the yeast, as well as the interaction between varietal aromas and other components, the volatile compounds in wine are altered during the fermentation process[21]. Aging further influences the chemical profile of red wine, with factors such as oak wood barrels affecting the concentration of certain acids[22]. In addition, research has shown that the profile of aroma compounds, anthocyanin, polyphenol, yeast, protein and even biogenic amines in wine differ based on geography, grape type and vintage age, which can be analyzed by analytical techniques and thus as markers for the authentication of wines.

The chemical compositions of red wine can vary due to the production and storage process, and they are influenced by factors such as geography, grape type and vintage age. Currently, in the field of wine analysis, a large number of biological and chemical

techniques have been utilized to determine various compounds. Biologically, DNA-based methods have been employed for varieties authentication, however, issues such as degradation and complex DNA separation processes limit the amplification of this application[23, 24]. Chemical techniques, on the other hand, are widely studied and involve the analysis of elements, phenolic compounds, volatiles, and isotopic ratios. The wine elements that are associated with the geographical origin can be quantitatively determined by inductively coupled plasma mass spectrometry (ICP-MS), but such analyses cannot be extended to the proof of year or variety[25, 26]. Techniques such as ^{1}H nuclear magnetic resonance (NMR), ultraviolet-visible (UV-Vis) spectroscopy and Fourier transform infrared (FT-IR) spectroscopy are prevalent in studying grape varieties, vintage years, and regions[27-29]. However, these methods have limitations such as lower sensitivity, lower efficiency, and inability to provide accurate information for complex mixtures.

Mass spectrometry is considered to be a powerful analytical technique, with increased applications in wine characterization, particularly by coupling with gas chromatography (GC-MS), high-performance liquid chromatography (HPLC-MS) and isotopic ratio (IR-MS)[30-32]. While GC-MS mainly detects volatile components and LC-MS prefers polar ones, both of them require complicated sample preparation and chromatographic separation, making them time-consuming. IR-MS can provide accurate isotopic abundances but misses the molecular information, which is not ideal for wine component profiling. Direct mass spectrometry methods, such as matrix-assisted laser desorption ionization mass spectrometry (MALDI-MS) and direct analysis in real time mass spectrometry (DART-MS), requiring neither sophisticated extraction nor separation steps, can provide rich information from numerous samples

in a relatively short time.

1.1.3 MALDI-MS

MALDI-MS was originally developed in 1988 by Karas et al.[33] and is based on the use of a laser. MALDI-MS enables soft ionization of the sample by introducing a matrix, which prevents direct interaction between the laser and the analytes, thus minimizing fragmentation. The matrix is first irradiated by the laser, and then the absorbed energy is transferred from the matrix to the analyte for ionization. Several types of matrices can be chosen, depending on the mixing properties and the ability to uniformly co-crystallize with the analytes[34].

MALDI-MS has a high tolerance to contamination, high sensitivity, rapid analysis and especially high-throughput as hundreds of sample spots can be analyzed automatically on the same MALDI plate. MALDI-MS has been extensively employed in various fields, such as compound profiling and differentiation of blended oils and herbal medicines[35, 36].

1.1.4 DART-MS

The DART-MS technique, introduced by R.B. Cody et al. in 2005[37], has gained significant interest with the development of ambient desorption ionization techniques. The mechanism of DART can be divided into two steps in general: ionization and reaction[38]. During the ionization step, gas flow is introduced through an axially segmented tube, where gas atoms are excited by a corona glow discharge between a needle electrode and a perforated disk electrode. The gas flow then passes through an additional electrode, a heated area and a third grid electrode to remove anions and

electrons, allowing the remaining heated neutral or uncharged ground-state gas atoms to flow out from the ionization source into the atmosphere. During the reaction step, the excited gas atoms first ionize the surrounding gases (mainly nitrogen, oxygen, and water), and through various reactions, ionize the analyte material placed in the atmosphere. Protonated and deprotonated ions are observed in positive and negative ion modes, respectively, with specific species depending on the compounds and the presence of dopants. In many studies, ammonia or methylene chloride dopants can be used to enhance signals by forming $[\mathrm{M} + NH_4]^+$ or $[\mathrm{M} + \mathrm{Cl}]^-$ in positive mode or negative mode[39], respectively. Desorption electrospray ionization (DESI) is a similar ambient ionization technique to DART and is widely used in many fields. DESI uses pneumatic-assisted electrospray to generate charged aerosols containing low-concentration electrolyte solvents, the highly charged aerosol droplets then hit the surface of the object, causing the release of analyte-containing charged droplets from the surface. DESI relies purely on liquid-phase processes, requiring large amounts of solvents, and is typically used for larger molecules than DART. DART is primarily suited for small molecules, enabling molecular weights between 50-1000 Da. In addition, considering the volatility of the analyte in wine analysis here, DART is more suitable as solution-phase processes are excluded.

The major advantage of DART is minimal or no sample preparation is needed under ambient environment conditions, making it a powerful and potential analytical technique in rapid and high-throughput analysis with MS. This technique has been demonstrated in diverse fields, such as food quality and safety, forensic and security, and has been successfully applied to analyze solid, liquid and gas samples[40-42].

Up to now, literature on red wine using MALDI-MS or DART-MS is still very few, primarily focusing on specific compounds or simplified samples at a small scale[43, 44]. MALDI-MS is commonly used for detecting large compounds and has been employed in the analysis of grape seed proteins and peptides in wine to differentiate grape varieties and geographical regions[45, 46]. Additionally, MALDI-MS has the potential to analyze small molecules such as anthocyanins, tannins, proanthocyanins, procyanidins and even yeasts. DART-MS is often used to investigate residual pesticides[47] and quickly quantify trace-level volatiles[48, 49]. However, there have been limited applications of MALDI-MS or DART-MS in wine discrimination, despite their potential in this field. What's more, while both targeted and untargeted methods have been used for wine characterization, the former has limitations when it comes to various wine characteristics, as some important but rarely reported compounds may be missing. In contrast, untargeted methods aiming to reveal changes in global chemical profiles have great superiority in discovering discriminative markers, including metabolites and secondary metabolites produced during fermentation and aging[50]. In this study, the untargeted method is utilized.

1.1.5 Multivariate statistical modeling tools

To obtain the best classification results, various multivariate statistical modeling tools have been routinely applied based on quantitative and qualitative information. Among them, principal component analysis (PCA), partial least squares discrimination analysis (PLS-DA), and orthogonal partial least squares discrimination analysis (OPLS-DA) are the most employed. PCA is a straightforward method that can handle multiple classes simultaneously and classify unknown observations. Three different varieties of Lambrusco wines were analyzed by HPLC, and PCA was applied to the profiles and

characterize the wines in terms of varieties[51]. However, PCA exhibits high intra-class variation, in other words, it can only separate significantly different classes with small variation. It is an overview and unsupervised statistical method that does not consider the category information of the sample. Maximum class separation is not the objective, and the explanation of group differences is not satisfactory. PLS-DA is an extension of PCA but outperforms PCA in classification. PLS performs supervision and involves information about sample classes and can evaluate the relationship between the descriptor and the response, helping to characterize the data structure. PLS-DA proves to be a powerful yet simple tool for analyzing microarray data with good predictive capability for clinical outcomes[52]. All samples before and after chemotherapy were overlapping in PCA, whereas they were apart and distinctly grouped with PLS-DA. But PLS-DA also suffers from low intra-class variability and lacks convincing explanatory ability when the number of classes increases.

OPLS-DA[53] is an extension of PLS-DA, which uses Y matrix to decompose X matrix into components that are related and unrelated to Y. One notable advantage of OPLS-DA is its ability to differentiate between predicted and non-predicted changes. Removing orthogonal components enhances classification accuracy independent of the sample class. OPLS-DA is a powerful multivariate statistical modeling tool when dealing with complex samples and large groups, and has been widely used in the analysis of food samples, such as white wine[54], peanut kernels[55] and dried slices of shiitake[56]. In a study on determining the geographical origins of Korean Panax ginseng, PCA analysis failed to separate samples due to heavy peak overlap. However, OPLS-DA was successful in clustering the samples, demonstrating excellent predictive and fitting abilities. Validation using testing samples yielded a prediction accuracy of

99.7%[57]. Authentication of red wine could also be accomplished by OPLS-DA. By coupling solid phase microextraction online with GC–MS, the red varietals were successfully determined with OPLS-DA[58]. Furthermore, with the assistance of OPLS-DA, liquid chromatography/ion mobility quadrupole time-of-flight mass spectrometry, NMR and infrared-based techniques enabled to tracing back geographical origin of red wines[59-61].

In this chapter, OPLS-DA models will be used as there are multiple classes to be differentiated with large internal differences: vintage years, grape varieties, produced areas, wine types and almost thoroughly different brands. Herein, we developed untargeted and high-throughput methods for rapid authentication of wine using MALDI-MS and DART-MS, coupling to OPLS-DA. Neither method can achieve the distinction of wine independently, but they were found to be complementary, mainly due to their different ionization methods and different analyte preferences. Though simple and rapid analysis can be performed without chromatographic separation, signal suppression may simultaneously cause loss of analyte information. For MALDI-MS, the high vacuum status inside makes it preferable to non-volatile compounds, besides, matrices used may result in background effects. For DART-MS, ambient ionization facilitates the analysis of volatile compounds, still, the water vapor and other components in the open air could bring high background signals and influence the protonation of sample molecules[38, 62].

Thereby, we hypothesize that they would improve the classification of wines after combination. To our knowledge, the approach of combining MALDI-MS and DART-MS was first presented in this work, which leads to remarkably enhanced discrimination

results. The approach was successfully conducted on 535 wine samples from 8 key wine-producing countries with high correct rates, and it was also extended to the differentiation of other features, such as vintage years and grape varieties, suggesting the feasibility of controlling wine quality in the market. Furthermore, this study provided a train of thought to combine multiple mass spectrometry methods to screen as many components as possible.

1.2 Experimental

1.2.1 Chemicals

α-Cyano-4-hydroxycinnamic acid (CHCA), 2, 5-Dihydroxybenzoic acid (DHB) and trifluoroacetic acid (TFA) were from Sigma-Aldrich (St. Louis, USA). HPLC-grade acetonitrile (ACN) and methanol were purchased from Anaqua Chemical Supply (Houston, USA), and acetone was from Acros Organic (Waltham, USA).

1.2.2 Wine samples

535 wine samples were kindly provided by Shenzhen Customs, China[31], which were collected directly from the original countries and were already certified by Customs to ensure the authenticity of samples. They were collected from 8 major wine-producing countries (America, Australia, Chile, China, France, Italy, Spain and South Africa), with vintage years ranging from 1999 to 2014, more than 10 types of grape varieties with a considerable number of blended wines, and they were from different brands and manufacturers, indicating the complexity of our samples (see Table 1-1 for their detailed information). The samples were randomly divided into the calibration set for the establishment of OPLS-DA models (nearly 2/3 of total samples) and the validation set for external validation of the classification ability of models (nearly 1/3 of total samples). Before the analysis, the samples were stored at 4 ℃.

Table 1-1. Wine samples collected for this study.

Country	Number	Grape cultivar	Vintage year
America	48	Zinfandel, Merlot, Cabernet Sauvignon, Shiraz, Pinot Nior	2005-2011
China	43	Cabernet Sauvignon, Cabernet Gernischt	2007-2014
France	78	Pinot Nior, Cabernet Sauvignon, Merlot, Cabernet Franc, Grenache, Cariñena	2005-2014
Italy	57	Cabernet Sauvignon, Shiraz, Merlot, Nero d' Avola, Rosso, Nebbiolo, Barbera	2001-2013
Spain	94	Cabernet Sauvignon, Pinot Nior, Cabernet Sauvignon, Merlot, Tempranillo	1999-2013
Australia	109	Pinot Nior, Cabernet Sauvignon, Merlot, Shiraz, Tempranillo	2001-2012
Chile	58	Cabernet Sauvignon, Merlot, Shiraz, Carménère, Malbec	2006-2012
South Africa	48	Cabernet Sauvignon, Merlot, Shiraz, Pinotage	2006-2012

1.2.3 MALDI-MS Analysis

The sample preparation method was utilized, including solvents, matrices and their concentrations, as well as loading methods. Briefly, a concentration of 20 mg mL^{-1} CHCA matrix in 75:25 acetone: water (v/v) containing 0.2% TFA was prepared. Aliquots of 10 µL wine samples were vacuum dried, to remove water and ethanol that were found to negatively influence the uniform crystallization and the signals of analytes. the dried samples were then dissolved with 10 µL of 50:50 ACN: H_2O for further use. The two-layer loading method was applied here: first, aliquots of 0.5 µL CHCA solution were loaded onto the MTP 384 target plate ground steel BC (Bruker, Billerica, USA), forming evenly distributed matrix layers after fast air-dried (Figure 1-1a). Then aliquots of 0.5 µL dissolved sample solution were dropped onto the matrix layer and air-dried before being introduced into the mass spectrometer (Figure 1-1b). Each wine sample was prepared with 8 spots.

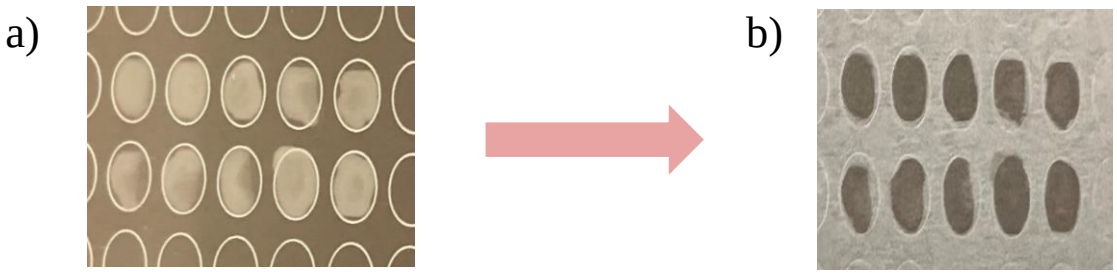

Figure 1-1. The two-layer loading method used in MALDI-MS.

An UltrafleXtreme MALDI-TOF-TOF mass spectrometer (Bruker, Billerica, USA) was applied to acquire the spectra (*m/z* 380-1000) under positive and reflectron mode, with a 355 nm smartbeam-II laser. The voltages for the ion source voltage 1 and 2, lens voltage, and reflector voltage 1 and 2 were set to 20.00 kV, 17.75 kV, 7.00 kV, 21.10 kV and 10.85 kV, respectively. The automatic acquisition was applied with a completely random walk to analyze hundreds of sample spots rapidly, and both the external and internal calibrations were performed using the CHCA matrix. For each spectrum, eight shots were accumulated with a total of 8000 laser pulses, and a high-signal mass range of *m/z* 400-600 with a resolution higher than 3000 was used for evaluation. MS/MS spectra of interest peaks were acquired by the same equipment using the LIFT function. The ion source voltage 1 and 2, lens voltage, reflector voltage 1 and 2, and lift 1 and lift 2 of the spectrometry were set to 7.50 kV, 6.30 kV, 3.90 kV, 29.50 kV, 19.2 kV and 3.40 kV, respectively. The flexAnalysis (Bruker, Billerica, USA) was used for processing the spectral results, applying centroid peak detection algorithm, signal to noise over 4, peak width over 0.2 Da and TopHat baseline subtraction.

1.2.4 DART-MS Analysis

Aliquots of 2 μL wine with 0.2% ammonium acetate were directly spotted onto a clean mesh sampling strip without any prior purification or extraction. Each sample was loaded with 5 spots, separated by a blank spot (Figure 1-2) to diminish the interferences from the nearby spots during the DART-MS analysis.

The calibration was performed with the standard Tuning Mix (Agilent Technologies, Santa Clara, USA) before assembling the DART-SVP ion source (IonSense Inc. Saugus, MA, USA) to the mass spectrometer. Spectra with a mass range of 100-1000 Da were

acquired under positive mode, with the ion source coupling to quadrupole-time of flight mass spectrometer (Agilent Technologies, Santa Clara, USA) by a VAPUR® interface, connecting with a membrane pump to maintain low vacuum. Semi-automatic analysis of samples was performed using a 1-D transmission module (P/N JCL-2100-A) fixed on a holder. To obtain information-rich and intensity-high mass spectra, the settings of the system were optimized. The settings for DART ionization included the distance between the DART source outlet and the ceramic tube inlet: 9.5 mm, the gap between the ceramic tube outlet and the capillary inlet of MS: 2 mm, module moving speed: 2 mm s^{-1}, helium flow rate: 2 L min^{-1}, gas temperature: 150 °C; and the settings for mass spectrometric detection included gas flow: 3 L min^{-1}, capillary voltage of ESI+: 1000 V, fragmentor voltage: 200 V. The acquired spectra were processed by MassHunter Qualitative Analysis (Agilent Technologies, Santa Clara, USA) with a threshold of relative intensity over 2%. Each sample-loaded spot was measured several times, and the spectral results of the second measurements, which were found to offer higher abundances as well as better reproducibility in the optimization study, were used for the data analysis.

Figure 1-2. The metal mesh trip with samples loaded for DART-MS analysis.

1.2.5 Data analysis

The procedures for the establishment and optimization of the OPLS-DA models are shown in Figure 1-3. For the better utilization of both MALDI-MS and DART-MS, all peaks as well as isotopic peaks were taken into account. A total of 611 and 192 variables were obtained from the MALDI-MS and DART-MS results, respectively. Automatic peak picking from samples was achieved using RStudio Desktop (RStudio, Inc., Boston, USA) to form datasheets with variables in columns and samples in rows. Variables from the matrix or backgrounds were removed, and the remaining data were normalized by dividing the intensity or abundance of each peak by the sum of the total intensity or abundance. Replicates were averaged and peaks with more than 50% missing values in all groups were excluded., after the removing, the normalization was performed again. Finally, 180 and 100 variables were left from MALDI-MS and DART-MS, respectively, for further data analysis.

Data pretreatment is an essential issue in multivariate analysis. Different methods can be used to maximize the variance of the inter-group variance while minimizing that of intra-group, e.g., centering, Pareto scaling, log transformation and power transformation[63]. In this study, all data were subjected to third root power transformation as it led to the best results among the transformations tested and mean-centered to improve the statistical model performances before performing supervised OPLS-DA in the software (Simca 16.0; Umetrics, Andover, MA, US).

The discrimination then can be achieved by using multivariate statistical modeling tools. Reliable OPLS-DA models based on the calibration set were established, and hundreds of wine samples could be simultaneously discriminated in our established models.

Several criteria for data screening should be considered. OPLS-DA can reduce dimension from a large original data, thereby selecting statistically important variables while removing redundant ones. Generally, the fitting ability increases with the number of OPLS-DA components, while the predictive ability is not necessary and, in most cases, decreases with the number of components after autofitting the software, indicating that the model is trying to fit dataset characteristics that are no longer representative. Too many components may lead to overfitting of the model, where the calibration is good but the prediction accuracy of the validation set is low. So there needs a proper predictive and orthogonal components number to balance the fitting and predictive abilities. Herein, all models established were estimated based on these two rules along with the predicting accuracy results of the testing set, and the optimal one was used when the overall correct classification rates of validation samples came up to the highest. Outliers may exist due to experimental or other errors, so only samples with standard deviations (SDs) between +4 and −4 remained. Though lots of variables were obtained, not all of them were important enough to the establishment of the model, and variables were selected with variable importance on projection (VIP) values no lower than 0.5. The outliers and unimportant variables were excluded to form a new data set to obtain models with higher fitting ability, going back to step 2 was then repeated until both SDs and VIP values met the criterion.

In the next step, the goodness of fitting ability (R^2Y) and the cross-validated predictive ability (Q^2) were evaluated, which suggests good models when both over 0.5 and excellent models when close to 1.0[64]. Besides, a permutation plot with 200 numbers was tested to avoid over-fitting of a model. Afterward, the calibration set was qualified to review models.

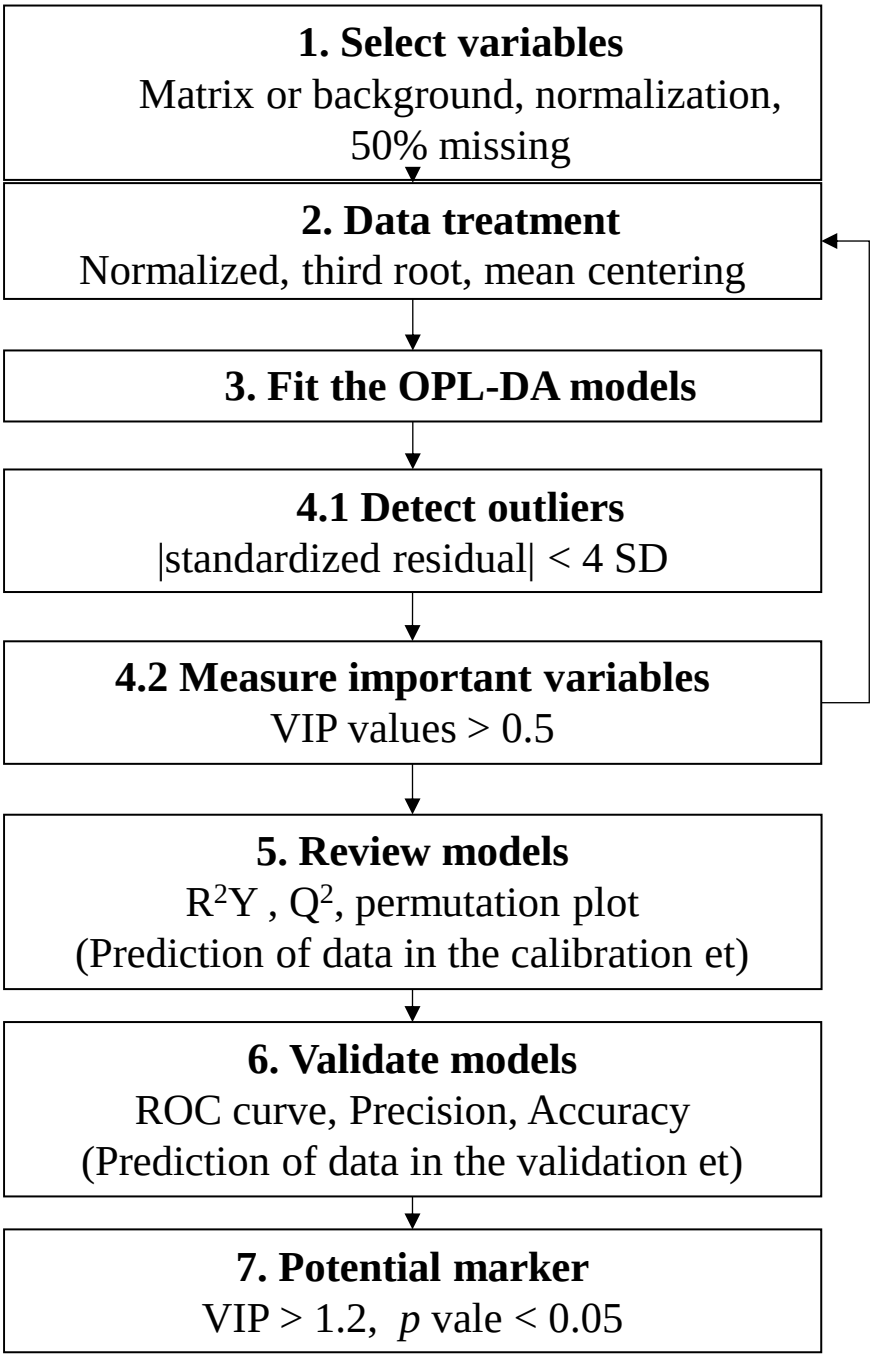

Figure 1-3. Outline for establishing and optimizing the OPLS-DA models.

For validation of the models, the validation set was qualified to verify the classification ability. The validation samples were external samples for these models, as they were not involved in the development process. The high correct classification rate of the validation set demonstrated the reliability of the models. In addition, it is almost impossible or hard to build OPLS-DA models with perfect identification from the validation set, the prediction results were thus inspected by measurements of accuracy, precision, receiver-operating characteristic (ROC) curve and area under curve (AUC)[65]. There are four types of prediction results: true positive (TP), true negative (TN), false positive (FP) and false negative (FN). A clear description is shown in Figure 1-4. Accordingly, precision and accuracy were calculated as

$$\text{Precision} = \frac{TP}{TP + FP} \qquad Equation\ (1)$$

$$\text{Accuracy} = \frac{TP + TN}{P + N} \qquad Equation\ (2)$$

where P is the total positive samples and N represents negative ones.

In addition, the false positive rate (FPR) and true positive rate (TPR) expressed as

$$\text{FPR} = \frac{FP}{N} \qquad Equation\ (3)$$

$$\text{TPR} = \frac{TP}{P} \qquad Equation\ (4)$$

On this basis, a set of points (*FPR, TPR*) was used to obtain the ROC curve. The AUC indicating the quality of a classified group to distinguish positive samples from negative samples is denoted as

$$AUC = \int_0^1 \frac{TP}{P}\, d\frac{FP}{N} = \frac{1}{PN} \int_0^N TP\, dFP \qquad Equation\ (5)$$

According to equation 5, the AUC value is 0 ~ 1: less than 0.5 is a random classifier, and 1.0 is a perfect classifier.

In the final step, potential characteristic markers were picked out based on VIP value > 1.2 and *p*-value < 0.05, which indicated the highest discriminative potentials in the OPLS-DA score plot. Characteristic markers were identified based on the MS and MS/MS results by referring to the literature or databases[66, 67].

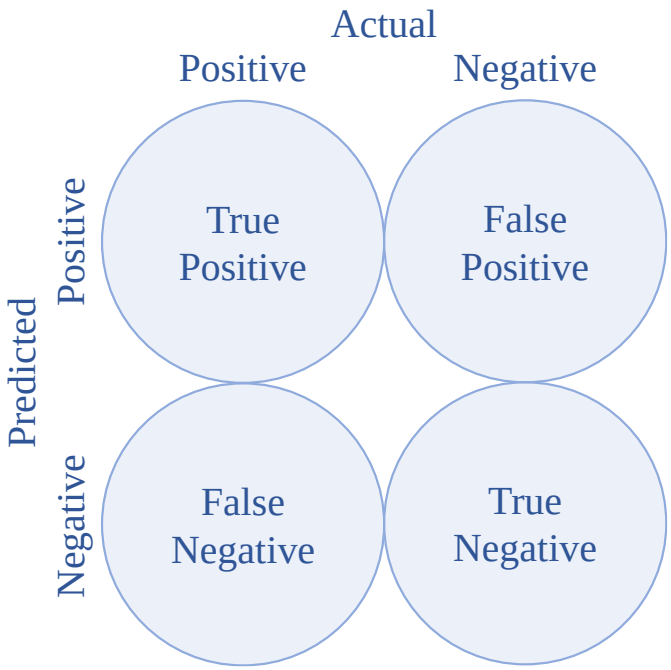

Figure 1-4. Description of prediction results.

1.3 Results and discussion

1.3.1 Rapid authentication of red wine by MALDI-MS

1.3.1.1 Optimization of sample preparation

To build a protocol of sample preparation with good quality and reproducibility, several parameters needed to be optimized, including the MALDI plate, matrix, organic solvent, addition of acid, and loading method. The results after optimization were listed in Table 1-2, and some important conditions were discussed next.

Table 1-2. Description of the different conditions studied for the implementation of wine identification by MALDI-MS.

Conditions studied	**Margin**	**Selected**
MALDI plate	384 ground, Anchorchip	384 ground
Matrix	CHCA, DHB, THAP	CHCA
Organic solution for matrix	ACN, methanol, acetone	Acetone
Percentage of acetone in water	25%, 50%, 75%, 100%	75%
Matrix concentration mg/mL	2, 6, 10, Saturated	Saturated
Percentage of TFA	0%, 0.1%, 0.2%, 0.5%, 1.0%	0.2%
Loading method	Dried-drop, two-layer	Two-layer
Ratio of matrix: sample (*v*:*v*)	1:1, 1:2, 1:3, 2:1, 3:1	1: 1

More than 86% of the composition of red wine is water, which cannot be detected using MALDI-MS because it evaporates before analysis. However, its presence largely affects the analysis of other components, which are present in very low concentrations in wine. In addition, water evaporates much slower than organic solvents, negatively affecting crystallization formation on the MALDI plate. To mitigate the influence, we tried to vacuum-dry the wine samples first to remove water and then re-dissolve the sample with 50% ACN. This led to improved crystallization and a better signal.

The selection of matrix plays an important role, which depends on the characteristics of the analytes. There are no universal rules in this regard, so experiments are conducted to enhance the signal. Three matrixes, namely CHCA, DHB and THAP, were tested. When using THAP as the matrix, low intensity was observed and only a few peaks were detected. When using DHB as the matrix, nearly no signals over 400 Da were observed. Even below 400 Da, compound ions that are well reported were not observed. On the other hand, CHCA exhibited significant matrix suppression effects but provided the highest intensity. Hundreds of peaks were detected between 400 Da and 1000 Da. As for the concentration, no significant changes were observed, therefore, the easily prepared saturated CHCA solution was applied.

The method of loading the analyte onto the MALDI plate can vary depending on the properties of the sample, its interaction with the matrix, and the type of plate used. Typically, there are three methods: dried-droplet, two-layer and direct sample loading. The dried-droplet technique, where the sample is mixed with a matrix and dropped to the MALDI plate for co-crystallization, is the most widely used. The two-layer method is a modification of the first one, where the matrix is first loaded onto the plate and then

the sample solution is added onto the dried matrix layer. Based on this, the sandwich method has been further developed, where the sample is applied between two dried matrix layers. The direct sample loading method is typically applied to samples that can absorb the energy from the UV-laser directly without the assistance of a matrix. However, this method is not suitable for wine samples. In this study, both the dried-droplet method and the two-layer method were tried to find the optimal approach. It was found that the dried-droplet method caused uneven co-crystallization and thus the existence of the "sweet spot", where signals could only be found in these specific spots. This resulted in poor reproducibility (Figure 1-5). In contrast, the two-layer method, with evenly distributed layers of both the CHCA and the sample, enabled better crystallization, resulting in better reproducibility (Figure 1-6).

The choice of solvent to dissolve the matrix was another important issue, as the evaporation of the solvent would impact the crystallization outcome. Herein, three different types of organic solvents were tested. It was observed that acetone evaporated the fastest, leading to an extremely even layer of CHCA matrix. Specifically, three replicates of the same wine sample showed the most similar spectral results when CHCA was dissolved in acetone, compared to ethanol and methanol (Figure 1-7).

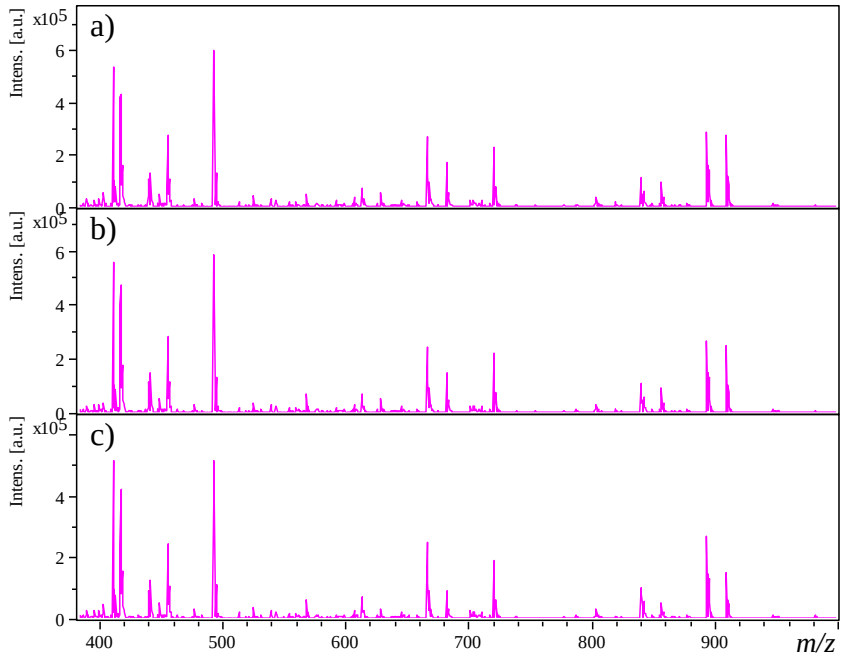

Figure 1-5. Three replicates of spectra using the dried-droplet method.

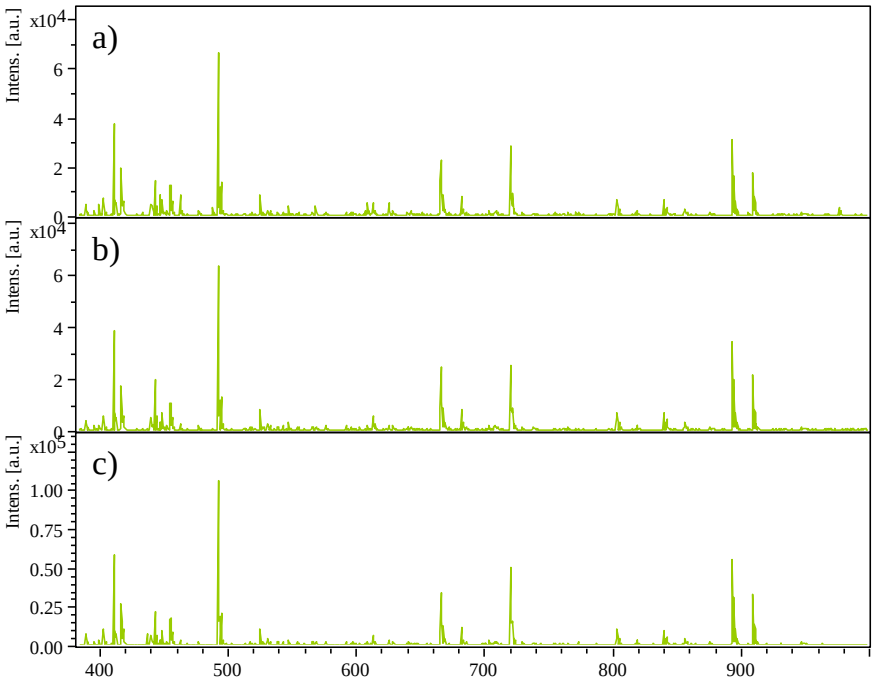

Figure 1-6. Three replicates of spectra using the two-layer method.

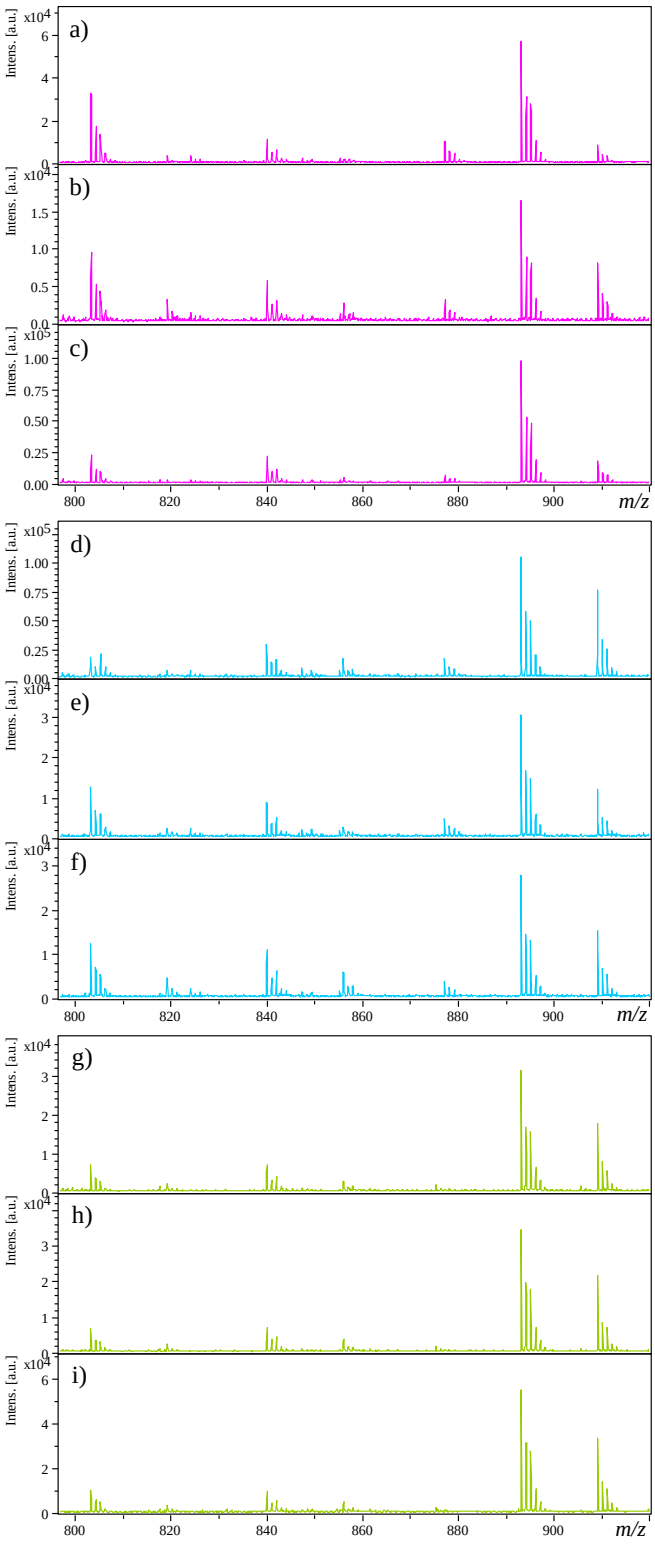

Figure 1-7. Spectra of a wine obtained by MALDI-MS using CHCA dissolved in a-c) ethanol, d-f) methanol and g-i) acetone.

1.3.1.2 Automatic data acquisition

Our previous research has demonstrated that MALDI-MS analysis can achieve automatic data acquisition with high-quality spectra for blended oils, comparable to manually obtained spectra. It indicates that manual acquisition can be replaced by the automatic mode, increasing efficiency and enabling high-throughput sample analysis. Automatic data acquisition was also applicable to this study: for each sample spot, it only took 30s, and even for 8 replicates, only 4 min was required. With a MALDI plate containing 384 spots, the detection time for hundreds of wine samples is significantly reduced. As shown in Figure 1-8, 8 spectra acquired from the sample using the automatic modes showed extremely identical profiles. Precision calculations using peaks of high and low relative intensity demonstrated high reproducibility, with the relative standard deviation (RSD) below 15% (Table 1-3), further highlighting the advantage of MALDI-MS for the rapid analysis of red wine.

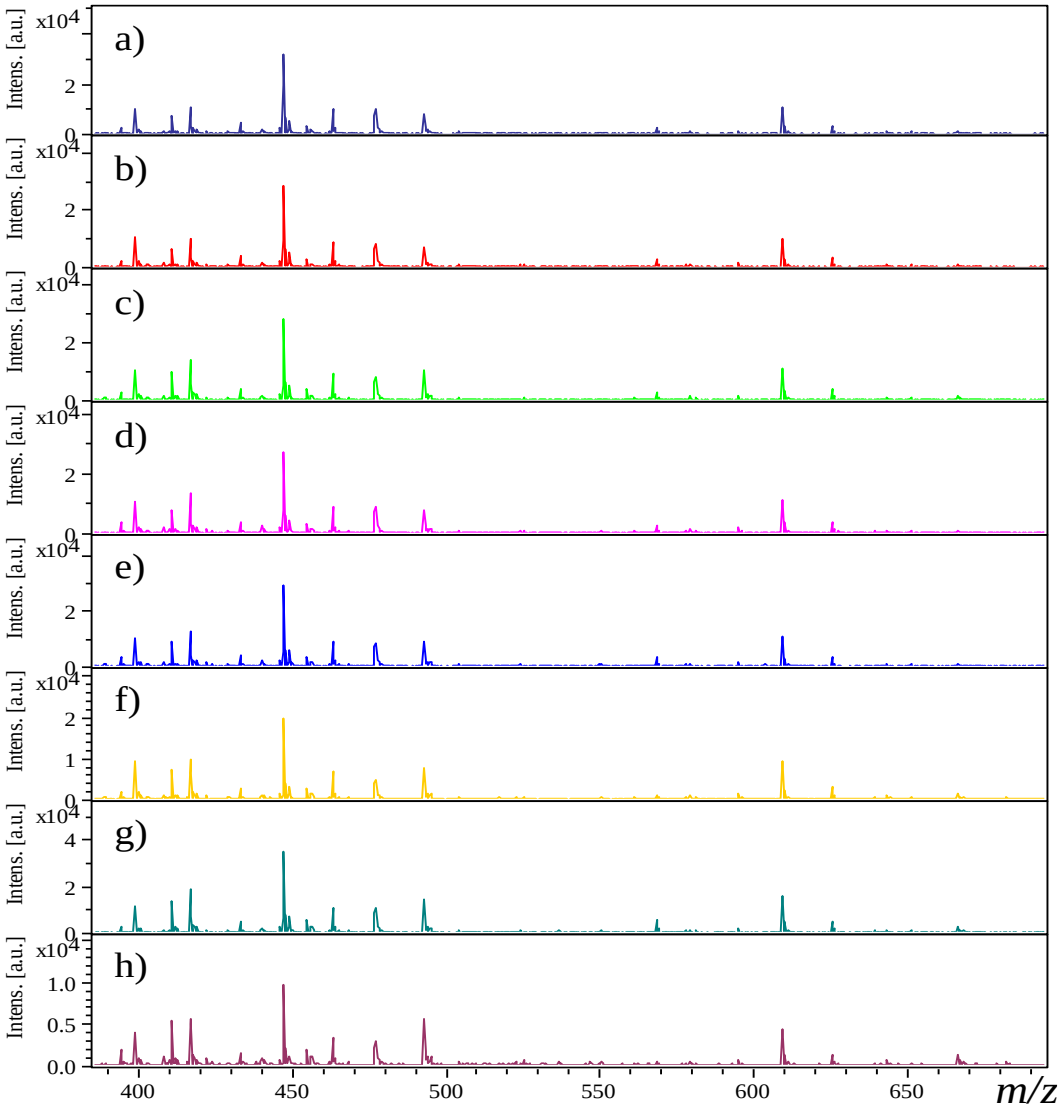

Figure 1-8. 8 spectra of a wine sample obtained by MALDI-MS under automatic acquisition mode.

Table 1-3. The precision of some peaks from a wine sample obtained by MALDI-MS under automatic acquisition mode.

m/z	Relative intensity (%)	RSD (%)
399	4.38±0.46	10.5
448	2.97±0.29	9.8
477	3.26±0.26	7.9
493	5.30±0.63	11.9
581	0.60±0.06	10.3
609	8.77±0.69	7.8
610	2.58±0.21	8.2
625	3.28±0.20	6.2
651	0.87±0.06	6.6
720	1.10±0.16	14.9
755	0.75±0.08	10.7

1.3.1.3 Spectral results from MALDI-MS

Applications of MALDI-MS in wine differentiation are mainly focused on target compounds, mostly anthocyanins. We try to propose an untargeted protocol, taking full advantage of wine information to evaluate hundreds of complicated samples. Figure 1-9 shows a representative spectrum of a sample from France obtained by MALDI-MS. Notably, the mass range below 380 Da was excluded because the strong signal from the CHCA matrix, especially the peak at *m/z* 379, would result in a significant reduction in the relative intensity of the sample ions. The most intensive peaks such as *m/z* 447, 493, 609, 625, 720 and 755 could be observed in almost all samples, which were commonly reported anthocyanins and their derived pigments that are associated with wine color[68, 69]. Anthocyanin composition has been proven to be an important factor for the classification of wines in terms of their regions, grape varieties and even wine-making methods[70]. Accordingly, 20 compound ions tentatively identified by MALDI-MS/MS were summarized in Table 1-4. Taking a peak at *m/z* 609 as an example, it was preliminarily identified as malvidin-3-O-glucoside-4-vinyl phenol as the neutral loss of glucoside (162 Da) and the remaining fragment ion 447 Da that corresponded to the malvidin residue (Figure 1-10a). Similarly, 625 Da was identified as peonidin-3-O-caffeoylglucoide by losing a glucoside (162 Da) and remaining the peonidin residue (Figure 1-10b).

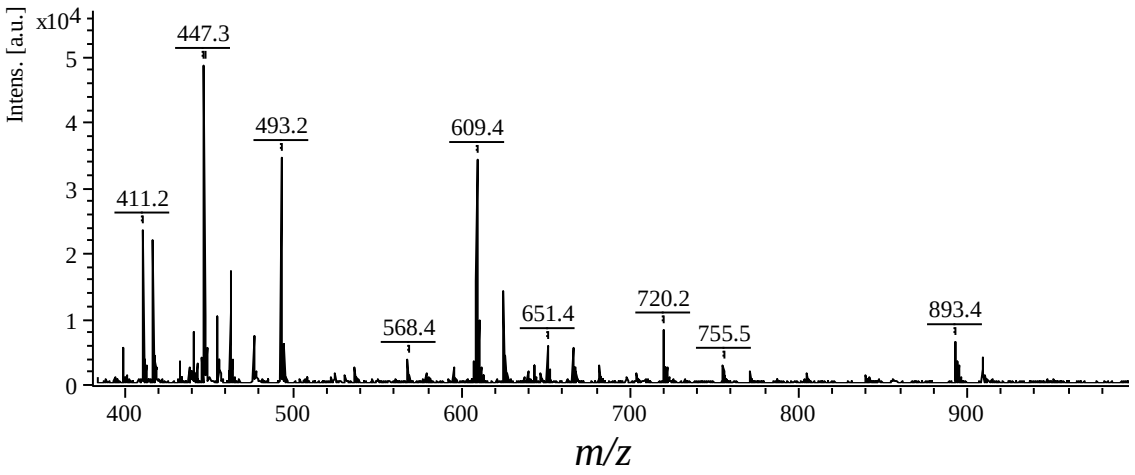

Figure 1-9. A representative spectrum of a sample from France obtained by MALDI-MS.

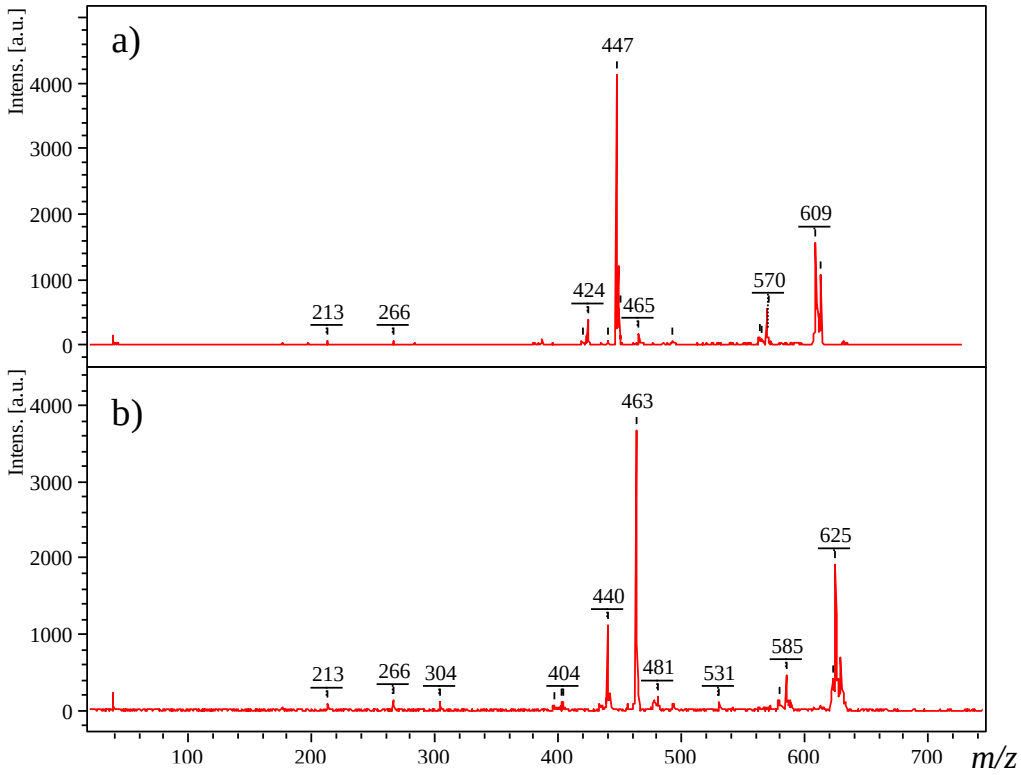

Figure 1-10. The MALDI-MS/MS result of the peak of 609 Da and 625 Da.

Table 1-4. Analytes in the red wine that were tentatively identified by MALDI-MS/MS.

Detected mass (Da)	Major fragment ions (Da)	Analytes
449	303	Astilbin
493	331	Malvidin-3-glucoside
531	369	Peonidin-3-glucoside-pyruvic acid
561	399	Vitisin A
581	419	Delphinidin-3-glucoside-4-vinyphenol adduct
595	287	Cyanidin-3-glucoside-coumarate
603	399	Malvidin-3-(6-O-acetylglucoside)-pyruvate
609	447	Malvidin-3-O-glucoside-4-vinyl-phenol
611	449	Cyanidin-3,5-O-diglucoside
625	463	Peonidin-3-O-caffeoylglucoside
627	465	Delphinidin-3,5-O-diglucoside
651	477	Acetyl-pigment A
667	463	Acetyl-pinotin A
707	399	*p*-Coumaroyl-vitisin A
720	493, 531	Malvidin procyanidins
755	477	Pigment B
771	463	Coumaroyl-pinotin A
787	625	Petunidin-3-(6-O-*p*-coumaroyl),5-O-diglucoside
805	643, 491	Malvidin-3-glucose-4-vinyl-catechin
951	643	Malvidin-3-*p*-cumaroylglucoside-4-vinyl-catechin

1.3.1.4 Establishment of OPLS-DA models for the discrimination of wine origins

It is widely recognized that proof of origin is a critical issue for food authentication, not to say for valuable red wine. However, most studies were confined to priced wines from the Old World, such as Italy, France and Spain. With the development of wines in the New World (America, Chile, China, Australia and South Africa), origin authentication of global wine including more key wine-producing regions has become necessary. Therefore, the main objective of this study is to develop a method for rapid differentiation of 535 wines from 8 key wine-producing countries using MALDI-MS. Comparing the MALDI-MS spectra of 8 countries, differences could be observed in Figure 1-11, which can be further amplified by OPLS-DA, bringing about significant distinguishment of samples from eight countries.

As a comparison, a PCA plot was first applied to classify wines from 8 countries. As shown in Figure 1-12, All samples after chemotherapy were overlapping in PCA, and even with multiple optimizations, they still could not be apart from each other, whereas samples from the same countries tended to cluster closely, which can be distinctly grouped with OPLS-DA.

Initially, an OPLS-DA model was performed to interpret two-thirds of the samples as the calibration set based on the MALDI-MS results. OPLS-DA can identify the variables with the greatest discriminatory power and is suitable for recognizing differences between groups. In the OPLS-DA plots, the horizontal direction will catch variations between groups, and the differences between the groups will locate them to the left and right sides, respectively, while the vertical direction will catch variations within groups. As shown in Figure 1-13a, samples were grouped into eight clusters

according to countries, with some overlap observed in the center, the relative 3D score curves of the model in Figure 1-13b and Figure 1-13c showed more details. It should be noted that wines were collected in a way that covered a wide variety of regions, vintages, grape varieties and manufacturers, all of which are known to influence the wine compositions. The complexity of the samples would narrow the differences between groups, making the spectral results similar and difficult to distinguish. However, an interesting trend in the scattering plot was that northern hemisphere countries (green circle) cluster to the left side and southern hemisphere countries (blue circle) cluster to the right side, suggesting that the difference between the two hemispheres was more pronounced than that between the eight countries. The opposite climate change might account for this, as the ripeness period of grapes is April to October and October to April in the northern hemisphere and southern hemisphere, respectively. The growth of grapes largely relies on climatic conditions, e.g., temperature, rainfall and solar radiation, which can critically impact grape ripeness and consequently the quality of wine[71]. In this way, the separation of two hemispheres would be the first step.

When OPLS-DA was applied to characterize countries within the two hemispheres, those from the southern hemisphere were well separated. As for the northern hemisphere, three European countries (Spain, Italy and France, red circle) were distinguished from America and China (Figure 1-13d). Since interactions between physical and biological environments lead to unique characteristics of a region, the climate has a remarkable impact on grape types and overall wine styles[71, 72]. These three European countries are located close to each other, which are more likely to share a similar climate that contributes to similar wine styles.

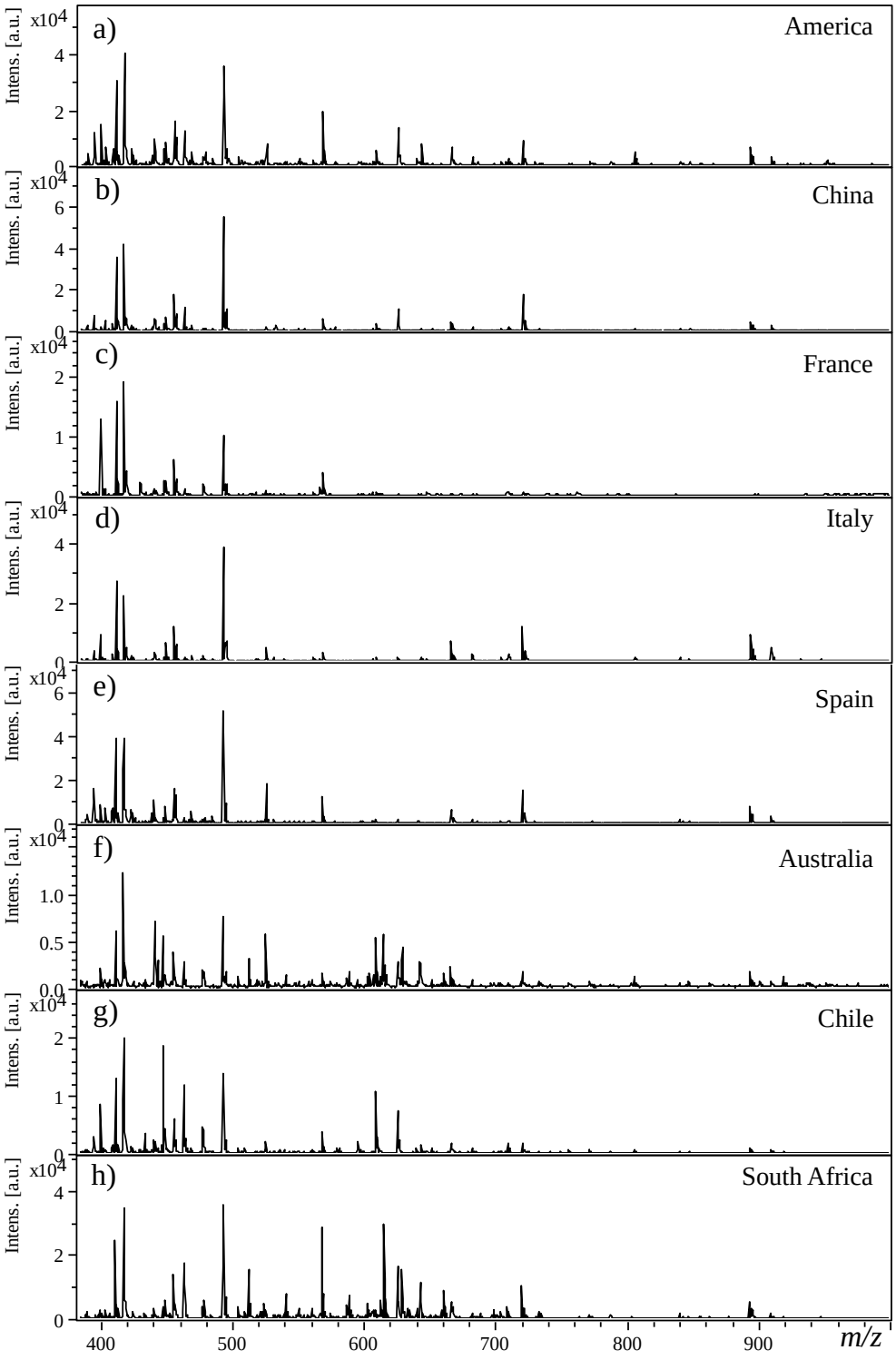

Figure 1-11. The spectra of 8 countries obtained from MALDI-MS.

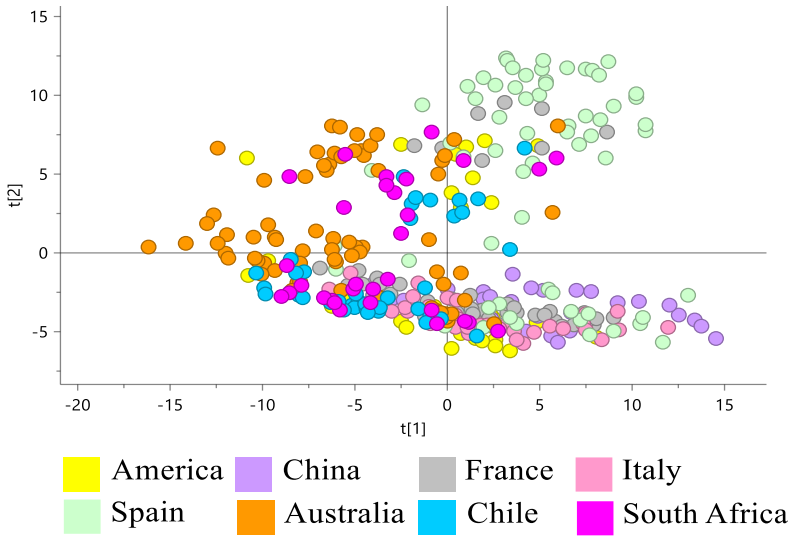

Figure 1-12. PCA plot of the wine samples for differentiation of eight countries.

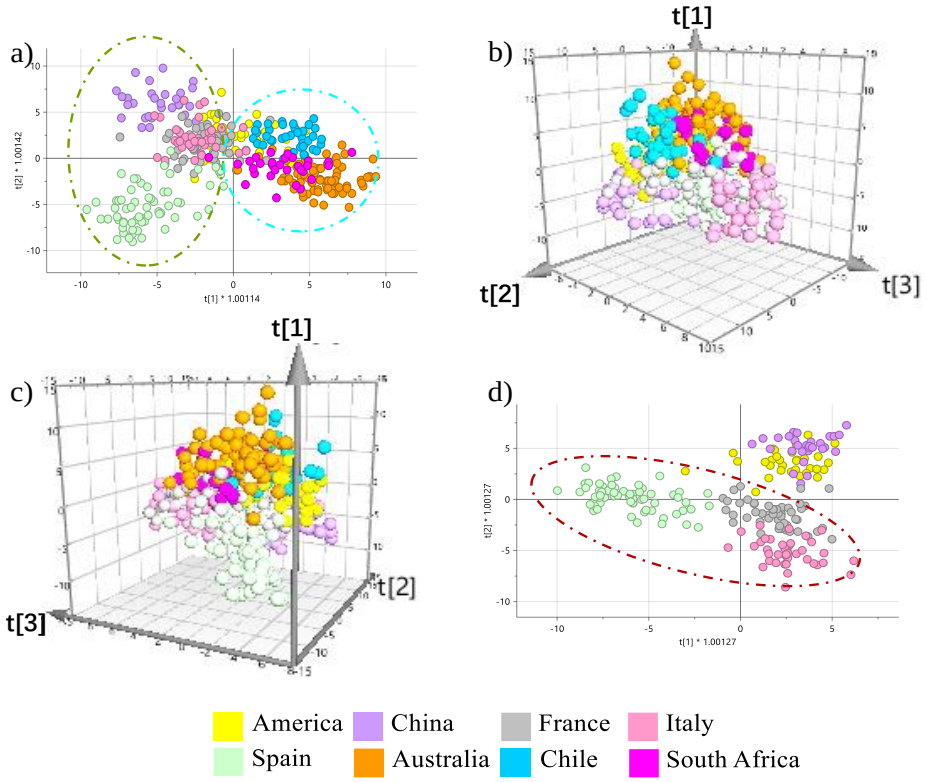

Figure 1-13. OPLS-DA classification of the wine samples for differentiation of a) eight countries, the relative 3D score curves of the model b) the front and c) the back, and d) OPLS-DA for countries from the northern hemisphere based on the MALDI-MS results.

In this case, wine classification could be accomplished step by step. As discussed above, the differences between the two hemispheres were found to be more significant than those among eight countries, and thus model M1 was first established to separate the two hemispheres. Two other models (M2 and M3) were carried out to discriminate countries in the northern hemisphere and southern hemisphere, respectively, with Spain, Italy and France as a whole (labeled as Europe). Model M4 was ultimately conducted to distinguish three European countries.

Optimal four OPLS-DA models were subsequently generated, and the separations were significantly improved. It was found that two hemispheres were located at two different sides of the x-axial, with some spots overlapped near zero (Figure 1-14a). In Figure 1-14b and Figure 1-14c, South Africa lied on the upper side of the plot, and Chile and Australia were separated along the t[1] axis, which were located at the negative and positive sides, respectively. Europe, America and China showed similar trends, with Europe at the center left of the plot, China at the right and America at the upper side. Three European countries were subsequently distributed in Figure 1-14d, where along the t[1] axis direction, Spain on the left side could be separated from another two on the right side, furthermore, France and Italy were separated in the t[2] direction.

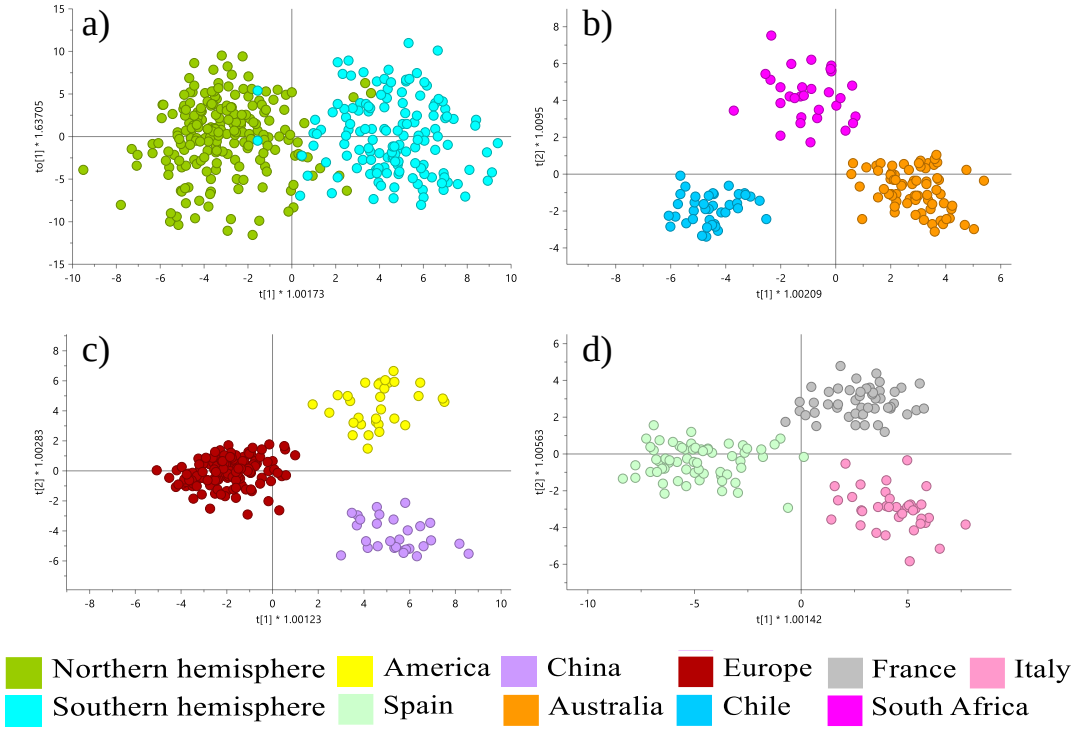

Figure 1-14. OPLS-DA classification of the wine samples for differentiating a) the two hemispheres, b) countries from the southern hemisphere, c) countries from the northern hemisphere with Spain, Italy and France as a whole (Europe), and d) three European countries based on the MALDI-MS results.

1.3.1.5 Review and validation of the established OPLS-DA models

To review four models, both the fitting ability and predictive ability were displayed in Table 1-5. Notably, the R^2Y values were all larger than 0.78 but lower than 0.87, and the Q^2 values were between 0.66 and 0.75, suggesting that they were good but not excellent models. The good results of the permutation plot with 200 numbers further indicated that there was no overfitting (Figure 1-15), as all Q^2 values（left）were lower than the original points (right), and the regression line for Q^2 points intersected the left vertical axis at zero or below.

The classification results of the calibration set were shown in Table 1-6, where the general correct rates of M1-M1 were 96.61%, 100%, 100% and 99.3%, respectively. In more detail, using the aforementioned four OPLS-DA models, the correct classification rates were as high as 100% for 7 countries and 98.4% for Spain, illustrating the good establishment of the models.

The established models were then applied to classify the external validation samples. The general correct rates of the validation set were shown in Table 1-6, respectively. The prediction results of 7 countries were over 81.3%, with Spain and South Africa displaying the highest two at 90.3% and 88.2% respectively. The exception was the samples from Italy, for which the model gave 68.4% discrimination accuracy merely, and this was consistent with the previous study[31]. It can be observed from Table 1-7 that the mis-assigned samples (25 out of 95) were primarily grouped to Spain, suggesting that there might be some similarities between the wines from two countries, and studies have shown that they had similar contents of titratable acidity and proportions of volatile compounds[73, 74].

As illustrated in Figure 1-16, the ROC of four models all made an upward bend with TPR>FPR, which indicated AUC values were over 0.5. The precision, accuracy and area AUC values were then calculated to evaluate the four OPLS-DA models for distinguishing the wine samples (Table 1-8). Precisions ranging from 68.4% to 92.9%, accuracies of all above 85.9%, and AUC values of all exceeding 0.796 and even up to 1.000 were obtained, proving the practicality of the established OPLS-DA models. Overall, the wine samples from different counties could be discriminated well using the method of MALDI-MS coupled with OPLS-DA.

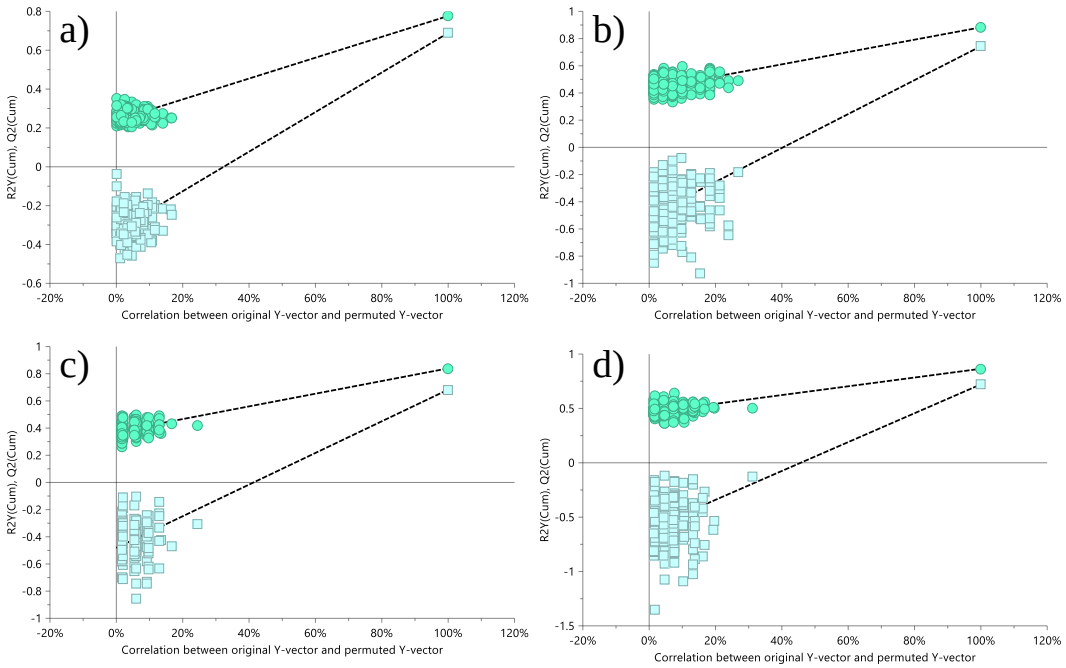

Figure 1-15. Permutation plots with 200 numbers for M1-M4.

Table 1-5. The statistical parameters of OPLS-DA models obtained by MALDI-MS.

Technique	Models	$R^2Y(cum)$	$Q^2(cum)$
MALDI-MS	M1	0.78	0.69
	M2	0.87	0.73
	M3	0.86	0.75
	M4	0.86	0.66

Table 1-6. The overall correct classification rates (%) of the OPLS-DA models by MALDI-MS.

	Calibration	Validation
M1	96.9	91.2
M2	100.0	86.3
M3	100.0	90.7
M4	99.3	82.1
America	100.0	81.3
China	100.0	85.7
France	100.0	82.1
Italy	100.0	68.4
Spain	98.4	90.3
Australia	100.0	86.5
Chile	100.0	84.2
South Africa	100.0	88.2

Table 1-7. The classification results of the validation set using M1-M4.

Countries	No.	France	Italy	Spain	Australia	Chile	South Africa	America	China	Europe
France	28	23	0	5	/	/	/	/	/	/
Italy	19	4	13	2	/	/	/	/	/	/
Spain	31	2	1	28	/	/	/	/	/	/
Australia	37	/	/	/	32	1	4	/	/	/
Chile	19	/	/	/	3	16	0	/	/	/
South Africa	17	/	/	/	2	0	15	/	/	/
America	16	/	/	/	/	/	/	13	2	1
China	14	/	/	/	/	/	/	1	12	1
Europe	78	/	/	/	/	/	/	5	0	73

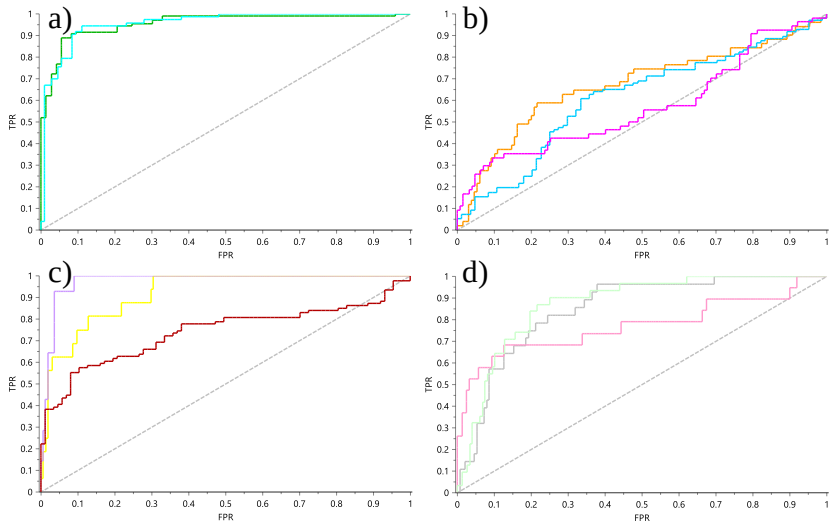

Figure 1-16. Description of receiver operator characteristic (ROC) curve of M1-M4.

Table 1-8. Summary of the predictive quality acquired by the four OPLS-DA models by MALDI-MS.

Country	Precision	Accuracy	AUC
America	68.4%	91.7%	0.973
China	85.7%	96.3%	0.968
France	79.3%	85.9%	0.850
Italy	92.9%	91.0%	0.772
Spain	80.0%	87.2%	0.872
Australia	86.5%	86.3%	0.796
Chile	94.1%	94.5%	0.809
South Africa	78.9%	91.8%	0.883

1.3.2 Rapid authentication of red wine by DART-MS

1.3.2.1 Optimization of sample preparation and semi-automatic data acquisition

The preparation of the samples was very straightforward as DART-MS is capable of directly detecting the samples. Here, we only treated wine samples by adding 2% ammonium acetate to enhance the signal. Although DART-MS is not as efficient as MALDI-MS in terms of high throughput and automaticity, the 1-D transmission module loaded with a mesh sampling trip allowed for semi-automatic data acquisition. The 5 replicates were analyzed at a time, taking less than 3 min. Various parameters, including working gas type, gas flow and temperature, sampling speed, matrix effect, dopant selection, sampling method and the distance between ion source outlet and mass spectrometer inlet, etc, play a crucial role in DART-MS, some of these parameters would be discussed later.

The gas temperature has an impact on the thermal desorption process of the analyte from the sample surface and its ionization. Experimental findings reveal that increasing the gas temperature can enhance the ionization ability of excited helium atoms and the thermal desorption rate of the sample[75], but at the same time, it is necessary to avoid thermal decomposition of the analyte. As displayed in Figure 1-17, a range from 50 ℃ to 300 ℃ was investigated with increments of 50 ℃. The results demonstrate that as gas temperature increased, the abundance initially increased and then decreased. Significantly different spectral results were obtained at temperatures above 250 ℃, mainly due to the decomposition of the analyte. Although the highest abundance occurred at 100 ℃, the relative abundance of other peaks was higher at 150 ℃, which was selected in this study.

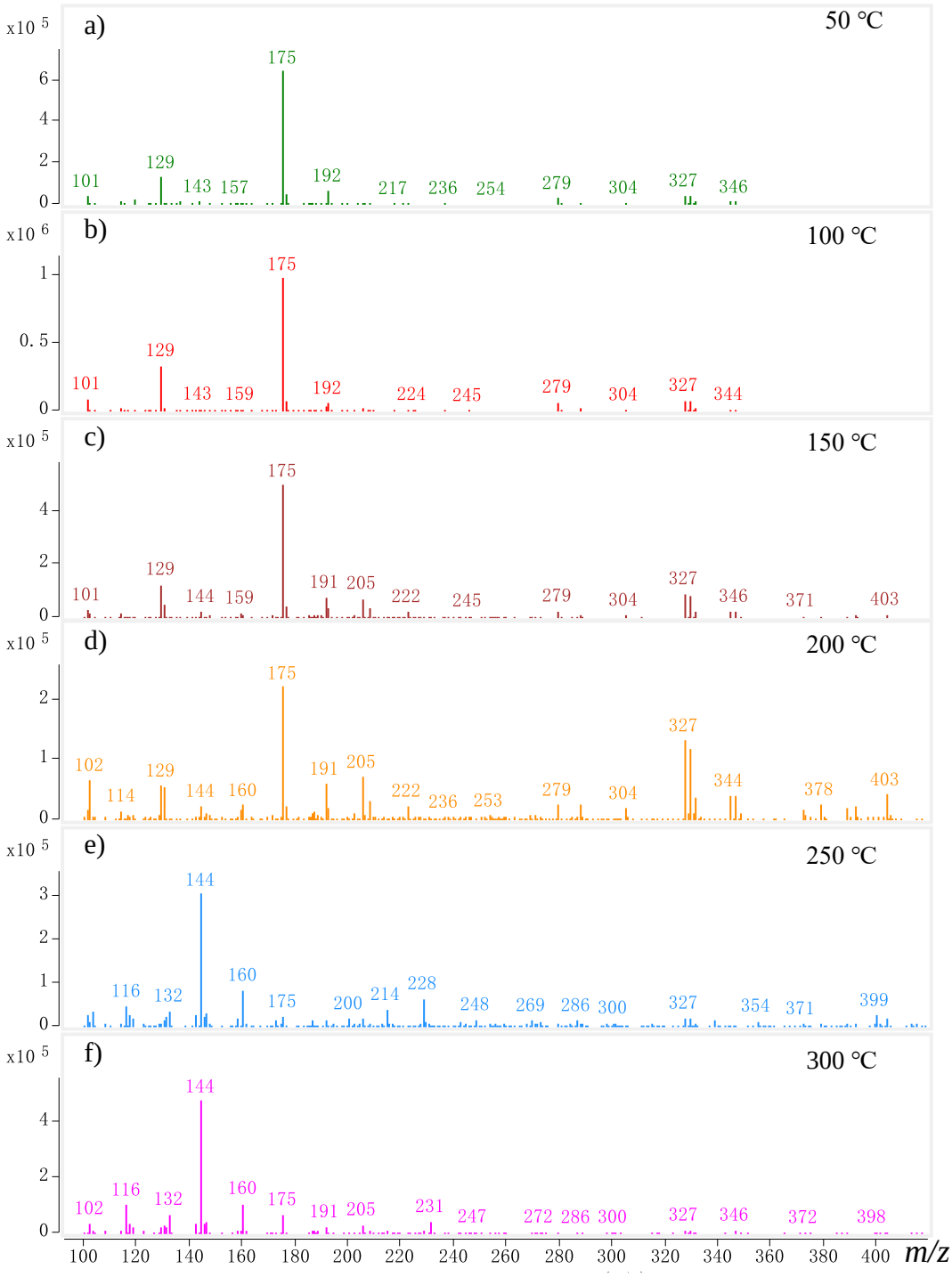

Figure 1-17. Spectra obtained from DART-MS under different gas temperatures.

A common method used for sampling with DART involves mounting a module, for example, a stainless-steel screen, onto a software-controlled rail. This rail sweeps through the desorption/ionization zone, causing the analyte on the sample surface to be thermally desorbed and ionized. The resulting ions enter the mass spectrometer. The speed of the rail is typically controlled between 0.2-10 mm/s[76]. Generally, a slower moving speed allows for more exposure to the ionizing reagent, increasing the likelihood of the analyte colliding with the reagent and improving ionization and detection. However, excessively slow speeds can be time-consuming. To balance efficiency and speed, a rate of 2 mm s^{-1} was employed.

Dopants are volatile additives that are often introduced to form a relatively durable microenvironment and provide sufficient ionizing reagents to further ionize or form adducts with the analyte to improve the detection signal. Ammonium is the most applied one to form adducts of $[M+NH_4]^+$. As illustrated in Figure 1-18, spectra obtained with or without ammonium were obviously different. The introduction of ammonia resulted in significantly improved overall abundance and more detected ions.

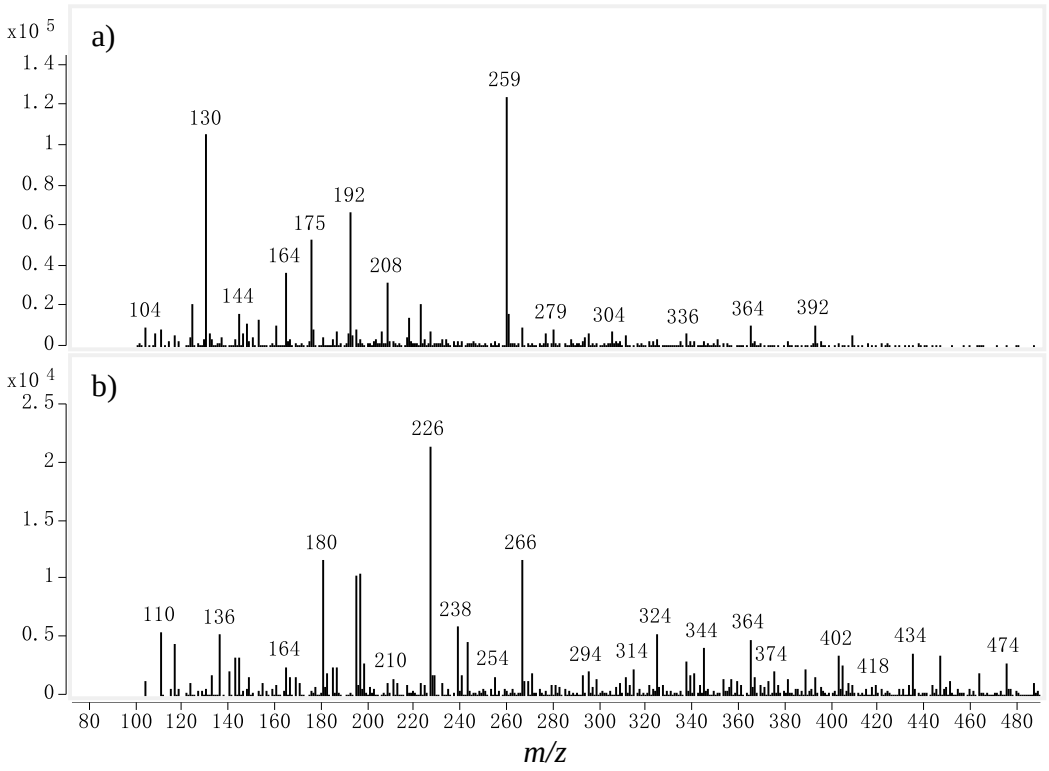

Figure 1-18. Spectra of a wine sample obtained from DART-MS a) without and b) with ammonium acetate added.

Whereas, the repeatability of DART-MS is another crucial concern, as samples are exposed to open air, where water vapor around the ion source can cause high background signals and influence the protonated molecules. 5 replicates of the same sample presented dramatical variation, besides, blank intervals also showed signals from previous loading spots, indicating residual influence. To improve the repeatability, the metal mesh was run multiple times. The spectral results of the second measurements, which were found to offer higher abundances as well as better reproducibility with the optimization study, were used for the data analysis. It could be observed that 5 replicates became highly similar (not shown) and fewer sample signals were shown in the spectra of blank intervals. Though some volatile compounds may be excluded in the second run, the results could be more reliable in data analysis. Hence, two runs were carried out for each sample.

1.3.2.2 Spectral results from DART-MS

DART-MS has been employed in qualitatively detecting specific compounds or residual pesticides in wine[47], but its applications in authentication of wine based on non-targeted analysis have received little attention, particularly at a large scale. A typical spectrum acquired by DART-MS is shown in Figure 1-19. Although a mass range of 100-1000 Da was scanned, nearly no signals were observed over 420 Da, which was in concordance with a previous study[77]. The commonly observed peaks may be related to volatile compounds that contribute to the wine sensory, which are also parameters for grouping wines[78].

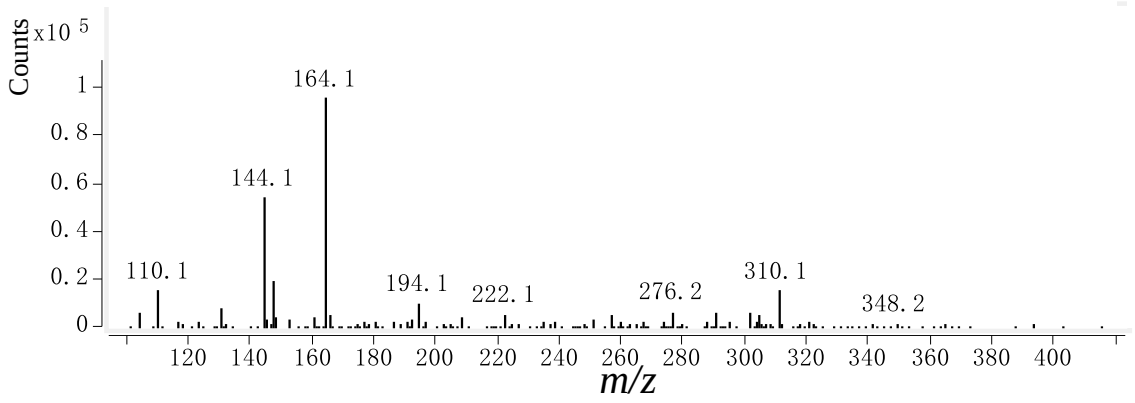

Figure 1-19. A representative spectrum of a sample from France obtained by DART-MS.

1.3.2.3 Establishment of OPLS-DA models for the discrimination of wine origins

The procedures of building 4 optimal OPLS-DA models were applied to the DART-MS results as well, and very similar clustering trends could be observed (Figure 1-20). Except for D4, where the separations of France and Italy were swapped, indicating the different predominant variances from MALDI-MS and DART-MS. Slight separation along the vertical direction was observed in Figure 1-20a, which might be caused by the differences in sample collection, storage and analysis. However, this intra-group difference was much smaller than the inter-group difference and did not affect the discrimination results. Compared with MALDI-MS, worse R^2Y and Q^2 values were obtained by D1, D2 and D3, but better ones were provided by D4 (Table 1-9). The permutation plot with 200 numbers was also measured with good results (Figure 1-21). When the calibration set was classified by the established models, correct classification rates of 78.1%-100% were obtained by DART-MS (Table 1-10), generally lower than those using MALDI-MS. As for the validation group, the correct classification rates were from 64.5% to 100%, with higher ones for the America, France and Italy samples, and lower ones for China, Spain, Australia, Chile and South Africa samples, as compared to the MALDI-MS results. The lowest one was from Spain, and the misassigned samples (15 out of 155) were mainly classified as Italian samples (Table 1-11) further proving our assumption that wines from Spain and Italy are much identical.

Similarly, the ROC of four models as well as other measurements were measured (Figure 1-22, Table 1-12), to evaluate the performance of DA-D4, with 53.6%-100% for precisions, 76.6%-100% for accuracies, and over 0.572 for AUC values. As indicated, there were significant differences between the results obtained by M1-M4 and D1-D4.

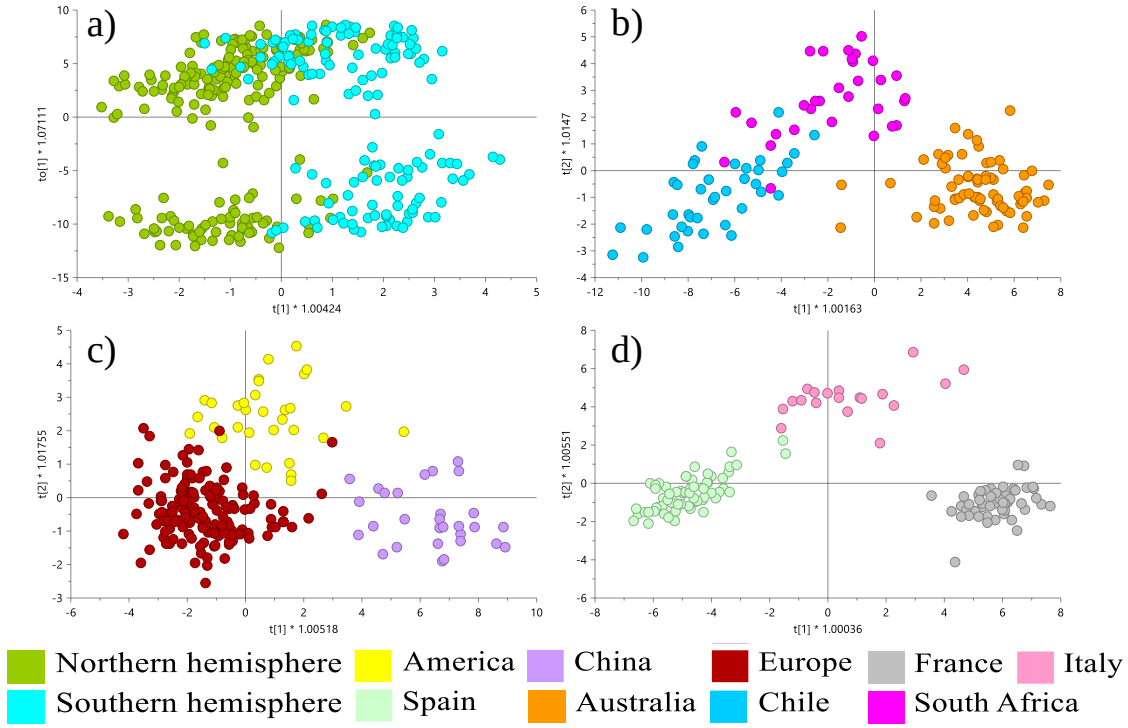

Figure 1-20. OPLS-DA classification of the wine samples for differentiating a) the two hemispheres, b) countries from the southern hemisphere, c) countries from the northern hemisphere with Spain, Italy and France as a whole (Europe), and d) three European countries based on the DART-MS results.

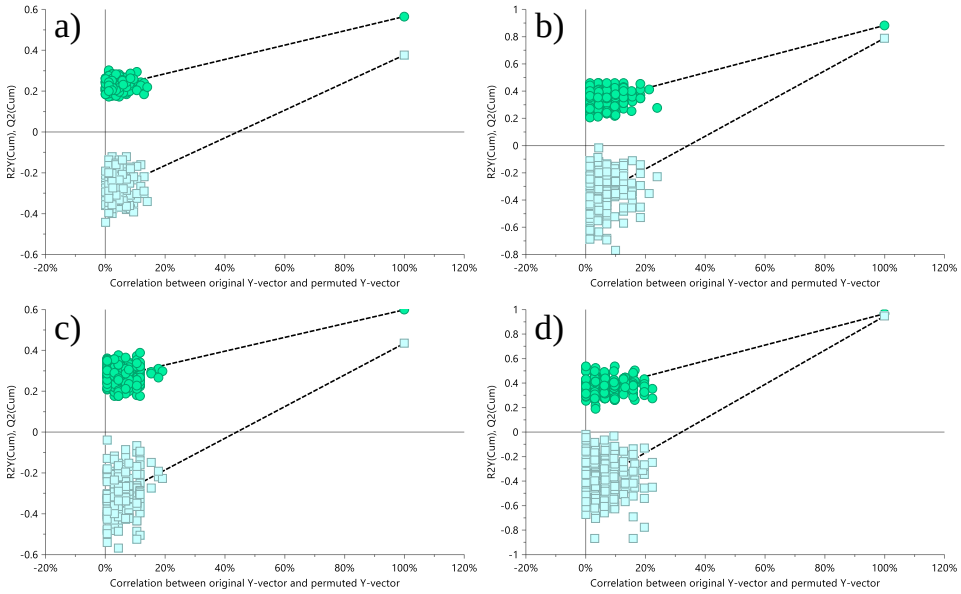

Figure 1-21. Permutation plots with 200 numbers for D1-D4.

Table 1-9. The statistical parameters of OPLS-DA models obtained by DART-MS.

Technique	Models	$R^2Y(cum)$	$Q^2(cum)$
DART-MS	D1	0.57	0.38
	D2	0.76	0.64
	D3	0.71	0.55
	D4	0.89	0.73

Table 1-10. The overall correct classification rates (%) of the OPLS-DA models by DART-MS.

	Calibration	Validation
D1	86.7	70.7
D2	96.5	74.0
D3	95.8	89.8
D4	99.3	83.5
America	78.1	87.5
China	100.0	71.4
France	100.0	100.0
Italy	95.0	84.2
Spain	100.0	64.5
Australia	100.0	75.7
Chile	94.9	79.0
South Africa	90.3	64.7

Table 1-11. The classification results of the validation set using D1-D4.

Countries	No.	France	Italy	Spain	Australia	Chile	South Africa	America	China	Europe
France	28	28	0	0	/	/	/	/	/	/
Italy	19	0	16	3	/	/	/	/	/	/
Spain	31	3	8	20	/	/	/	/	/	/
Australia	37	/	/	/	32	1	4	/	/	/
Chile	19	/	/	/	3	16	0	/	/	/
South Africa	17	/	/	/	2	0	15	/	/	/
America	16	/	/	/	/	/	/	13	2	1
China	14	/	/	/	/	/	/	1	12	1
Europe	78	/	/	/	/	/	/	5	0	73

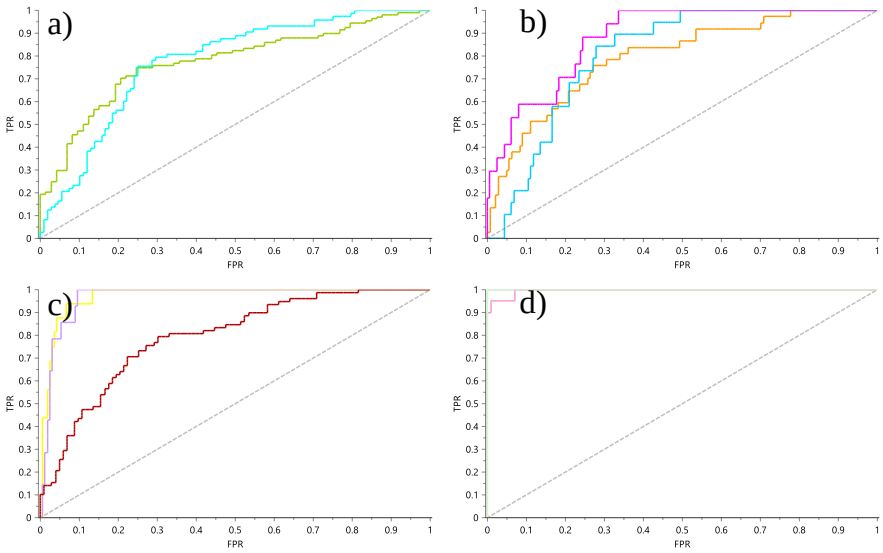

Figure 1-22. Description of receiver operator characteristic (ROC) curve of D1-D4.

Table 1-12. Summary of the predictive quality acquired by the four OPLS-DA models by DART-MS.

Country	Precision	Accuracy	AUC
America	77.8%	94.4%	0.920
China	90.9%	95.4%	0.977
France	90.3%	96.2%	0.998
Italy	66.7%	85.9%	0.914
Spain	89.0%	82.1%	0.889
Australia	100.0%	87.7%	0.671
Chile	53.6%	76.7%	0.611
South Africa	64.7%	83.6%	0.572

1.3.3 Rapid authentication of red wine by MALDI-MS combined with DART-MS

The above results showed that both MALDI-MS and DART-MS were individually applicable in distinguishing original countries of wine on a large and complex scale, yielding barely satisfactory prediction results, underscoring that compounds in wine have a specific relationship with origin. But neither of them was robust enough for unambiguous differentiation of all the countries studied. As mentioned above, MALDI-MS and DART-MS have different ionization mechanisms and favor different types of molecules. MALDI-MS underlined a mass range from 380 Da to 1000 Da in this study, mainly for the detection of anthocyanins and their metabolites, beneficial for characterizing two hemispheres and southern hemispheric countries, but it has limitations in analyzing smaller compounds because of the interferences from the matrix ions. The major mass range of DART-MS is 100-420 Da in this study, and most of the detected compounds were volatiles, showing advantages in determining Northern Hemispheric countries. These indicated the complementary roles of these two analytical techniques in the mass range and detectable compounds for the analysis, suggesting that combining their spectral results in data analysis to screen a wider range of wine compound ions (m/z 100-1000) might be a way to improve the classification results.

1.3.3.1 Data analysis

The use of different techniques for determining different wine features[28, 31] and a combination of NMR and differential sensing array datasets for differentiation of grapevines[79] have been reported. However, combining different MS techniques to distinguish complex wine samples on a large scale has received little attention. A study combining LC-MS and GC-MS to detect non-volatile and volatile components

respectively was developed to distinguish bourbon whiskeys, proving the feasibility of combining two different MS techniques[80]. However, traditionally used LC-MS and GC-MS are time-consuming and labor-intensive. We hypothesize that the direct MS, MALDI-MS and DART-MS, can perform as powerful alternatives.

An approach of combining spectral results from MALDI-MS and DART-MS for wine analysis was for the first time proposed in this study. As described in Figure 1-23, in this approach, the calibration dataset from MALDI-MS was integrated with the calibration dataset from DART-MS with equal contribution to form a new combined dataset and then followed the procedures from step 2 to step 7 in Figure 1-3 for the data analysis. As the intensities of the MALDI-MS spectra did not match with the abundances of the DART-MS spectra, in step 2, the data treatment was conducted within each dataset rather than normalizing them as a whole.

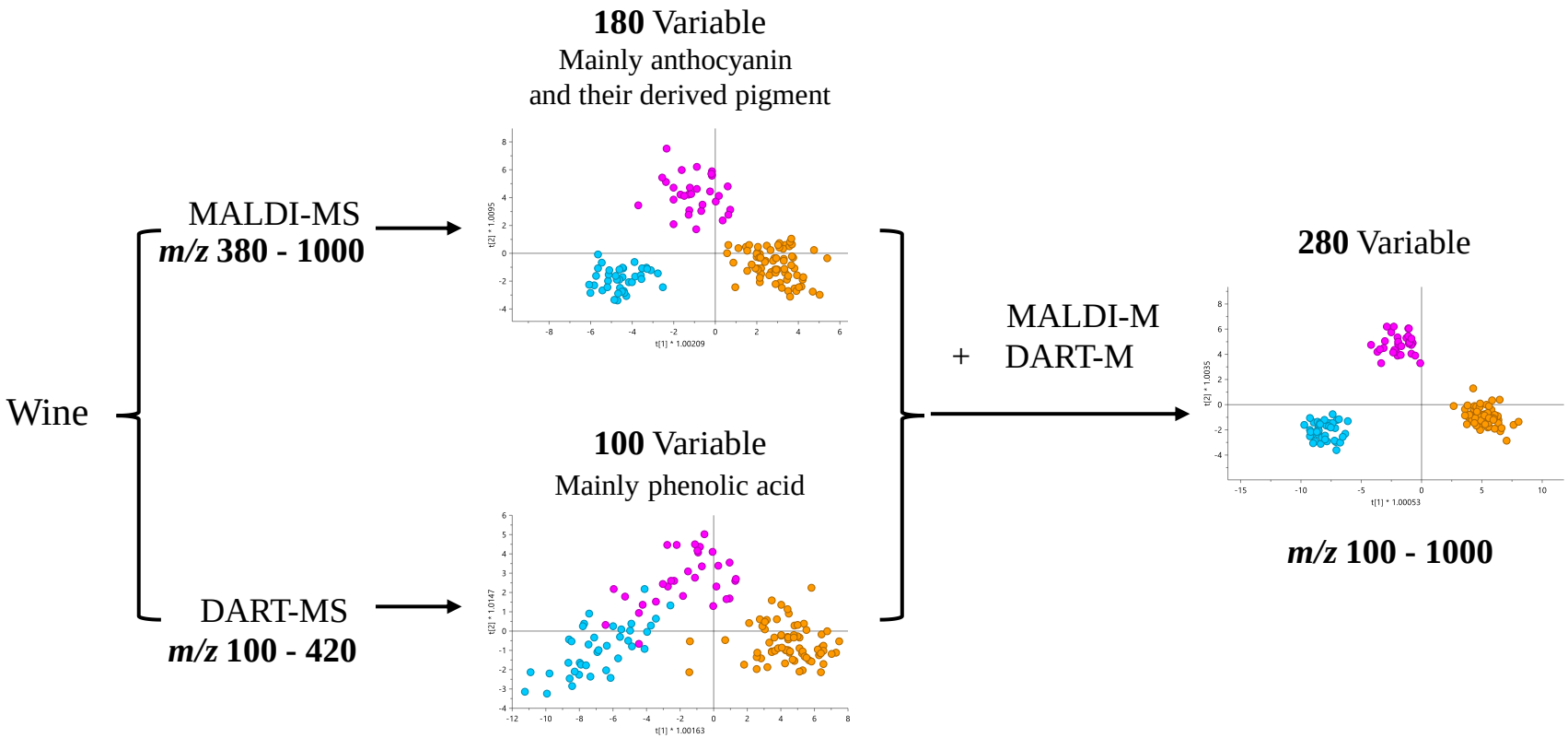

Figure 1-23. Scheme of combining spectra results from MALDI-MS and DART-MS.

1.3.3.2 The improved performance of the OPLS-DA models after the combination

The performance of the OPLS-DA models after the combination was superior to those of the individual ones as shown in Figure 1-24. The trend of separation was just the same as described above, but each group had a clearer cluster and less dispersion. Compared with those with the single techniques, significant increases in both R^2Y and Q^2 values were obtained by the current four models up to 0.95 (Table 1-13, MD1-MD4), implying the reliability and better differentiating ability of the models, which were further verified by the results of the permutation plot with 200 numbers（Figure 1-25）. The calibration set was then employed to review the new models. Notably, the correct classification rates in all countries reached 100.0% (Table 1-14), which was remarkably higher than those obtained by MALDI-MS or DART-MS alone.

The prediction abilities of the established models on external samples were confirmed by the validation set, and the results showed that the validated samples were well matched with the calibration ones as the correct classification rates were typically higher than 90%, with 100% for China and France. The exception was still the samples from Italy, and 6 of 19 samples were misassigned to Spain (Table 1-15), consistent with the previous results. As listed in Table 1-16, better outputs of the precision, accuracy and area under curve (AUC, Figure 1-26) values were achieved using the newly built four OPLS-DA models, with 82.4% to 100% of Precisions, all above 88.5% of accuracies, and all exceeding 0.86 of AUC values, illustrating the feasibility of these established models. These results demonstrated that combining the spectral results of the two complimentary techniques, MALDI-MS and DART-MS, enabled improved results for the differentiation of the wine samples from different countries. For an unknown sample, MD1 can be applied first to determine the hemisphere, and MD2 or

MD3 then for the determination of countries. If it is from European countries, MD4 can be further employed.

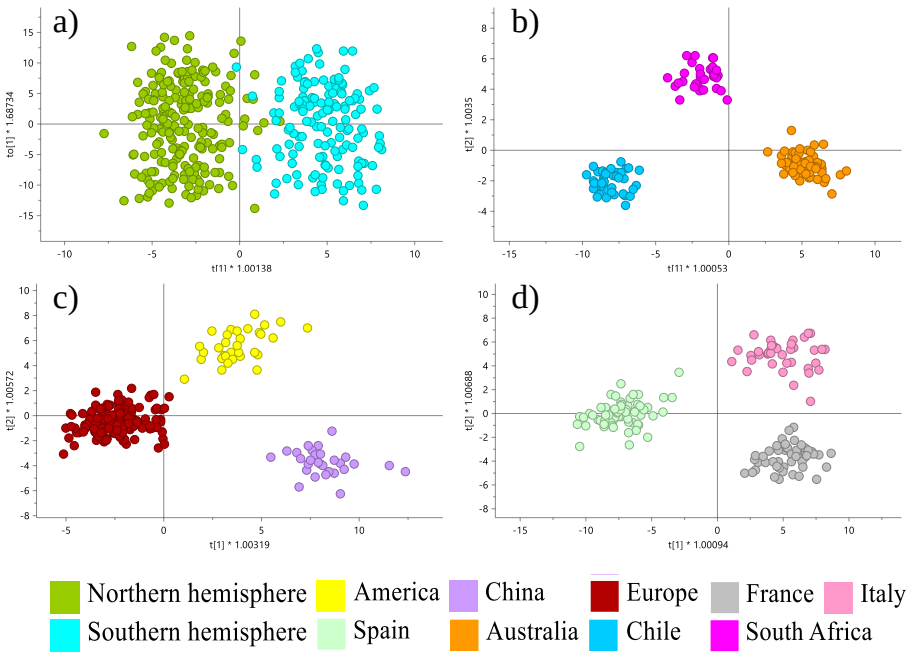

Figure 1-24. OPLS-DA classification of the wine samples for differentiating the two hemispheres, countries from the southern hemisphere, countries from the northern hemisphere with Spain, Italy and France as a whole (Europe), and three European countries based on the MALDI-MS+DART-MS results (a-d).

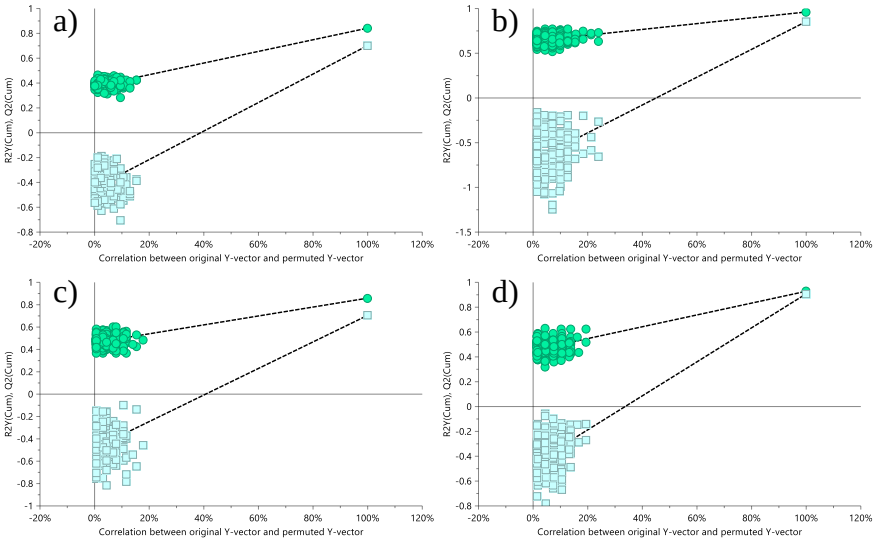

Figure 1-25. Permutation plots with 200 numbers for MD1-MD4.

Table 1-13. The statistical parameters of OPLS-DA models obtained by MALDI-MS+DART-MS.

Technique	Models	$R^2Y(cum)$	$Q^2(cum)$
MALDI-MS +DART-MS	MD1	0.84	0.70
	MD2	0.95	0.83
	MD3	0.89	0.77
	MD4	0.92	0.84

Table 1-14. The overall correct classification rates (%) of the OPLS-DA models by MALDI-MS+DART-MS.

	Calibration	Validation
MD1	98.3	89.0
MD2	100.0	93.2
MD3	100.0	96.3
MD4	100.0	88.5
America	100.0	93.8
China	100.0	100.0
France	100.0	100.0
Italy	100.0	68.4
Spain	100.0	90.3
Australia	100.0	91.9
Chile	100.0	94.7
South Africa	100.0	94.1

Table 1-15. The classification results of the validation set using MD1-MD4.

Countries	No.	France	Italy	Spain	Australia	Chile	South Africa	America	China	Europe
France	28	28	0	0	/	/	/	/	/	/
Italy	19	0	13	6	/	/	/	/	/	/
Spain	31	2	1	28	/	/	/	/	/	/
Australia	37	/	/	/	32	1	4	/	/	/
Chile	19	/	/	/	3	16	0	/	/	/
South Africa	17	/	/	/	2	0	15	/	/	/
America	16	/	/	/	/	/	/	13	2	1
China	14	/	/	/	/	/	/	1	12	1
Europe	78	/	/	/	/	/	/	5	0	73

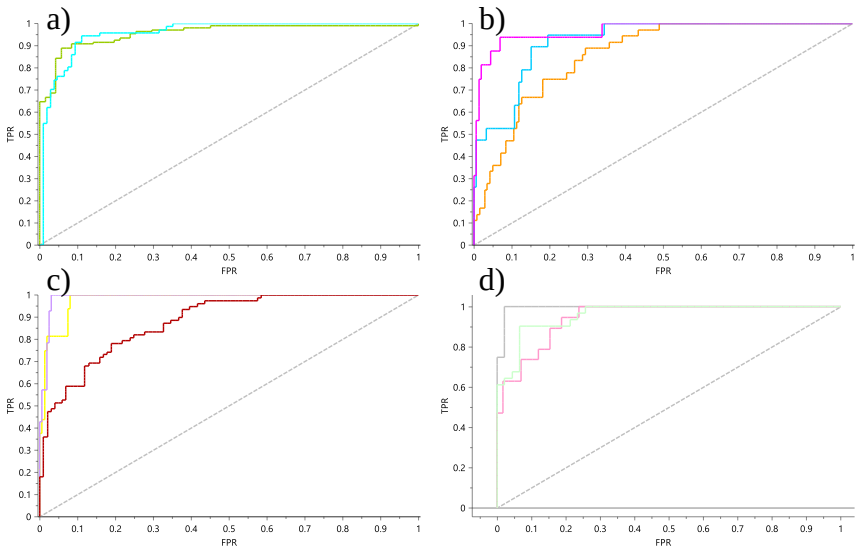

Figure 1-26. Description of receiver operator characteristic (ROC) curve of MD1-MD4.

Table 1-16. Summary of the predictive quality acquired by MD1-MD4.

Country	Precision	Accuracy	AUC
America	83.3%	96.3%	0.980
China	93.3%	99.1%	0.990
France	93.3%	97.4%	0.995
Italy	92.9%	91.0%	0.945
Spain	82.4%	88.5%	0.961
Australia	97.1%	94.5%	0.862
Chile	90.0%	95.9%	0.923
South Africa	88.9%	95.9%	0.967

1.3.3.3 Potential characteristic markers of the eight countries

Different compositions in red wine have been proven to be related to their origins[81, 82]. Therefore, it is important to find out the characteristic markers that have the greatest impact on country discrimination. As shown in Table 1-17, a total of 26 marker ions were selected by applying VIP value > 1.2 together with *p* value < 0.05. The majority of these marker ions were of too low intensities for conducting MS/MS, and the identities of some marker ions were tentatively assigned based on their mass-to-charge ratios and relevant literature (Table 1-18). These assigned compounds were typically phenols and volatiles, which are most involved in the wine sensory evaluation. The remaining unknown ones might be metabolites and secondary metabolites produced during fermentation and storage. When looking into the relative intensities/abundances, it was found that some markers were country-characteristic, such as *m/z* 144 was higher in Chinese wines, and *m/z* 116 was significantly lower in Australia wines compared with that in Chile and South Africa. The relative abundances of ions *m/z* 110 and *m/z* 194 for France wines were almost twice as high as for Italy and Spain wines. These may provide an easy and improved method for wine authentication for future studies, the identification of which needs to be done with improved intensity.

Table 1-17. Potential wine marker ions obtained by MALDI-MS+DART-MS coupled with OPLS-DA models.

Model	**Marker ions (Da)** (VIP value > 1.2, *p* value < 0.05)
MD2	352.3, 414, 446, 447, 448, 581, 609, 610, 625, 626, 867
MD3	458, 606, 720, 721, 722, 773, 896
MD4	129, 159, 194, 202, 219, 250, 256, 280

Table 1-18. Potential markers that were tentatively assigned.

Detected mass (Da)	Markers	Remark
194	Phenylacetylglycine	$[M + H]^+$ (DART-MS)
219	Tyrosol 4-sulfate	$[M + H]^+$ (DART-MS)
250	Vanillin 4-sulfate	$[M + NH_4]^+$ (DART-MS)
280	Dihydrocaffeic acid 3-sulfate	$[M + NH_4]^+$ (DART-MS)
446	Fragment ion of derivatized resveratrol	$[M]^+$(MALDI-MS)
447	Fragment ion of anthocyanins	$[M]^+$(MALDI-MS)
448	Kaempferol-3-O-glucoside	$[M]^+$(MALDI-MS)
581	Delphinidin 3-glucoside 4-vinyphenol adduct	$[M]^+$(MALDI-MS)
609	Malvidin 3-O-glucoside 4-vinyl phenol	$[M]^+$(MALDI-MS)
610	Quercetin-3-O-rutinoside	$[M]^+$(MALDI-MS)
625	Peonidin-3-O-caffeoylglucoside	$[M]^+$(MALDI-MS)
720	Malvidin procyanidins	$[M]^+$(MALDI-MS)
722	Fumonisins B_1	$[M]^+$(MALDI-MS)
867	Procyanidin C1	$[M]^+$(MALDI-MS)
773	Delphinidin-3-glucoside-coumarate-5-glucoside	$[M]^+$(MALDI-MS)

1.3.3.4 OPLS-DA models for every two countries

From three series of models, an interesting observation is that when the number of countries interpreted in one model decreased, R^2Y, Q^2 and classification rates got higher, signifying that supervised OPLS-DA might perform better for the discrimination of fewer classes. It is more difficult to separate larger groups as different grape varieties, vintages and brands introduced complex within-group variations that complicated the analysis. Compared to previous studies that focused on simple samples or small groups, one of the major advantages of this study is that multiple classes of wines could be distinguished. In addition to the previously mentioned 4 models, we also attempted to build another 28 OPLS-DA models for every two countries (Figure 1-27), and it was found to allow enhanced differentiation as compared to those containing more than two countries. As shown in Table 1-19, every two countries were well distinguished with higher R^2 and Q^2 values. Among them, 19 models showed excellent correct classification rates of over 95.0% for the validation sets, with 12 models exhibiting 100%, which was better than that using 4 models. Furthermore, the classification of Italian samples also gained significant improvement with total correct classification rates varying from 90.9% to 100% when discriminated with other countries (Table 1-19, Models 3, 9, 14, 20, 21 and 22). Still, it was 84% when distinguished from Spain (Figure 1-27, Model 19), further suggesting that the wine samples from these two countries were similar. However, testing an unknown sample using 28 models one by one is incredibly time-consuming. Consequently, as the overall predictive ability is remarkable enough, 4 models are still applied in this study. These 28 models can be used as a complement to figure out confusing samples or to rapidly determine whether a sample belongs to country A or country B.

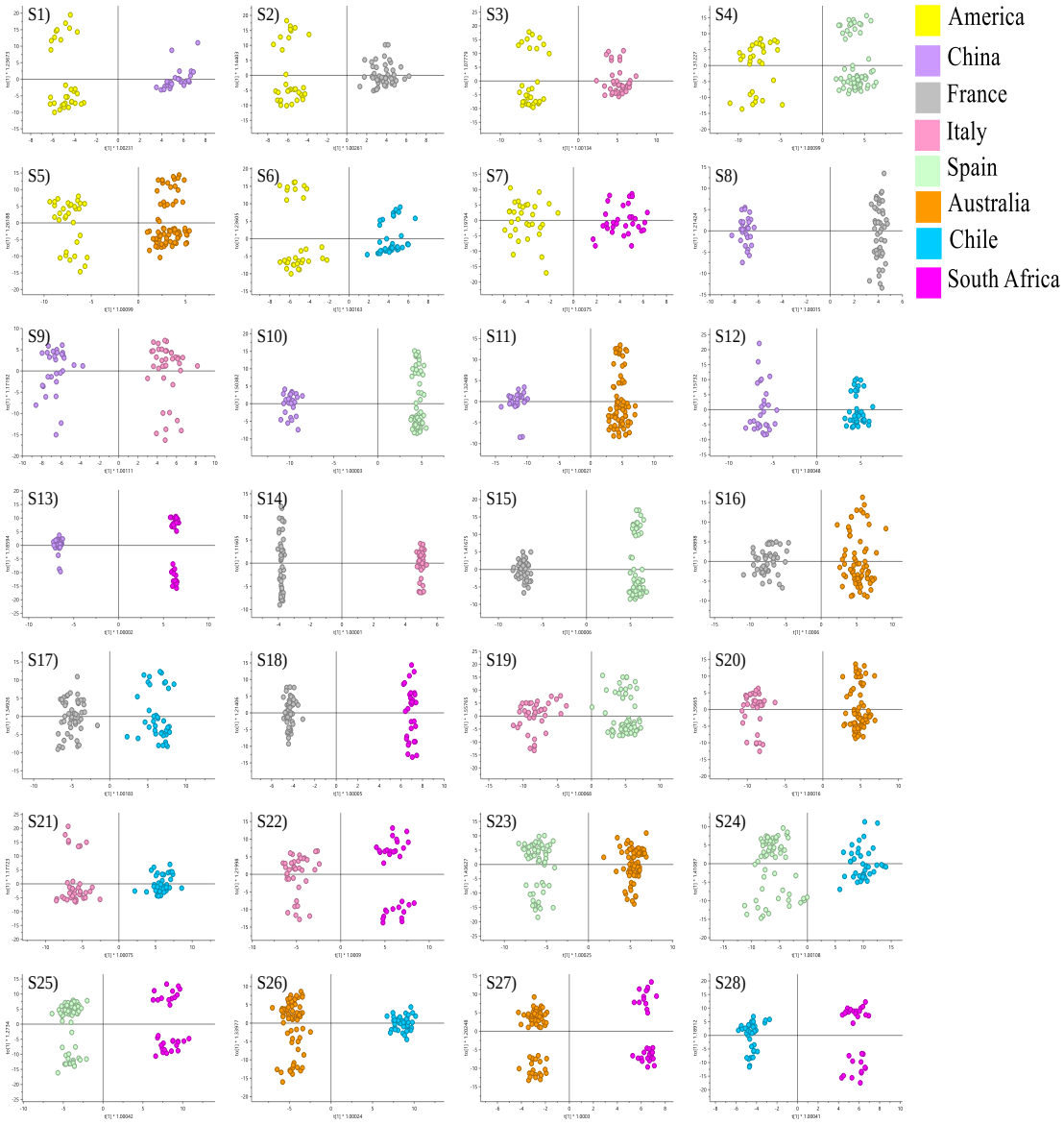

Figure 1-27. OPLS-DA classification of wines for every two countries by MALDI-MS+DART-MS.

Table 1-19. Performance of the 28 OPLS-DA models for discrimination of every two countries.

Model	$R^2Y(cum)$	$Q^2(cum)$	Correct (%)
1	0.97	0.93	93.3
2	0.96	0.83	100.0
3	0.97	0.93	94.3
4	0.96	0.87	95.7
5	0.95	0.77	94.3
6	0.95	0.82	100.0
7	0.92	0.79	100.0
8	1.00	0.96	100.0
9	0.97	0.94	90.9
10	1.00	0.90	100.0
11	0.98	0.95	100.0
12	0.98	0.93	93.9
13	1.00	0.94	100.0
14	1.00	0.95	100.0
15	1.00	0.96	94.9
16	0.96	0.86	96.9
17	0.96	0.87	95.7
18	1.00	0.96	100.0
19	0.96	0.84	86.0
20	0.98	0.92	100.0
21	0.96	0.91	94.7
22	0.96	0.86	97.2
23	0.98	0.88	94.1
24	0.93	0.85	98.0
25	0.97	0.86	100.0
26	0.98	0.91	98.2
27	0.99	0.84	96.3
28	0.98	0.90	100.0

1.3.3.5 OPLS-DA models for other features

Origin, vintage year and grape variety are known to affect the flavor of a wine. Since the country is a dominant feature for the wine samples collected in this study, the distinction among countries is easier to achieve. The vintage year holds significant significance for both wine enthusiasts and investors. It serves as a fundamental benchmark for determining the quality and attributes of a wine. Various meteorological elements during a particular year contribute to the distinct characteristics of wines. It is widely acknowledged that wines produced in specific years can possess exceptional value, as favorable weather conditions result in a distinctive flavor profile for red wines. Additionally, wines may also gain prestige when the yield for a particular year is low.

To demonstrate the further potential of our approach, we also tried to distinguish the vintages. The vintages of the collected wines spanned a wide range, from 1999 to 2014, while sample numbers for most years were insufficient for the collected samples. Since larger vintage differences allowed better differentiation[83], in this study, instead of grouping by specific years, we roughly divided samples into three groups according to their aging time: the young group (vintage year after 2010), the aged group (vintage year between 2008-2010) and the old group (vintage year before 2008). Supervised OPLS-DA models were performed to characterize three groups within each country. Though clear separation between the young group and the old group showed the potential of the method for the distinction, their overlapping with the aged group was observed (Figure 1-28), indicating that close vintages were difficult to discriminate. Therefore, the aged group was temporarily excluded, and the OPLS-DA models were built based on the young group and the old group. As shown in Figure 1-29, it could be discovered that the two groups exhibited good separation in most countries, with R^2 and

Q^2 values over 0.5 and even close to 1.0 (Table 1-22), while the Spain samples showed exceptionally low performance, which needs further investigation, and not enough samples of the old group from Chile were obtained for the investigation. The correct classification rates of America, Australia, China, France, Italy and South Africa all reached 100%, and 81.4% of Spanish samples were correctly classified (Table 1-21), illustrating the approach was also applicable to the differentiation of wine years.

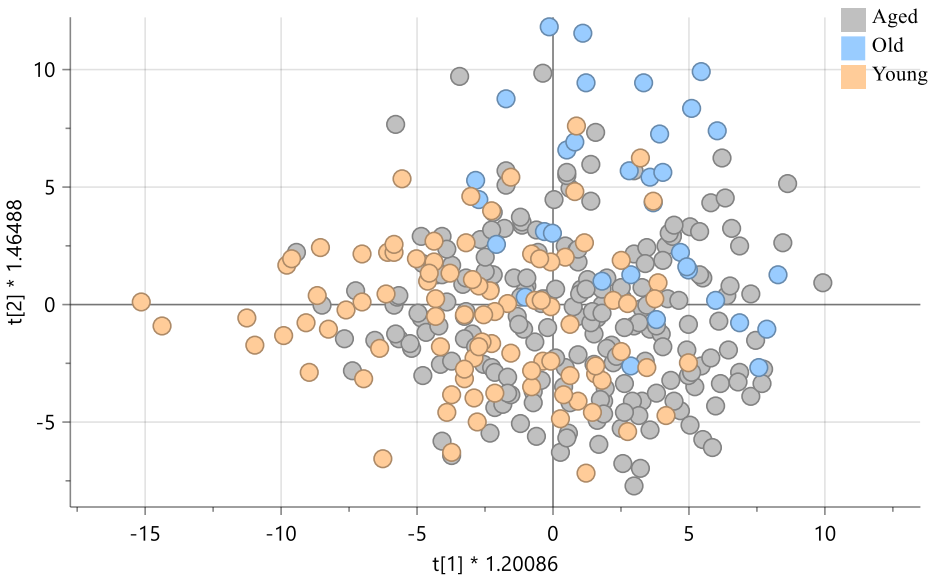

Figure 1-28. OPLS-DA classification of three different vintage groups.

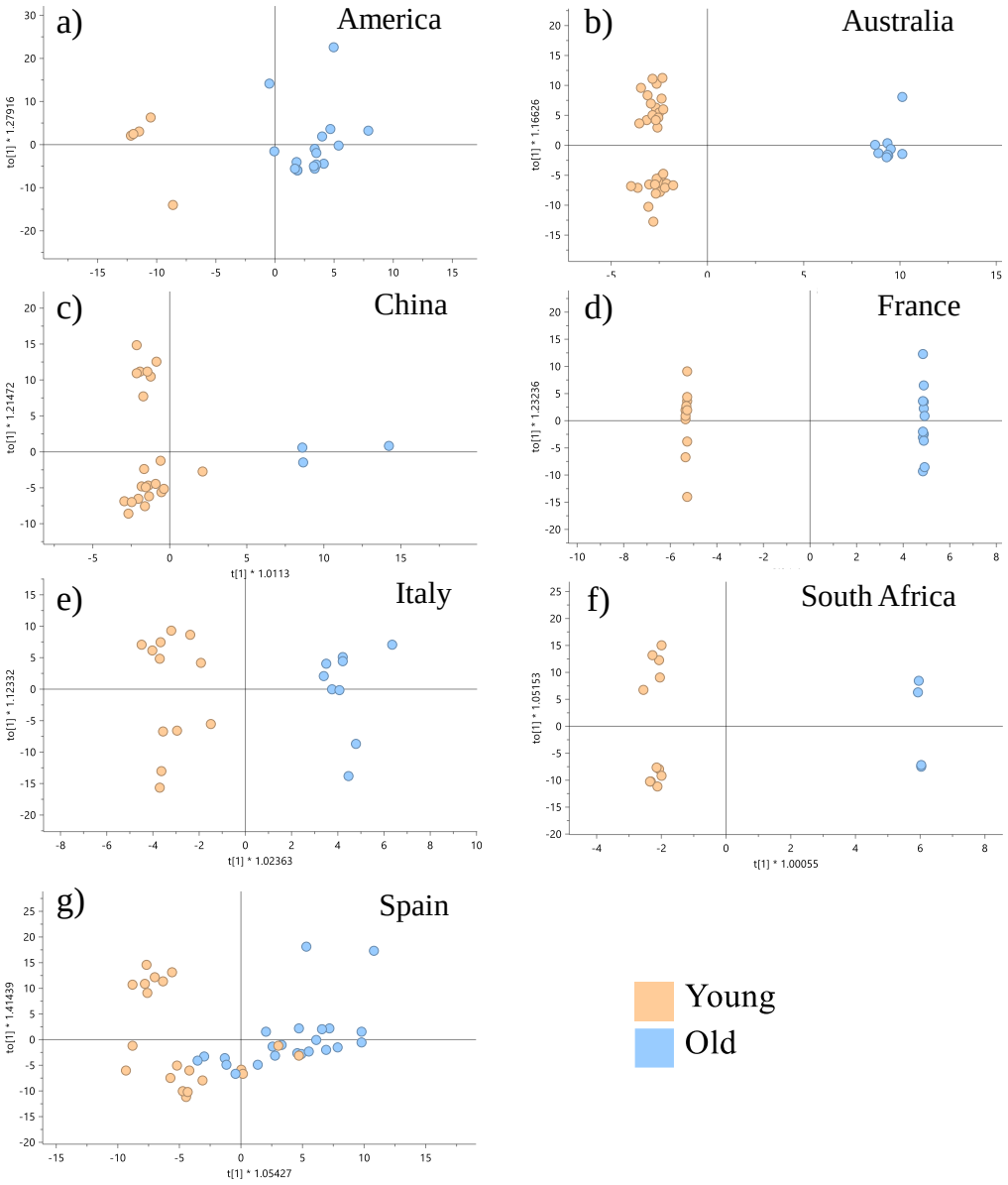

Figure 1-29. OPLS-DA classification of the young group and the old group from different countries.

Table 1-20. Performance of the OPLS-DA models for discrimination of vintage years.

Feature		America	Australia	China	Spain	France	Italy	Chile	South Africa
Vintage year	R^2Y(cum)	0.91	0.99	0.90	0.55	1.00	0.95	NA	1.00
	Q^2(cum)	0.51	0.88	0.51	0.16	0.77	0.53	NA	0.51

Table 1-21. The overall correct classification rates (%) of the young group and the old group from different countries using the combined OPLS-DA models.

Country	Correct (%)
America	100.0
Australia	100.0
China	100.0
France	100.0
Italy	100.0
South Africa	100.0
Spain	81.4

Discriminating the grape variety of the wine samples was also attempted by our combined approach. The main grape varieties in this study are Cabernet Sauvignon, Shiraz, Tempranillo, Merlot, Pinot Nior, Carménère, Pinotage and Zinfandel, and other varieties were removed as the numbers were insufficient for multivariate statistical analysis. When all data sets were taken into account, no clear discrimination of wines was observed. Subsequently, three OPLS-DA models were constructed according to the trend of each variety clustered in the scattering plot, which showed distinct clustering (Figure 1-30). The correct classification rates of the 8 varieties ranged from 82.8%-100% for the calibration set, with an average rate as good as 91.8% (Table 1-23), and more validation samples are needed to further verify the three models. These preliminary results demonstrate the ability of the approach to distinguish vintages and grape varieties, which, however, still needs further validation with unknown samples. Improved performance can be also expected with a larger number of representative samples for each variety or each year, and more investigations can be explored to develop classification models that cover all the features, and even for the identification of diluted, adulterated and mislabeling wines.

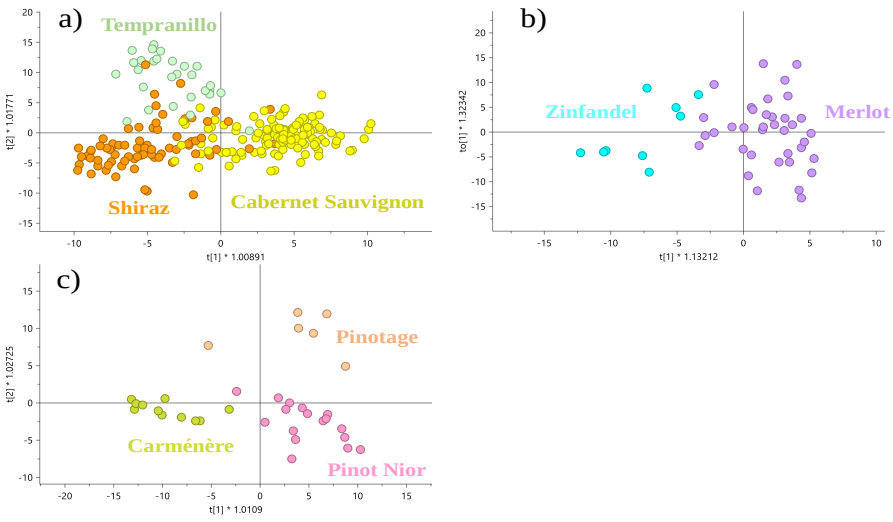

Figure 1-30. OPLS-DA classification of grape varieties from a) Cabernet Sauvignon, Shiraz and Tempranillo, b) Zinfandel and Merlot and c) Pinot Nior, Carménère and Pinotage.

Table 1-22. Performance of the OPLS-DA models for discrimination of grape varieties.

Feature		Cabernet Sauvignon, Shiraz and Tempranillo	Zinfandel and Merlot	Pinot Nior, Carménère and Pinotage
Grape variety	$R^2Y(cum)$	0.63	0.69	0.79
	$Q^2(cum)$	0.52	0.46	0.62

Table 1-23. The correct classification rates (%) of grape varieties using the combined OPLS-DA models.

Variety	Correct (%)
Cabernet Sauvignon	93.2
Shiraz	85.3
Tempranillo	82.8
Pinot Nior	94.1
Carménère	100.0
Pinotage	100.0
Zinfandel	88.9
Merlot	100.0
Overall	91.8

1.4 Conclusions

Authentication of commercial wine is significantly important, due to the economic and cultural values. In this study, 535 red wines with large variations were collected and investigated with MALDI-MS and DART-MS, two direct mass spectrometry methods which require no chromatographic separation. With minimal sample preparation, hundreds of wine samples could be analyzed within hours. Both MALDI-MS and DART-MS were proven to be applicable in the discrimination of wine from different origins, in coupling with OPLS-DA. However, none of them could achieve the perfect classification, showing advantages and disadvantages in classifying different countries. MALDI-MS worked better for hemispheres and northern countries, while DART-MS worked better for southern countries and European countries.

Interestingly, the two techniques were found to work complementarily for wine analysis, with MALDI-MS mainly for the detection of anthocyanin-related analytes and DART-MS for volatile compounds, due to their different ionization mechanisms. Their combination was utilized for the first time in the classification of 535 red wine samples from 8 countries. Combining spectral results from MALDI-MS and DART-MS expanded the chemical profiles and resulted in better fitting and predictive abilities as well as higher correct classification rates, even up to 100% for Chinese and French wines. A total of 26 potential characteristic markers were tentatively selected and some of them were tentatively identified. The approach was also attempted to distinguish

other features such as vintage years and grape varieties, with satisfactory classification results. The combined techniques enabled the analysis of different types of compounds under different ionization conditions, revealing more comprehensive chemical information. The combination of MALDI-MS and DART-MS is typically useful in analyzing both volatile and non-volatile compounds. Considering the overall time and workload demanded, our approach is profound to be a promising alternative to traditional GC-MS or LC-MS methods for wine analysis, because of its simplicity, minimal sample preparation, rapid analysis and high throughput. The thought of combining different types of mass spectrometric techniques and even other analytical techniques can also be extended to other fields for various applications.

Chapter 2. Chiral Recognition of Drugs by Mass Spectrometry

2.1 Introduction

Chirality is of great significance in various fields, such as mathematics, physics, chemistry, and biology. In chemistry, chirality refers to the property of a pair of molecules that are mirror images but non-superimposable on each other, like our left and right hands. These molecules possess at least one asymmetric center that is bonded to four different substituents. In most cases, carbon is typically the center, although sulfur, phosphorus, and nitrogen can also serve as the center[84-86]. The two mirror images are known as enantiomers or optical isomers, and they exhibit different optical activities when polarized light passes through them due to their different spatial arrangements. Many compounds that are important for life, such as amino acids, proteins, enzymes, nucleosides and a great number of alkaloids and hormones, are chiral[87]. The two enantiomers share similar physical and chemical properties, making it extremely challenging to differentiate them. However, molecules containing multiple chiral centers, referred to as diastereomers, can differ more in their physical and chemical properties, which allows for the separation of enantiomers through the introduction of chiral selectors.

Nowadays, chirality has significant implications in plants and animals, as well as in the pharmaceutical industry, and the important role of chiral drug separation has been

strengthened. In academic research, scientists have been recognized with the Nobel Prize for developing asymmetric chiral catalysts to produce specific enantiomer chemicals or drugs[88]. It is estimated that over 80% of the drugs on the market are chiral compounds, and 60% of new drugs approved by the U.S. Food and Drug Administration (FDA) in 2015 were chiral drugs[89]. As required by the FDA, both enantiomers of new drug candidates must undergo biological testing, making the development of optically pure chiral drugs a significant concern. Even though asymmetric synthetic methods have been elaborated for the synthesis of chiral drugs[90-92], these methods can lead to enantiomeric impurities as achieving 100% enantioselectivity is challenging. Therefore, great emphasis has been put on chiral analysis and discrimination.

Though two enantiomers share the same chemical formula, and very similar physical and chemical properties, each enantiomer might differ in biological activity, mechanism, and toxicity when interacting with chiral environments. There are three cases to consider. The first one is that one of the enantiomers is biologically active, and the other is not or is less active. Typically, its substituent functional groups interact with the appropriate binding points of the receptor, inducing advantageous biological effects. In contrast, the inactive enantiomer, due to the different spatial order of the substituent functional groups, cannot bind to the receptor in the same way[87]. Sometimes, this inactive enantiomer may bind to unintended receptors, resulting in toxicity in the body[93, 94]. The second case is that the two enantiomers have the same activity and

pharmacodynamics, such as cyclophosphamide and fluoxetine[87]. The final case is when one enantiomer is biologically active and the other one can be converted in vivo to its biologically active enantiomer by chiral inversion[95]. What really needs to be investigated is the first situation.

L-Dopa is significant for treating Parkinson's disease, however, *D*-Dopa shows grave toxicity towards agranulocytosis[96]. Angiotensin II receptor antagonist valsartan is employed as a single *S*-enantiomer, as it has significantly higher activity[97]. The *R*-isomer is more potent and less toxic than its *S*-antipode. Verapamil acts as a modulator for multidrug resistance in cancer therapy. It has been found to be cardiotoxic, with the *R*-verapamil showing less toxicity than the *S*-verapamil[98]. Tetramisole is a medication used to treat parasitic worm infections, but its d-isomer has great side effects and is no longer used in medicine. Only the (+)-isomer of ascorbic acid (vitamin C) displays redox activity, while its enantiomer is inactive[99]. In pharmaceutical research, it is an important issue to produce or select a useful enantiomer.

2.1.1 Current techniques for the chiral recognition of drug

Well-established advantageous technologies have been developed rapidly, involving chiral high-performance liquid chromatography (HPLC)[100, 101], chiral GC[102, 103], X-ray crystallography, supercritical fluid chromatography (SFC)[104, 105], nuclear magnetic resonance (NMR) spectroscopy[106, 107], and capillary electrophoresis (CE)[108, 109].

By applying the chiral stationary phases (CSPs), it is possible to separate two enantiomers using HPLC. However, there is no single CSPs that is suitable for all enantiomers, which means selecting the right column for this process can be a challenge. X-ray crystallography requires the formation of single crystals and a larger amount of the sample. NMR methods rely on creating diastereomers, which can be identified by NMR parameters. However, it is limited to compounds with suitable functional groups for derivatization. GC methods allow for direct separation of chiral compounds due to their different chemical and physical properties. SFC is increasingly utilized for separating chiral pharmaceuticals. CE, on the other hand, uses chiral selectors (CSs) for separation. However, the potential interference from nonvolatile chiral selectors needs to be considered.

In addition to the aforementioned techniques, MS is a powerful analytical technique that has been applied in various fields, and it has the advantages of high sensitivity, specificity and speed. Generally, it can be divided into two major groups: one involves coupling with other techniques, such as SFC, HPLC, or CE, significantly enhancing the capability to analyze complex samples[110-112]; the other involves direct MS by forming diastereomeric complexes.

2.1.2 Differentiation of chiral drugs by tandem mass spectrometry

Our previous study has demonstrated the feasibility of MS/MS in the discrimination of

chiral drugs, such as *R*- and *S*-Naproxen[113]. The MS/MS method will be used in this study. The two enantiomers show similar chemical and physical properties, making it difficult to distinguish them using MS alone, as chiral compounds produce similar spectra. However, by introducing another chiral compound as a chiral selector, diastereomers with two or more chiral centers can be formed (Figure 2-1). These diastereomeric complexes can have different stability and activation energy barriers, resulting in distinct thermodynamic and kinetic differences. These differences can be magnified or observed by performing MS/MS under collision induced dissociation (CID), and the enantiomers can be distinguished based on the different fragmentation patterns of their diastereomeric complexes. Figure 2-2 shows an example of *R/S*-naproxen, which could not be differentiated by MS directly. However, after introducing histidine (*L*-His) as the chiral selector, the formed diastereomers (*L*-His+*R*-naproxen and *L*-His+*S*-naproxen) resulted in different MS/MS spectral patterns, where the intensity ratio of the product ion (*m/z* 388.97) to the precursor ion (*m/z* 663.06) obtained from *L*-His+*R*-naproxen was higher than that from *L*-His+*S*-naproxen.

The interactions between analytes and chiral selectors can be either covalent or non-covalent. Covalent interactions are typically stronger and non-reversible, requiring complex chemical reactions. Non-covalent interactions[114], varying from weak to strong, aremore commonly applied. In many cases, metal ions are introduced to enhance the interactions. The chiral recognition process involves the formation of complexes

between the enantiomers and chiral selectors, either with or without metal ions. These complexes can form dimers, trimers, tetramers, or even octamers with multiple chiral centers[115]. By using MS/MS, the two complexes can produce different spectral patterns under the same CID value, allowing for measurement using chiral recognition methods.

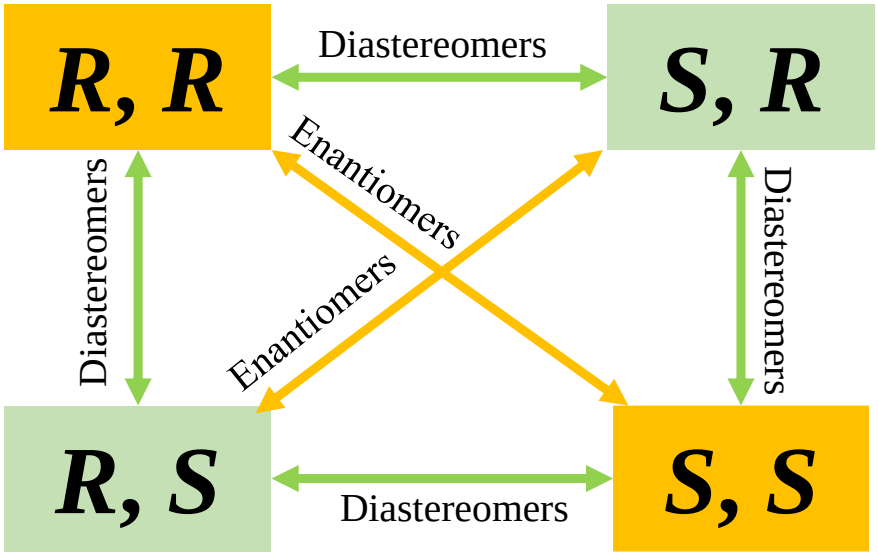

Figure 2-1. Difference between enantiomers and diastereomers.

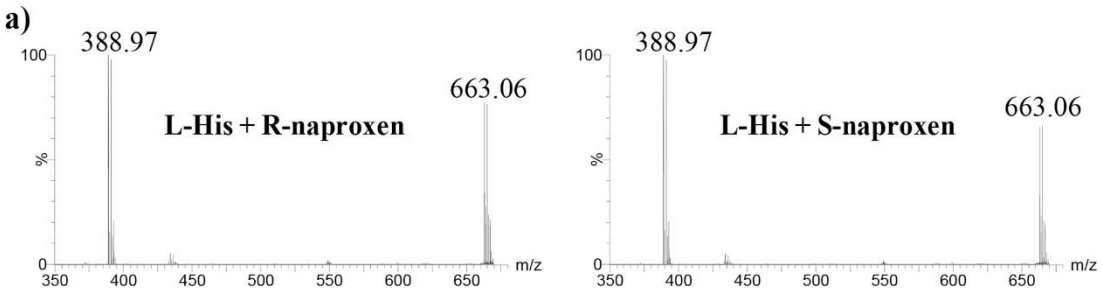

Figure 2-2. The CID spectra of $[(Cu(II))_2(R/S\text{-naproxen})(L\text{-His})_2-3H]^+$.[113]

2.1.3 Chiral recognition methods

There are two major methods for chiral recognition: the kinetic method (KM) and the chiral-recognition method (CR). The KM, pioneered by Cooks and Kruger[116] has been extensively applied in the differentiation of enantiomers such as amino acids and monosaccharides, quantified using R_{chiral}. The further the R_{chiral} value deviates from unity, the more effective the chiral differentiation. Yao et al.[117] in 1999 developed the CR method for chiral discrimination of 19 amino acids. Unlike using intensity ratios of product ions to product ions in KM, the CR method uses the intensity ratios between product ions and precursor ions. It is particularly suitable when merely one product ion is obtained with high intensity, where KM analysis is not applicable. Both methods yield reliable and reproducible results for chiral recognition and have been successfully employed in the investigation of various chiral compounds. In this study, the CR method was employed as in most cases, only one product ion was produced.

2.1.4 Chiral drugs

In this chapter, chiral recognition of four chiral drugs, ofloxacin, clopidogrel, omeprazole and bupivacaine were investigated.

Ofloxacin is an antibacterial drug with a broad antibacterial spectrum. The double-stranded DNA of bacteria would uncoil into a single-stranded structure during the replication and transcription process; ofloxacin then works as a specific inhibitor of DNA gyrase by binding to the subunit of the enzyme, which makes bacteria unable to replicate or synthesize proteins[118]. Such binding may even alter the compliance of the gyrase, causing bacterial cell death. The structure of ofloxacin contains a tricyclic ring with a carboxyl group and an asymmetric carbon at the C-3 position (Figure 2-3) that

enables the chirality of ofloxacin. Previous studies have proven that the *S*-enantiomer is 8 to 128 times more potent than the *R*-enantiomer, and the use of the *S*-enantiomer is preferred[119].

Clopidogrel is a well-marketed drug with an annual worldwide sale of 9.43 billion US dollars in 2010[120], and the demand is increasing. It is a potent antithrombotic and antiplatelet agent. Clopidogrel acts as an adenosine diphosphate receptor antagonist to inhibit platelet aggregation. The structure of clopidogrel contains a thienopyridine and an *O*-chlorobenzyl group (Figure 2-4). The chirality is induced by the carbon that is connected to a methoxycarbonyl group. Only the *S*-enantiomer shows antithrombotic activity, while the *R*-enantiomer does not, and high doses of *R*-enantiomer can cause convulsions in animals[121].

Omeprazole is one of the most frequently used proton-pump inhibitors that effectively and persistently reduces the production of gastric acid. Its mechanism involves binding to H^+, K^+-ATPase, and irreversibly blocking the enzyme system of gastric parietal cells. The structure of omeprazole is depicted in Figure 2-5, the sulfur of which contains three types of coordination and therefore results in two *S/R*-enantiomers. Extensive research has demonstrated that the *S*-enantiomer (ESZ) is far more effective than the *R*-enantiomer and the racemate in therapeutic efficacy, as it is less metabolized and minor oxidized in the metabolic pathway[122]. ESZ has already received FDA approval and was introduced to the market in 2001[123], showing great potential for various applications. Though omeprazole is currently used as the racemate and as the ESZ in the market, it is essential to develop a rapid and efficient analytical method for the separation and discrimination of these two enantiomers, as well as for assessing and checking their

enantiomeric purity.

Bupivacaine is a long-acting local anesthetic that is used for obstetric analgesia and epidurals to reduce sensation in specific areas. It is commonly combined with epinephrine to prevent systemic absorption and prolong the duration of action[124]. Bupivacaine is a piperidine carboxamide, and the chirality is induced by the carbon on piperidine connected to the carboxamide (Figure 2-6). Though the drug is marketed as a racemic mixture, the pharmacokinetics of two enantiomers differ when binding to plasma and proteins. The *R*-bupivacaine is proven to cause increased central nervous system and cardiovascular toxicity, however, the *S*-enantiomer is more active and less toxic. Clinical studies showed that increasing the ratio of *S*-bupivacaine in the mixture would result in increased safety of the drug[125].

Various methods including HPLC[126, 127], electrochemical detection[128], CE[129, 130], SFC[131] and thin layer chromatography (TLC)[132] have been developed for chiral analysis of chiral drugs. In this study, chiral analysis by direct MS/MS was herein applied. The main advantages of using MS/MS are easy sample preparation, no separation or extraction required, lots of diastereomeric complexes can be observed and thus dissociated due to the high sensitivity of MS, rapid sample detection once the best diastereomeric complex is found, low consumption of samples and low cost as no columns, reference standards or ionic liquids are involved. To perform MS/MS, ion trap mass spectrometry (IT-MS) was employed due its to numerous following-advantages: high ion capacity and sensitivity; mass-selected ions can be accumulated over time; MS^n is allowed to determine ion structures; ions with extremely low abundances in full MS can also be selected and isolated for MS/MS; and dissociation channels, which are

mild to complex ions, start from the lowest activation energy.

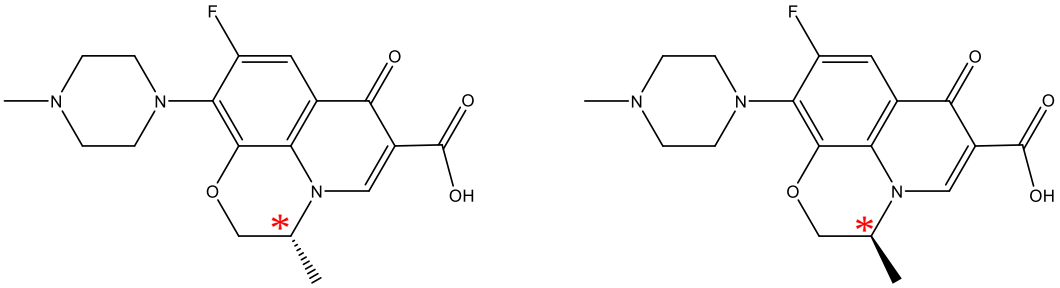

R-ofloxacin *S*-ofloxacin (Levofloxacin)

Figure 2-3. The chemical structure of *R*/*S*-ofloxacin.

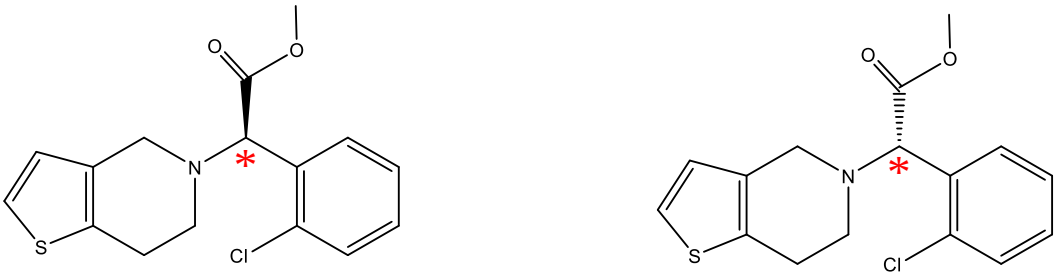

R-Clopidogrel *S*-Clopidogrel

Figure 2-4. The chemical structure of *R*/*S*-clopidogrel.

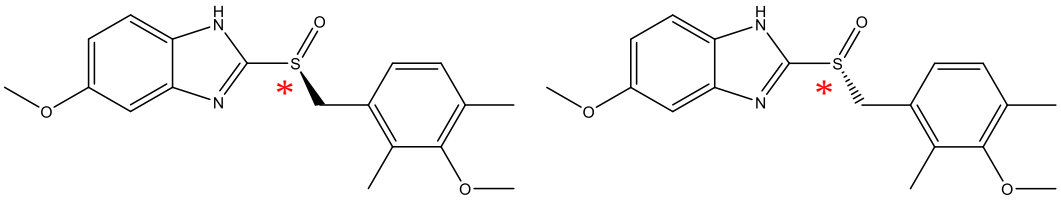

R-Omeprazole *S*-Omeprazole

Figure 2-5． The chemical structure of *R*/*S*-omeprazole.

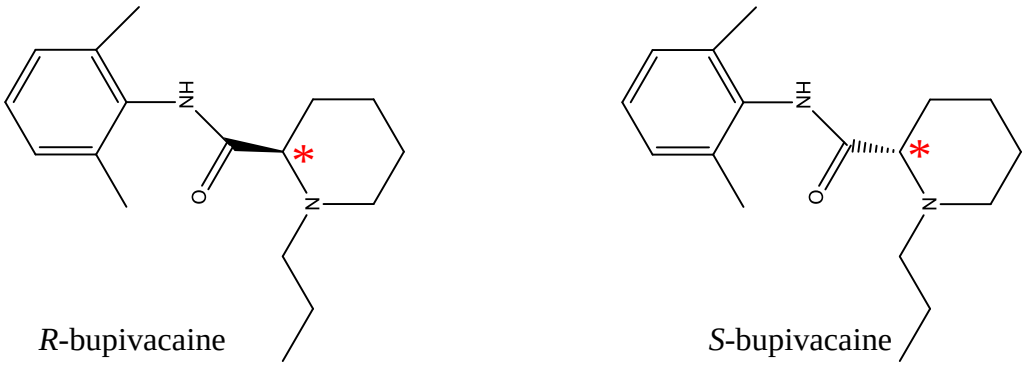

R-bupivacaine *S*-bupivacaine

Figure 2-6. The chemical structure of *R*/*S*-bupivacaine.

2.2 Experimental

2.2.1 Chemicals

Methanol (HPLC grade) was purchased from Anaqua Chemical Supply (Houston, USA). Milli-Q water was produced from a Milli-Q water purification system (Millipore, Bedford, USA). *R*- and *S*-ofloxacin were from Cayman (Michigan, USA) and Sigma-Aldrich (St. Louis, USA), respectively. *R/S*-clopidogrel were obtained from the National Institutes for Food and Drug Control (Beijing, China). *R*- and *S*-omeprazole were prepared from racemate by DAICEL (Shanghai, China). *R*- and *S*-bupivacaine were purchased from Macklin (Shanghai, China) and Toronto Research Chemicals (Toronto, Canada), respectively. *L*-Amino acids (proline, tyrosine, phenylalanine, and lysine) and metal salts (nickel(II) chloride, cobalt(II) chloride, and lithium chloride anhydrous) were purchased from Macklin (Shanghai, China). *L*-Amino acids (tryptophan, histidine, glutamic acid, and aspartic acid), metal salts of zinc(II) bromide and copper(II) nitrate, and α/β/γ-cyclodextrins were obtained from Sigma-Aldrich (St. Louis, USA).

2.2.2 Sample preparation

The workflow of the experiment was described in Figure 2-7, chiral drugs, selectors and metal salts were dissolved in methanol or 50% methanol in water at a concentration of 500 μM. Before analysis, the above stock solutions were mixed and diluted with 50% methanol in water to a certain concentration. The obtained solutions were then injected directly into the IT-MS at a certain rate through a syringe pump to perform MS/MS or even MS^n.

2.2.3 Mass spectrometry

MS/MS or MS^n experiments were performed under the positive ion mode using the amaZon speed ESI-ion trap-ETD mass spectrometer (Bruker, Billerica, USA). The ESI+ conditions were optimized in terms of capillary voltage, dry gas temperature, gas pressure, gas flow rate, and infusion rate: capillary voltage, 4500 V; dry gas temperature, 200 °C; gas pressure, 3 psi; gas flow rate, 4 L min^{-1}; and infusion rate, 6 µL min^{-1}. Gas-phase complex ions were generated by electrospraying. Ion fragmentation was performed and CID values varied, depending on the relative intensity of product ions to the precursor ion. All spectral data were collected for 1 minute and averaged, and each sample solution was detected three times to obtain an average value. The identification of complex ions was achieved by checking the monoisotopic mass, isotopic patterns, charge states and spectral results. Compact DataAnalysis software (Bruker, Billerica, USA) was used for processing row data.

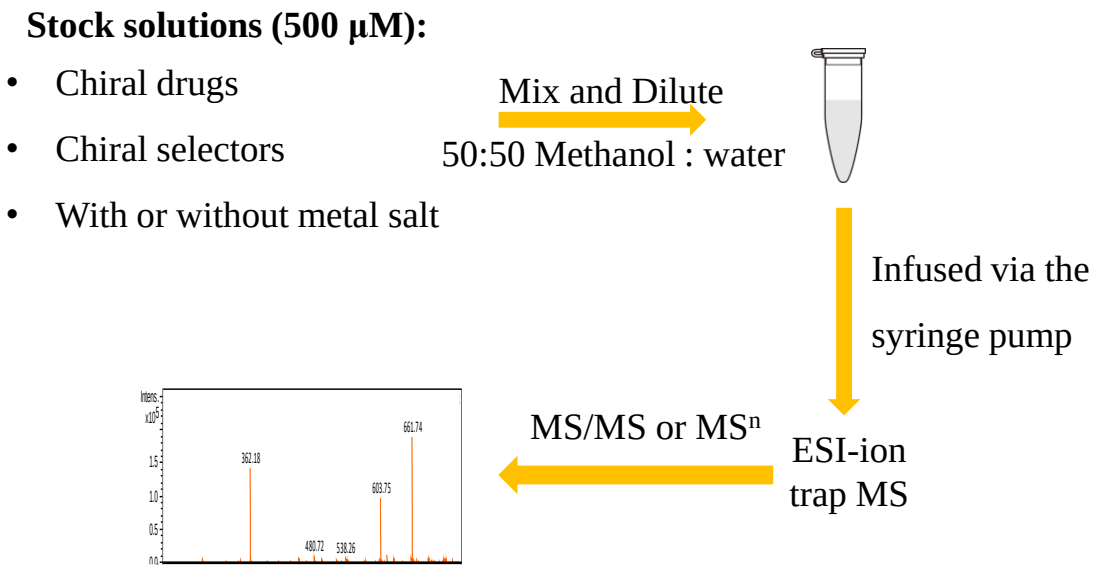

Figure 2-7. The workflow of the experiment.

2.3 Results and discussion

2.3.1 Chiral recognition of ofloxacin

Figure 2-8a showed the full MS spectrum of ofloxacin without the addition of chiral selectors. The highest intensity of protonated monomers ($[M+H]^+$, *m/z* 362.2, M represented the analyte) was observed, and to some extent, it suppresses the signal from any other peaks present in the spectrum. When the mass range starting from 400 Da was selected, more peaks became observable, such as protonated ions $[2M+H]^+$ at *m/z* 723.4 (Figure 2-8b), indicating the existence of dimers. No sodium adduct or potassium adduct ions were observed. Even though some peaks were too low in intensity to be observed in MS, when they were isolated, the accumulation function of IT-MS would lead to improved intensity for detection.

Figure 2-9a and Figure 2-9b showed the MS/MS spectra of $[M+H]^+$. A loss of 44 Da was observed for both diastereomeric complexes, possibly attributed to the loss of CO_2 from the precursor. The MS/MS spectra of protonated dimers $[2M+H]^+$ were shown in Figure 2-9c and Figure 2-9d, and a loss of an analyte was observed to form $[M+H]^+$. Though clear product ions were obtained for both $[M+H]^+$ and $[2M+H]^+$, there is nearly no difference in fragmentation patterns of the two diastereomers, indicating the similar bindings within the ions. The two enantiomers could not be differentiated directly by MS, therefore, the addition of chiral selectors was required.

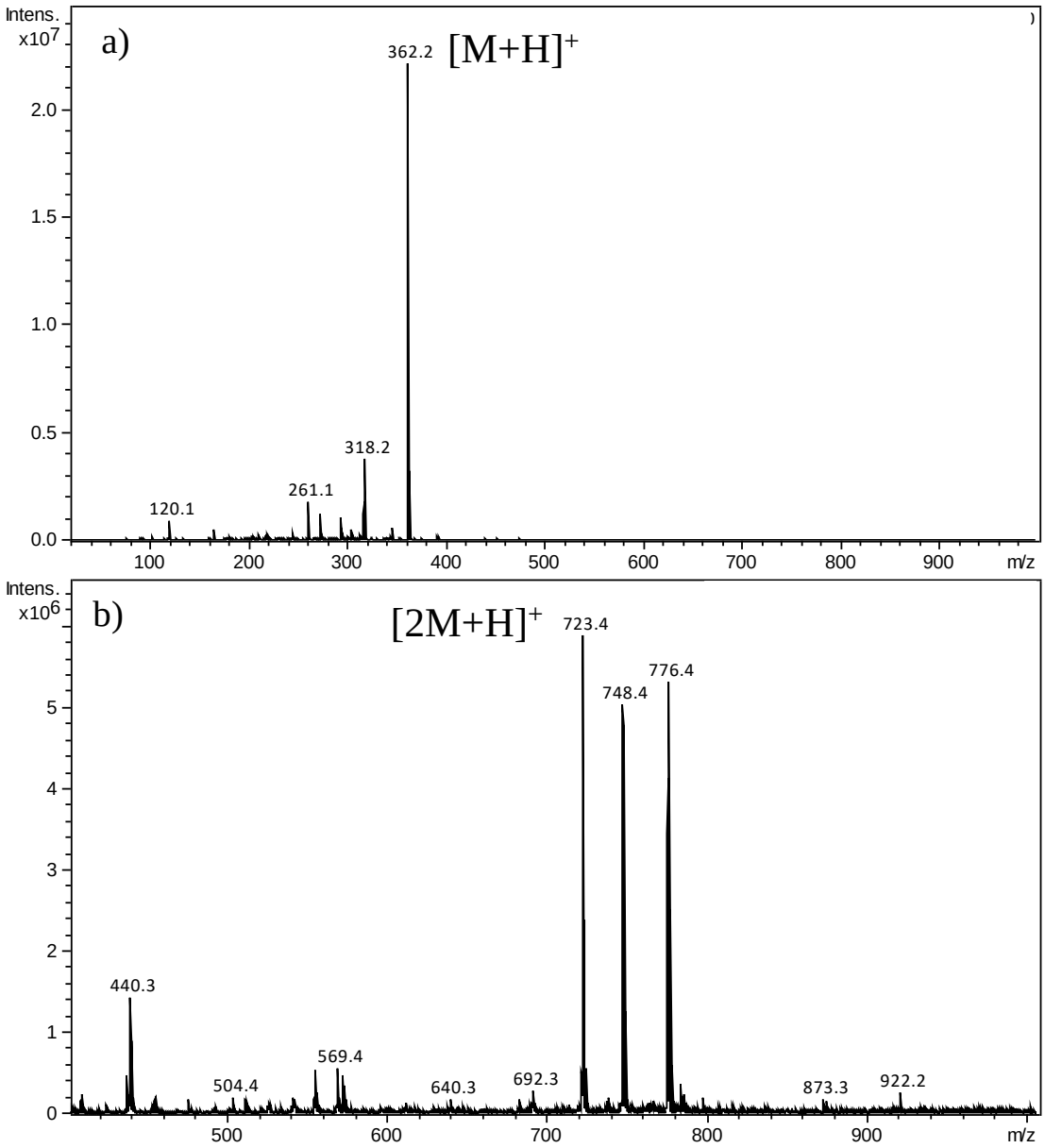

Figure 2-8. MS spectra of ofloxacin with mass ranges of a) *m/z* 20 - 1000 and b) *m/z* 400 - 1000.

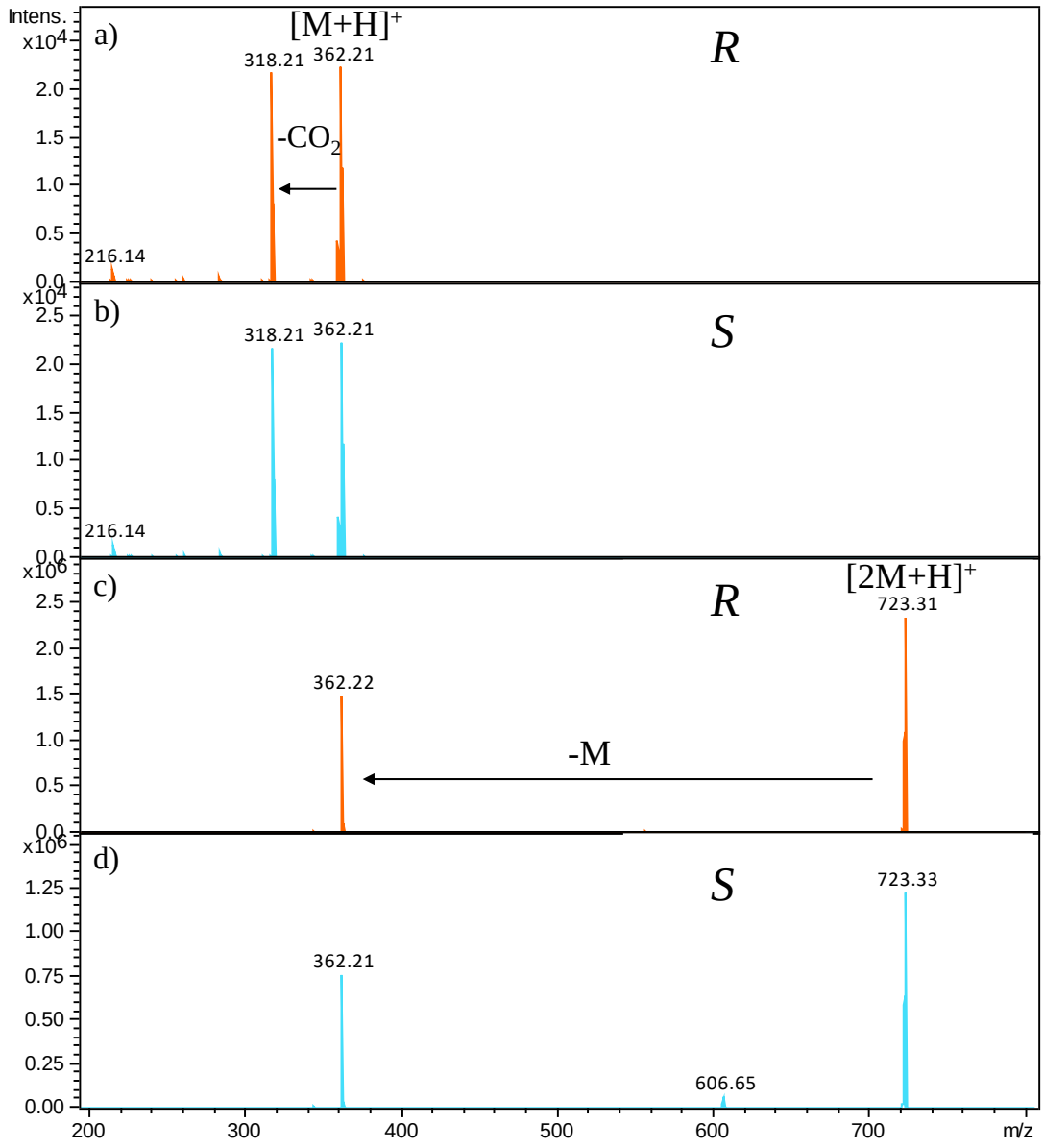

Figure 2-9. The MS/MS spectra of $[M+H]^+$ (a and b), and $[M+H]^+$ (c and d) without any chiral selectors. The product ions of *m/z* 318.2 and *m/z* 362.2 were identified as $[M-CO_2+H]^+$ and $[M+H]^+$, respectively.

2.3.2 Optimization of the experimental conditions

To improve the chiral differentiation of ofloxacin, a range of chiral selectors were utilized, among which amino acids (AAs) and cyclodextrins showed stronger binding affinities than the others. In this study, amino acids (*L*-type first) were chosen as the starting point due to their low cost and ability to form non-covalent interactions at groups of amino and carboxylate. Furthermore, the functional groups in its side chain might enhance these interactions. Among the twenty common AAs, all except glycine are chiral due to the presence of four different groups bonded to the α carbon, making them potential chiral selectors toward chiral compounds. This study revealed that AAs alone exhibited weaker binding affinities towards ofloxacin compared to metal-amino acid complexes, as the inclusion of metal ions facilitated strong coordination interactions with both AAs and ofloxacin, thereby enhancing the binding affinity. Metal ions were thus introduced into sample solutions.

Cu(II), Zn(II), Ni(II), Co(II) and Li(I), which had been reported as useful in chiral analysis, were compared in their ability to interact with ofloxacin, and relevant metal-bound complex ions that were formed were listed in Table 2-1. Among the metal ions tested, copper ions demonstrated the best interaction results. Several complex ions of varying sizes were detected when phenylalanine (Phe) was used as the selector, including dimers $[Cu+CS+M-H]^+$, trimers $[Cu+2CS+M-H]^+$, $[Cu+CS+2M-H]^+$ and $[Cu+3M-H]^+$, and tetramers $[Cu+3CS+M-H]^+$ (CS represented the chiral selector), whereas only two or three complexes were observed with the other metal ions. Similar results were observed when other AAs were used as CSs. This confirmed the superior performance of Cu(II) in the chiral analysis of ofloxacin, which was consistent with the results of our previous study for the analysis of naproxen[113]. Therefore, copper(II) ions

were selected for use throughout the entire study.

It was found that the relative intensity of the obtained cluster ions initially increased and then decreased as the concentration of Cu(II) increased from 5 μM to 20 μM, with the selector concentration being kept constant (results were not shown). The overall signal was better when 10 μM of Cu(II) was added. In contrast, the concentration ratio between ofloxacin and selectors did not have any significant effect on the results of MS and MS/MS for either *R*- or *S*-ofloxacin (Figure 2-10), therefore, the concentrations of ofloxacin and chiral selectors were fixed at 20 μM.

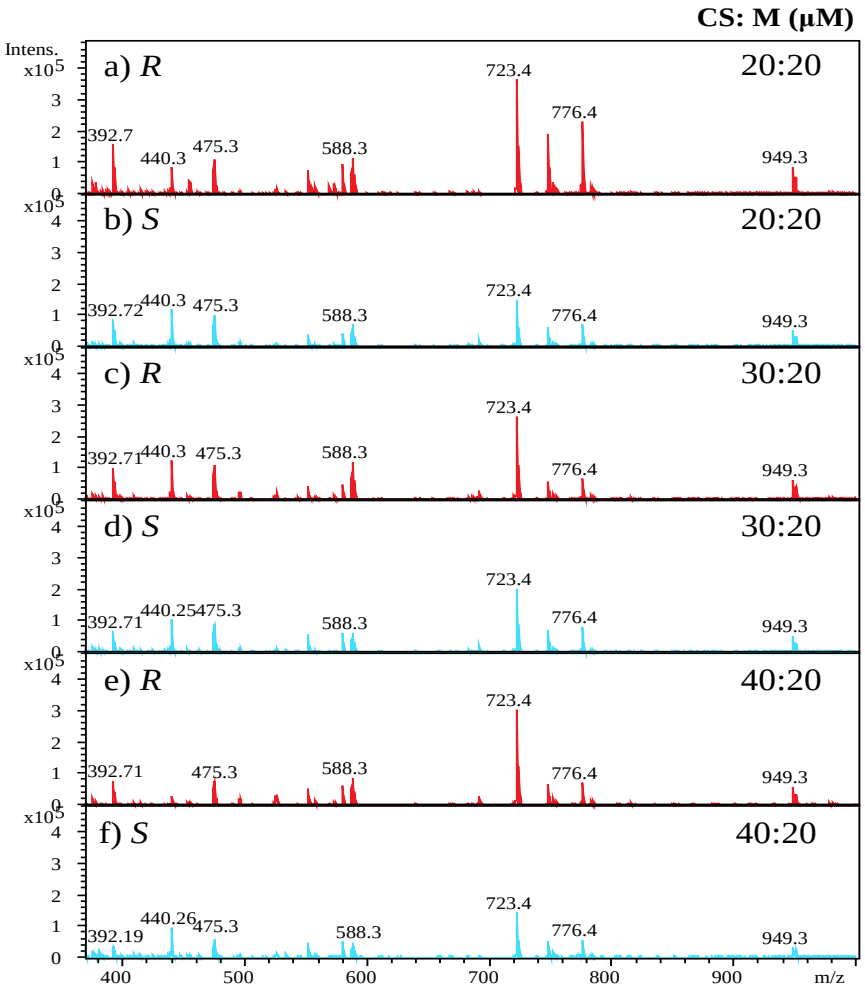

Figure 2-10. MS spectral results obtained with concentration ratios between the *R*/*S*-ofloxacin and selectors as a-b) 20 μM:20 μM, c-d) 30 μM:20 μM, and e-f) 40 μM:20 μM.

Table 2-1. Typical metal-bound complex ions observed using different metal ions of Cu(II), Zn(II), Ni(II), Co(II), and Li(I) (CS represents the chiral selector and M represents ofloxacin).

Cu^{2+}	Zn^{2+}	Ni^{2+}	Co^{2+}	Li^{+}
$[M+CS+Cu-H]^{+}$	$[M+CS+Zn-H]^{+}$	$[M+CS+Ni-H]^{+}$	$[M+CS+Co-H]^{+}$	$[M+CS+Li]^{+}$
$[M+2CS+Cu-H]^{+}$	$[M+2CS+Zn-H]^{+}$	$[M+2CS+Ni-H]^{+}$		$[M+2CS+Li]^{+}$
$[M+3CS+Cu-H]^{+}$	$[M+3CS+Zn-H]^{+}$		$[M+3CS+Co-H]^{+}$	
$[2M+CS+Cu-H]^{+}$				$[2M+CS+Li]^{+}$
$[3M+Cu-H]^{+}$				

Our previous findings have illustrated that the intermolecular forces between the chiral selector and the analyte play a crucial role in MS/MS analysis, and similar structures between them facilitate the formation of diastereomeric complexes, leading to better separation and detection of enantiomers. These findings are also applicable to this study. As displayed in Figure 2-13, few complex ions could be observed when lysine (Lys), glutamate (Glu) and aspartate (Asp) (their structures shown in Figure 2-11) were used as selectors. On the other hand, when AAs with rigid rings were applied, i.e., proline (Pro), tryptophan (Trp), tryptophan (Tyr), histidine (His) and Phe (structures shown in Figure 2-12), some typical diastereomeric complex ions containing the analyte and CS were observed (Figure 2-14), including dimers $[M+CS+Cu-H]^+$ (*m/z* 588.3, 627.3 and 538.3, respectively) and trimers $[M+2CS+Cu-H]^+$ (*m/z* 949.3, 988.3 and 899.3, respectively). A possible explanation for the formation of these complexes could be that the rigid tricyclic ring of ofloxacin is crucial for the strong π interactions, and utilizing AAs with similar structures can provide extra π interactions to form diastereomeric ions with ofloxacin. In addition to the amino and carboxylic groups, the coordination site for copper bound is provided by the rigid ring in the chain. Therefore, five amino acids, Pro, Trp, Tyr, His and Phe, were primarily employed.

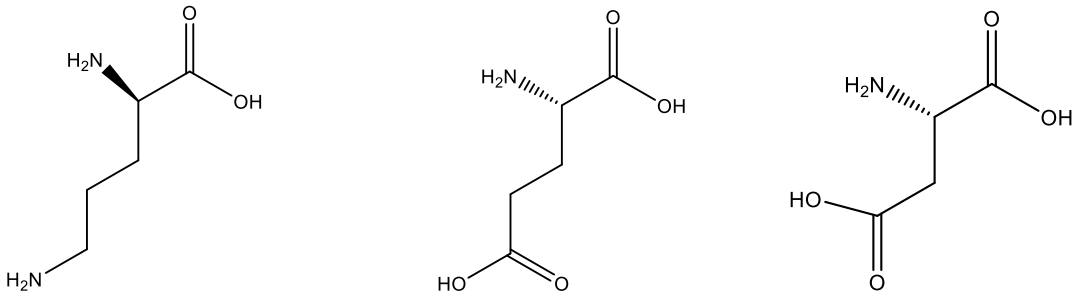

L-Lys *L*-Glu *L*-Asp

Figure 2-11. Structures of Lys, Glu, and Asp (all *L*-type).

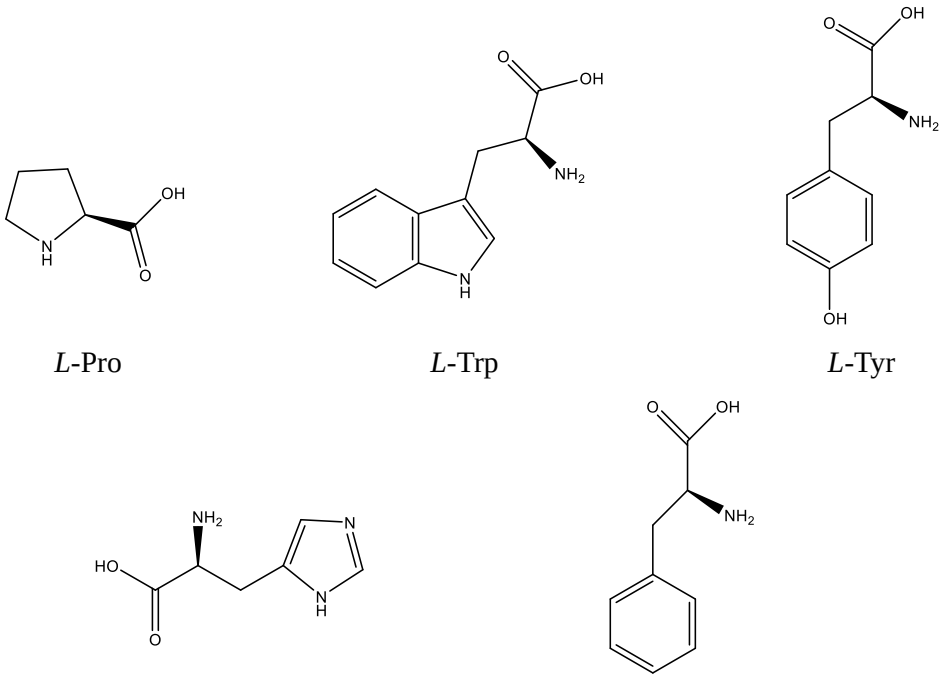

L-Pro *L*-Trp *L*-Tyr

L-His *L*-Phe

Figure 2-12. Structures of Pro, Trp, Tyr, His, and Phe (all *L*-type).

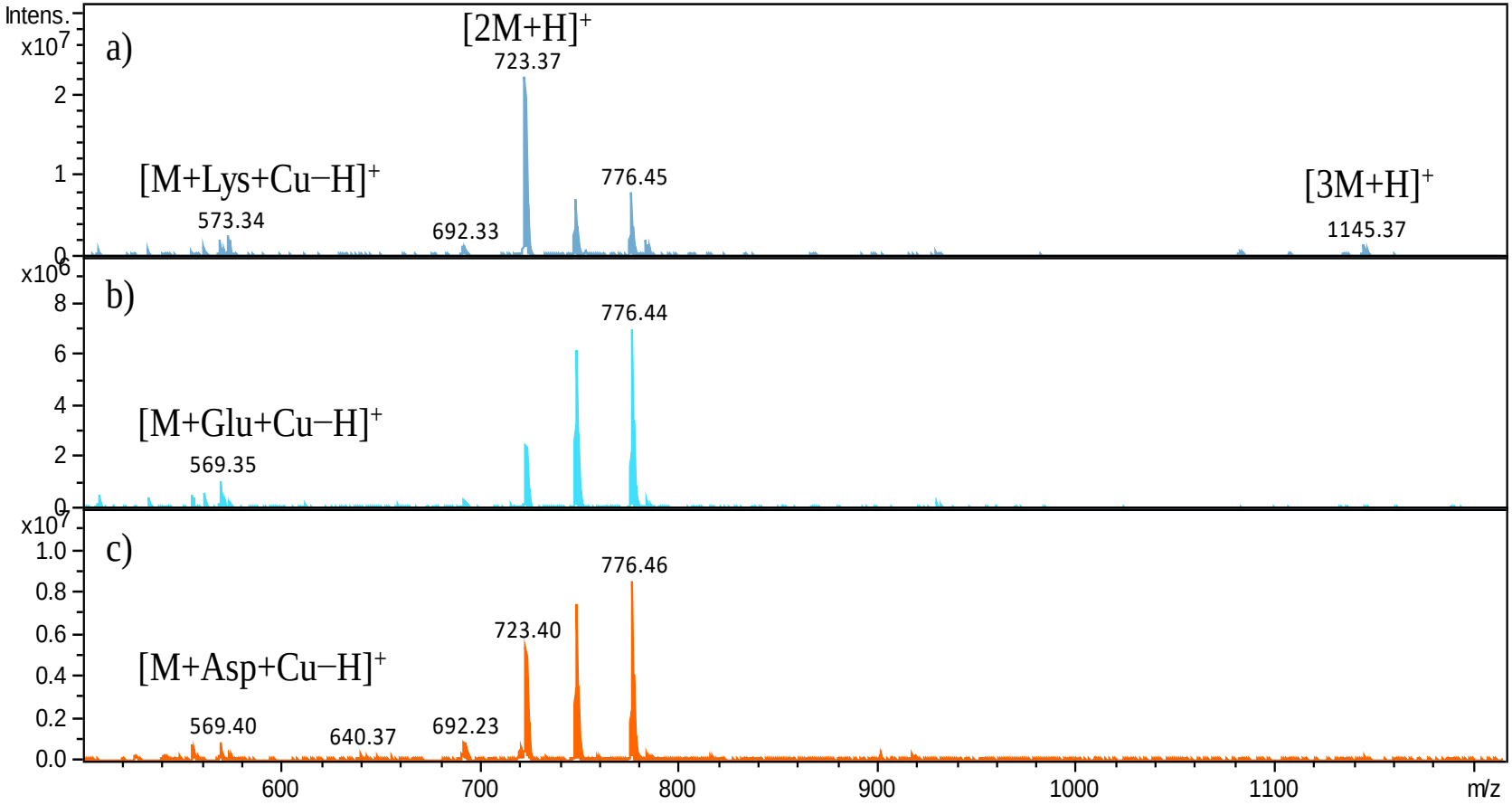

Figure 2-13. MS spectra of ofloxacin with added Cu(II) and chiral selectors of a) Lys, b) Glu and c) Asp.

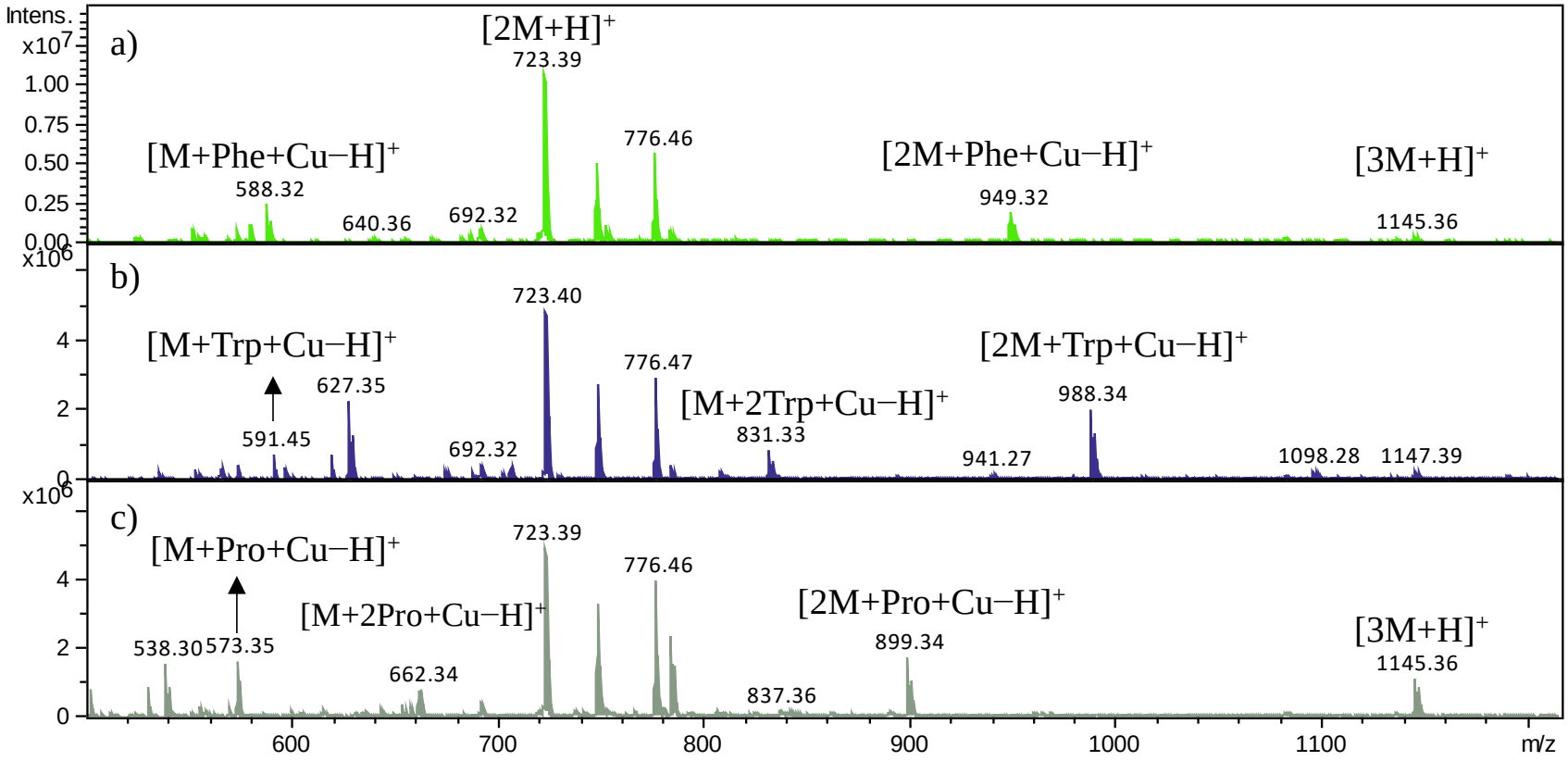

Figure 2-14. MS spectra of ofloxacin with added Cu(II) and chiral selectors of a) Phe, b) Trp and c) Pro.

In this study, chiral recognition was examined using MS/MS analysis. The collision energy was adjusted to a specific value for each complex ion in order to achieve an abundance ratio of the product ion that closely matched that of the precursor ion. To ensure the reliability of the results, only stable ions that showed sufficiently high intensities under the collision energy were considered. Figure 2-15 showed an example with Pro as the CS that copper-bound trimers $[M+2Pro+Cu-H]^+$ (*m/z* 653.3) were dissociated into fragments of $[M+Pro+Cu-H]^+$ (*m/z* 538.5) and $[M+H]^+$ (*m/z* 362.3) by losing one and two selectors, respectively. The Cu(II) was dissociated with two CSs, and no $[M+Cu-H]^+$ alone was observed. This might help to explain the binding affinity of Cu(II) ions towards CSs and ofloxacin. The abundance ratio of these fragments clearly distinguished between two diastereomers, as the relative intensity of $[M+Pro+Cu-H]^+$ to $[M+2Pro+Cu-H]^+$ obtained with *R*-ofloxacin was obviously higher than that obtained with *S*-ofloxacin. The stereoselectivity may be caused by the steric hindrance of the ofloxacin methyl group, which resulted in stronger π interactions between L-Pro and S-ofloxacin.

For another trimeric cluster ions $[2M+Pro+Cu-H]^+$, in addition to the loss of CSs, a loss of the analyte was also found, by forming $[M+Pro+Cu-H]^+$ at *m/z* 538.3 (Figure 2-16a). The intensity of $[M+Pro+Cu-H]^+$ was much lower than that of $[2M+Cu-H]^+$, suggesting the strong binding of ofloxacin within the complex ions. Interestingly, for the dimeric cluster ion $[M+Pro+Cu-H]^+$, the major fragment ion (*m/z* 494.3) was formed by losing CO_2 (Figure 2-16b). As no loss of CO_2 was obtained in $[M+2Pro+Cu-H]^+$, this further confirmed that $[M+H]^+$ was obtained from $[M+2Pro+Cu-H]^+$ by losing two selectors rather than from $[M+Pro+Cu-H]^+$ by losing one Pro. In $[M+Pro+Cu-H]^+$, no loss of analytes was observed, which suggested a

strong binding within the copper dimeric cluster ions[133]. According to previous studies, loss of CO_2 reflected the possible structure of $[M+Pro+Cu-H]^+$, with at least one deprotonated carboxylic group coordinated to Cu(II)[134, 135], as proposed in Figure 2-17. Compared to the dimeric cluster ions, the bindings within Cu-bound trimeric ions were looser, which was also evidenced by the lower collision energy required for fragmentation. The coordination sites of the analyte and Pro with Cu(II) within two dimeric ions also could be inferred, for $[M+2CS+Cu-H]^+$, there were two coordination sites for ofloxacin and one site for each Pro, and for $[M+2CS+Cu-H]^+$, there were two coordination sites for one ofloxacin and one site for each of another ofloxacin and Pro. These results were also confirmed by other CSs, such as Trp (Figure 2-18).

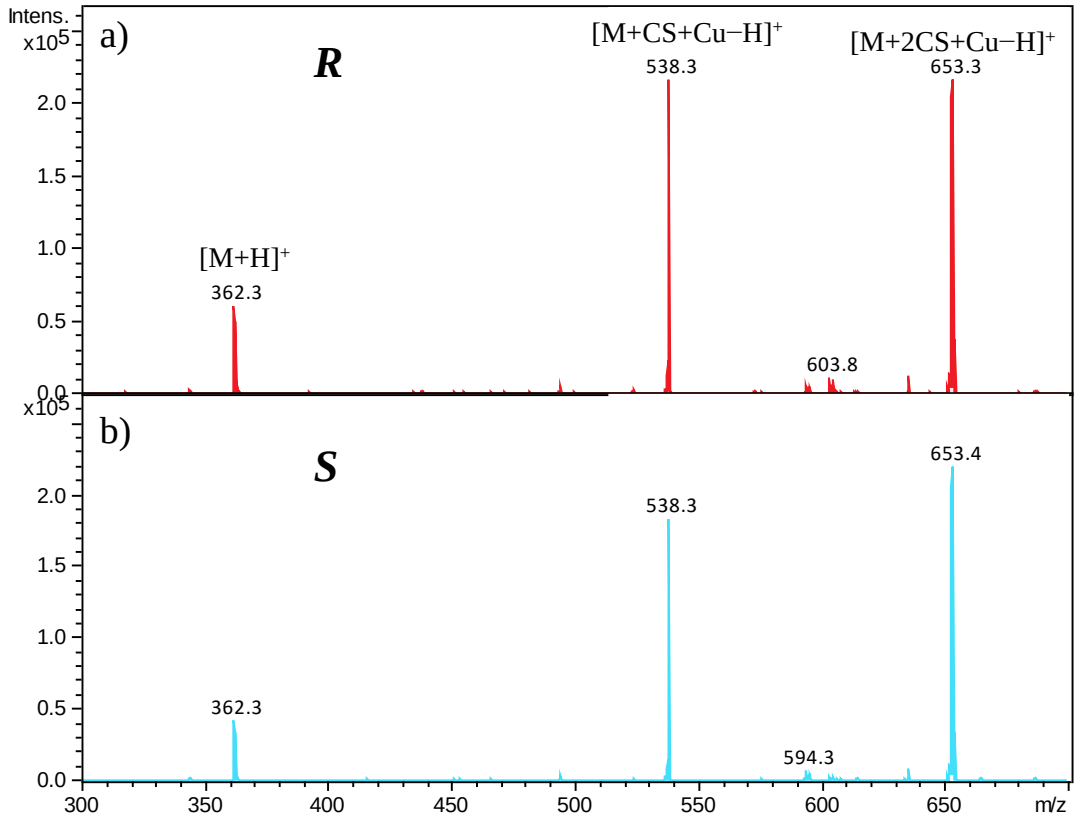

Figure 2-15. MS/MS spectra of *R*/*S*-ofloxacin on $[M+2CS+Cu-H]^+$ with Pro as the chiral selector.

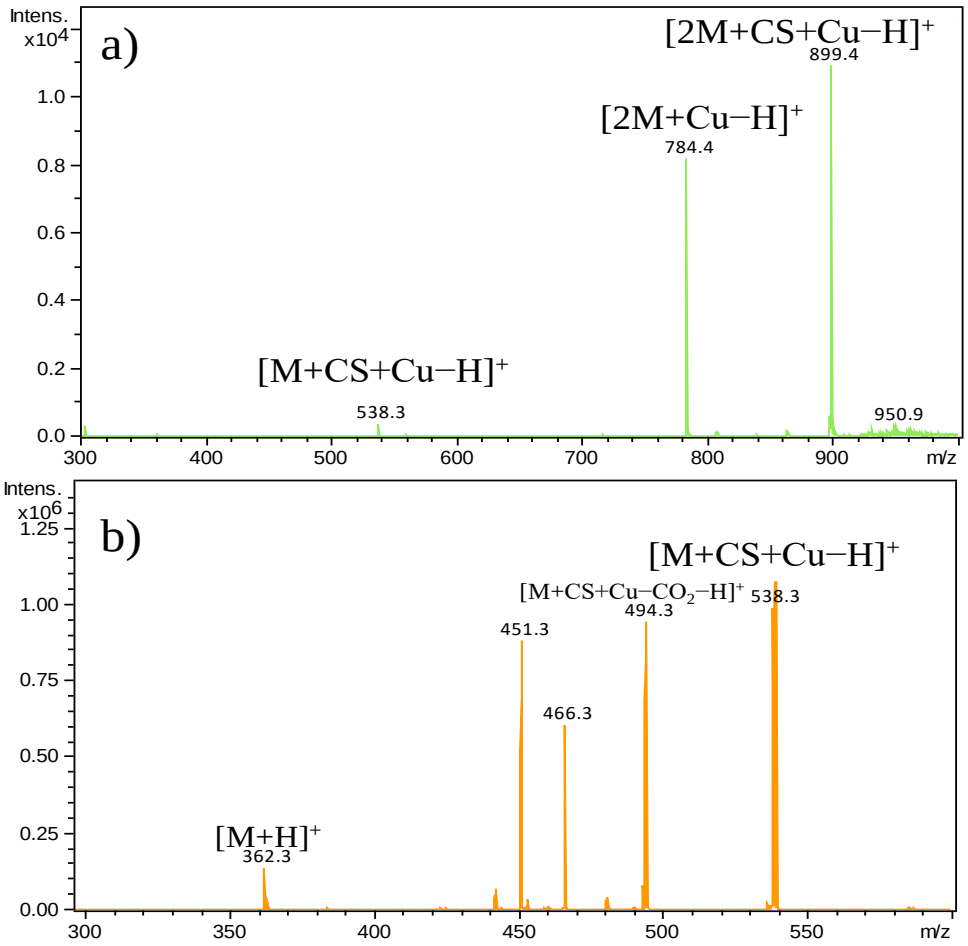

Figure 2-16. MS/MS spectra of ofloxacin on a) $[2M+CS+Cu-H]^+$ and b) $[M+CS+Cu-H]^+$ with Pro as the chiral selector.

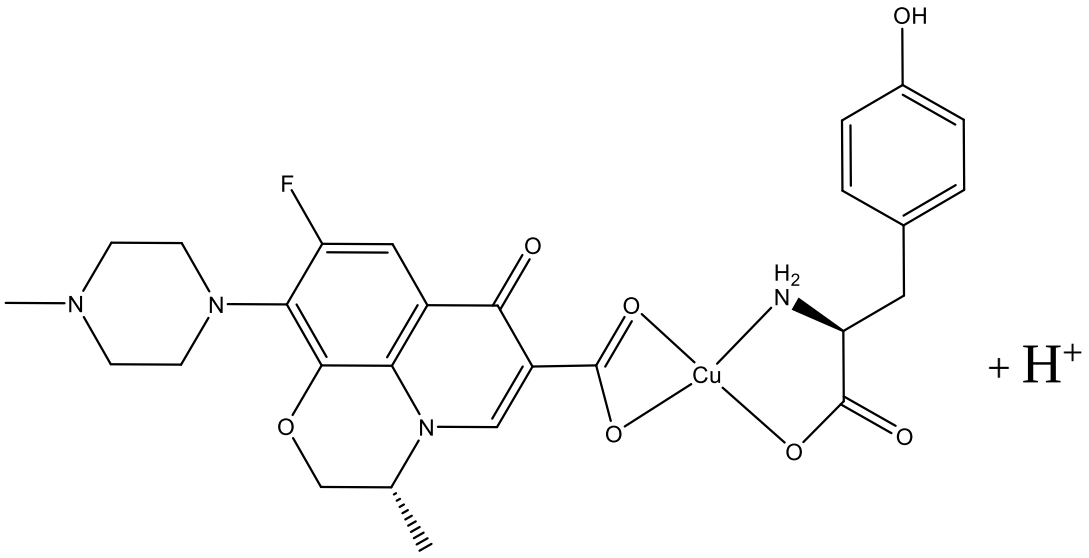

Figure 2-17. A possible structure of the dimeric ion [*R*-ofloxacin+Pro+Cu−H]$^+$.

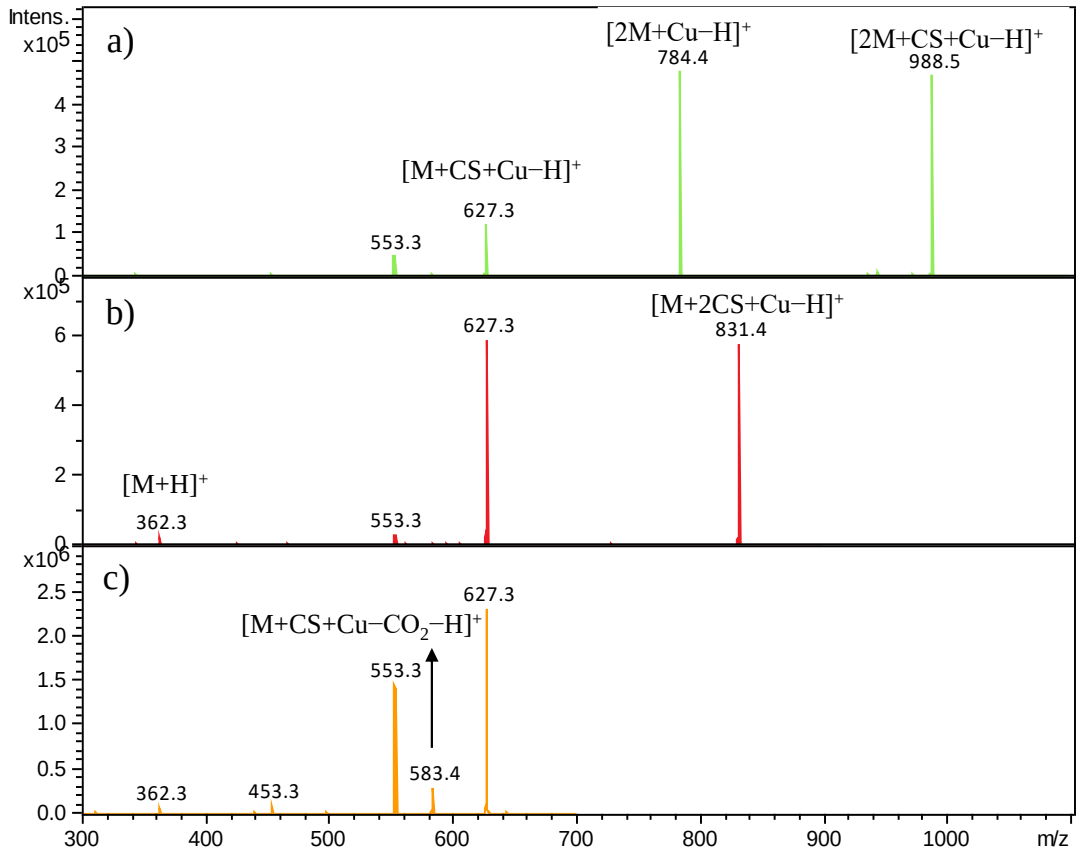

Figure 2-18. MS/MS spectra of ofloxacin on a) $[2M+CS+Cu-H]^+$, b) $[M+2CS+Cu-H]^+$ and c) $[M+CS+Cu-H]^+$ with Trp as the chiral selector.

As mentioned in Chapter 1, the chiral recognition results can be measured by two methods, one is the KM, and R_{chiral} of which is calculated by Equation 6:

$$R_{Chiral} = \frac{[(Cu)_m(M_S)_n(CS)_{Z-1} - H]^+ / [(Cu)_m(M_S)_{n-1}(CS)_Z - H]^+}{[(Cu)_m(M_R)_n(CS)_{Z-1} - H]^+ / [(Cu)_m(M_R)_{n-1}(CS)_Z - H]^+} \qquad \text{Equation (6)}$$

and the other is the CR method, the ratio of which is defined as Equation 7:

$$CR = \frac{[(Cu)_m(M_R)_n(CS)_{Z-1} - H]^+ / [(Cu)_m(M_R)_n(CS)_Z - H]^+}{[(Cu)_m(M_S)_n(CS)_{Z-1} - H]^+ / [(Cu)_m(M_S)_n(CS)_Z - H]^+} \qquad \text{Equation (7)}$$

where m, n and z are the number of copper ions, the analyte and the chiral selector, respectively.

For some diastereomeric ions, there was only one product ion produced in MS/MS, therefore, the second method was employed in this study. The magnitude of difference from unity plays a crucial role in chiral recognition, as it indicates the degree of chiral recognition. Here, CR > 1+3SD or CR < 1-3SD (SD, standard deviation) were defined as the criteria. The CR value larger than 1 indicates that the R-enantiomer-based ion has a higher tendency to dissociation. A summary of the results can be found in Table 2-2. Overall, when the same selector was utilized, larger complexes generally led to improved chiral recognition. $[M+2CS+Cu-H]^+$ tended to have better CR results than $[M+CS+Cu-H]^+$ for all selectors. However, this observation needs to be further explored with higher degrees of assembly.

As exhibited in Table 2-2, chiral selectors Pro and Tyr demonstrated the most significant chiral discrimination of ofloxacin. Particularly noteworthy was the enantioselectivity achieved when $[M+2Pro+Cu-H]^+$ dissociated into $[M+Pro+Cu-H]^+$ with a CR value of 1.26 ± 0.04. Pro, lacking long side chains with the carboxyl directly attached to the ring,

displayed a more rigid structure than the other four amino acids. It appeared that its CR value was higher than 1.0, indicating that the heterochiral cluster ion (*R*-ofloxacin, *L*-Pro) was less stable than the homochiral one (*S*-ofloxacin, *L*-Pro) at the same collision energy. In contrast, when $[M+2Tyr+Cu-H]^+$ was dissociated into $[M+Tyr+Cu-H]^+$, the obtained CR value was 0.85 ± 0.02, which was smaller than 1.00, indicating that the heterochiral cluster ion (*R*-ofloxacin, *L*-Tyr) was more stable than the homochiral one (*S*-ofloxacin, *L*-Tyr) at the same collision energy. The different preferences for the configurations of selectors and ofloxacin between Pro and Tyr main due to the small steric effect of proline. The specificity and strength of the binding interactions between the chiral selector and the analyte greatly influenced the fragmentation patterns and can be correlated with the stability and selectivity of the complexes formed. The different stability of the above complex ions strongly suggested the selectivity of different chiral selectors towards ofloxacin. The binding interactions will be further investigated in terms of the chemical structures of these formed complex ions.

Table 2-2. The CR values of complex ions of ofloxacin and amino acids.

Chiral selector	Precursor ion	Product ion	CR
Pro	$[M+CS+Cu-H]^+$	$[M+CS+Cu-CO_2-H]^+$	1.08±0.04
	$[M+2CS+Cu-H]^+$	$[M+CS+Cu-H]^+$	1.26±0.04
		$[M+H]^+$	1.44±0.13
	$[2M+CS+Cu-H]^+$	$[2M+Cu-H]^+$	1.05±0.15
Trp	$[M+CS+Cu-H]^+$	$[M+CS+Cu-CO_2-H]^+$	0.97±0.04
	$[M+2CS+Cu-H]^+$	$[M+CS+Cu-H]^+$	0.98±0.02
	$[2M+CS+Cu-H]^+$	$[2M+Cu-H]^+$	1.07±0.05
		$[M+CS+Cu-H]^+$	1.11±0.09
Tyr	$[M+CS+Cu-H]^+$	$[M+CS+Cu-CO_2-H]^+$	1.00±0.03
	$[M+2CS+Cu-H]^+$	$[M+CS+Cu-H]^+$	0.85±0.02
	$[2M+CS+Cu-H]^+$	$[2M+Cu-H]^+$	1.12±0.01
Phe	$[M+CS+Cu-H]^+$	$[M+CS+Cu-CO_2-H]^+$	0.98±0.10
	$[M+2CS+Cu-H]^+$	$[M+CS+Cu-H]^+$	0.93±0.02
His	$[M+CS+Cu-H]^+$	$[M+CS+Cu-CO_2-H]^+$	1.02±0.02
	$[2M+CS+Cu-H]^+$	$[M+CS+Cu-H]^+$	0.94±0.08

In addition to amino acids, three types of cyclodextrins (CDs) were investigated as well. Cyclodextrins are cyclic oligosaccharides consisting of multiple glucose units connected by α-1,4-linkages. Based on the number of glucose units, there are α/β/γ-CDs (6, 7, 8 glucose units respectively, Figure 2-19). This unique structure enables CDs to form clathrates with various chiral compounds. CDs are frequently utilized as chiral stationary phases involved in HPLC, GC, CE and SFC. In addition to being employed in the chiral column, CDs as dependent chiral selectors have also been studied[136]. In this study, when three α/β/γ-CDs were applied as CS, it was observed that α-CD and β-CD exhibited better detection of cluster ions, all of which were doubly charged (Figure 2-20). In contrast to amino acids, no addition of copper ions was needed, mainly due to the enhanced hydrogen bonds induced by multiple hydroxyl groups. Two complexes ($[M+CS+K+H]^{2+}$ and $[2M+CS+K+H]^{2+}$) containing α-cyclodextrin were detected, both of which dissociated into $[M+H]^{+}$. The potassium ion may be induced by the production of the α-CD. Similarly, only one complex of $[M+CS+2H]^{2+}$ was observed with β-CD, and interestingly, when using γ-CD as the chiral selector, no diastereomers were detected. This could potentially be attributed to the fact that ofloxacin was too small in size to effectively fit into the large cavity size of γ-CD and the weak hydrogen bindings between the selector and analyte.

However, as shown in Table 2-3, these three complexes did not result in any discernible chiral discrimination, with CR values close to 1.00. These findings collectively revealed that CDs might not be effective chiral selectors for achieving enantiomeric differentiation of ofloxacin. It was possible that both enantiomers of ofloxacin had similar binding affinities with CDs, resulting in no noticeable difference in dissociation.

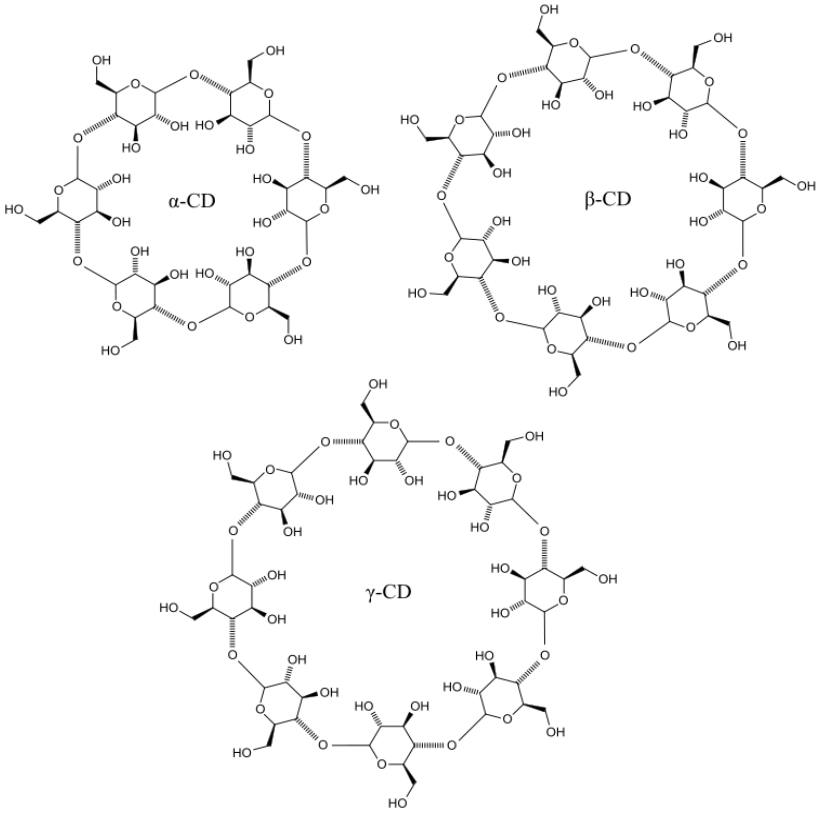

Figure 2-19. The structure of α/β/γ-cyclodextrins.

Table 2-3. The CR values of complex ions of ofloxacin and cyclodextrins.

Chiral selector	**Precursor ion**	**Product ion**	**$CR_{R/S}$**
α-cyclodextrin	$[M+CS+K+H]^{2+}$	$[M+H]^{+}$	1.02±0.03
		$[CS+K]^{+}$	0.99±0.02
	$[2M+CS+K+H]^{2+}$	$[M+H]^{+}$	1.00±0.03
		$[M+CS+K]^{+}$	1.04±0.07
β-cyclodextrin	$[M+CS+2H]^{2+}$	$[M+H]^{+}$	1.01±0.02

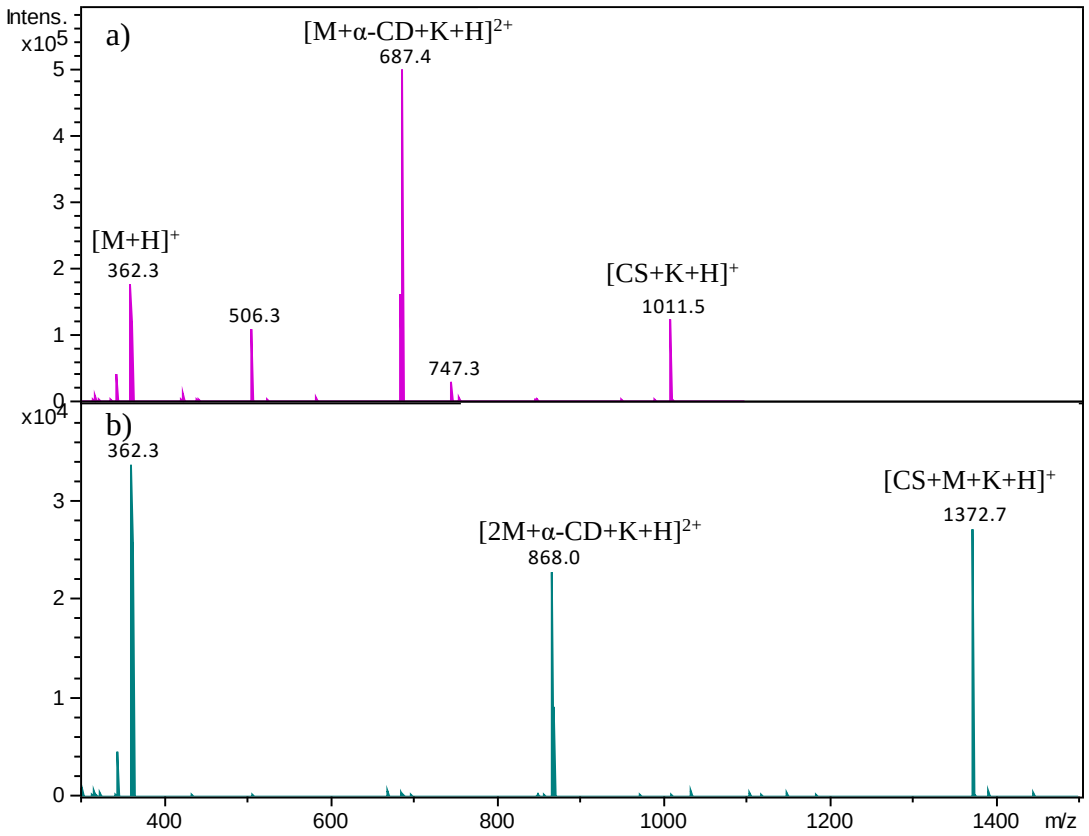

Figure 2-20. MS/MS spectra of *R*-ofloxacin on a) $[M+\alpha\text{-CD}+K+H]^{2+}$ and b) $[2M+\alpha\text{-CD}+K+H]^{2+}$.

2.3.3 Quantification of enantiomeric purities of ofloxacin

The enantiomeric purity of enantiomeric composition is described as enantiomeric excess (*ee*), indicating how the content of one enantiomer is over another enantiomer in a mixture. If the fractions of two enantiomers in the mixture are [R] and [S] respectively, then the *ee* is expressed as

$$ee = \frac{[R] - [S]}{[R] + [S]} \qquad \text{Equation (8)}$$

The [R]/[S] corresponds to the intensity ratio of the CID spectra obtained from two diastereomers. It was found that *ee* has a relationship with r

$$\frac{1}{r - r_0} = -\frac{c^2}{b} \cdot \frac{1}{ee} - \frac{c}{b} \qquad \text{Equation (9)}$$

where r is the ratio of the relative abundance of product ion to precursor ion, r_0=a+b/c (when [R] equals [S]), a, b and c are constants[117].

Based on this, quantification of the enantiomeric purity can be achieved by plotting a standard calibration curve with $1/(r - r_0)$ versus 1/*ee*. For the quantitative measurement of ofloxacin, a standard calibration curve was established by preparing a series of mixtures containing 0%, 20%, 25%, 75%, or 80% *R*-ofloxacin, then the corresponding *ee* values would be -100, -60, -50, 50 and 60 (Table 2-4). The measurement was carried out by dissociating $[M+2Pro+Cu-H]^+$ into $[M+Pro+Cu-H]^+$ by losing one chiral selector, as it enabled the most chiral discrimination of ofloxacin according to the results mentioned earlier. All measurements were performed in triplicate. As shown in Figure 2-21, a satisfactory linear coefficient of 0.9878 was obtained, suggesting the reliability of the calibration curve, which could provide a fast quantification of the

chirality of unknown ofloxacin.

Table 2-4. Values for Different Enantiomeric Compositions of ofloxacin.

Solution composition (percentage of *R* in *R*+*S*)	*ee* of *R*-ofloxacin	r	SDr
0	-100	0.8157	0.0136
20	-60	0.8295	0.0010
25	-50	0.8351	0.0022
75	50	0.8868	0.0060
80	60	0.8870	0.0041

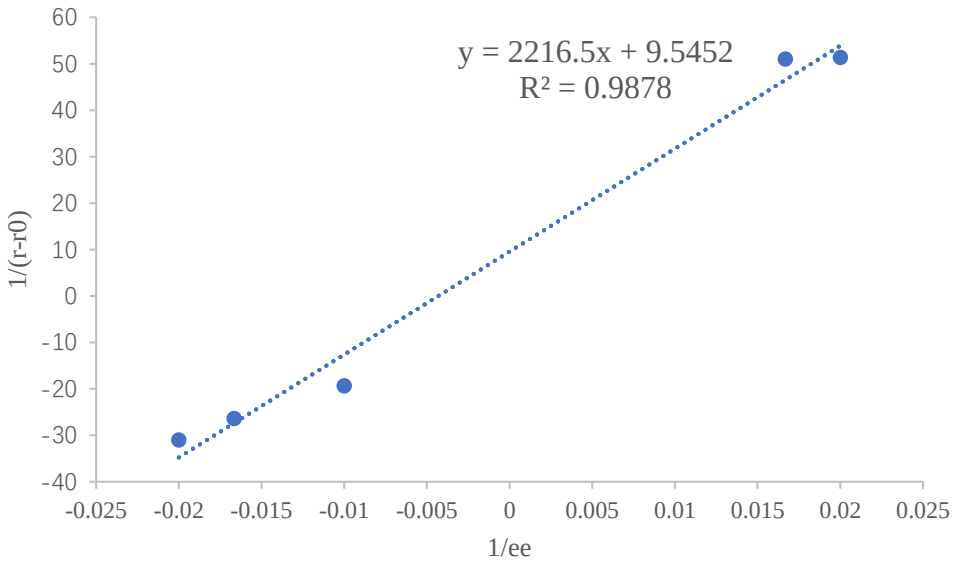

Figure 2-21. Plot of $1/(r - r_0)$ value as a function of 1/ee.

2.3.4 Chiral recognition of clopidogrel

The structure of clopidogrel contains pyridine and benzyl group (Figure 2-4), suggesting that chiral selectors with chiral discrimination towards ofloxacin may also be applicable in the differentiating of clopidogrel enantiomers. The above five amino acids were applied (Pro, Trp, Tyr, His and Phe). Compared with ofloxacin, the most interesting observation was that clopidogrel generated no or less intensive copper-containing complexes with Pro. This indicated that clopidogrel might not interact strongly with copper-containing complexes formed by Pro. Additionally, when using the other four amino acids, trimeric ions $[2M+CS+Cu-H]^+$ were hardly detected, even though the structure of clopidogrel was smaller than that of ofloxacin. However, trimeric cluster ions $[M+2CS+Cu-H]^+$ containing two CSs were still detected. This could be attributed to the more dimensional 3D structure of clopidogrel, which potentially hinders the formation of larger complexes, particularly the self-assembled clopidogrel, as unlike ofloxacin, there was no $[2clopidogrel+H]^+$ observed (Figure 2-22).

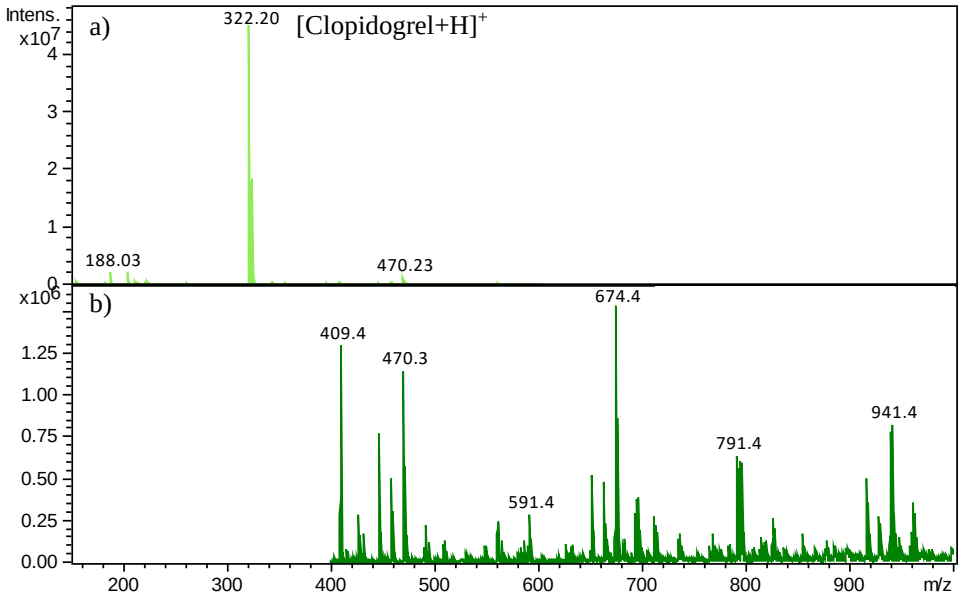

Figure 2-22. MS spectra of *R*-clopidogrel with mass ranges of a) 150-600 Da and b) 400-1000 Da.

The chiral discrimination induced by clopidogrel was found to be stronger, as enantioselectivity was obtained with Trp, Tyr and Phe as the chiral selectors by loss of CO_2 from $[M+CS+Cu-H]^+$. Table 2-5 summarizes the recognition results of the four types of amino acids. Overall, the heterochiral complex was more stable against dissociation than the homochiral complex for all investigated copper-bound dimers. The most significant result was obtained with Trp, and both copper-bound dimers and trimers were found, leading to distinctive MS/MS spectra between two diastereomers (Figure 2-23 and Figure 2-24). An outstanding CR value of 2.16 ± 0.04 was obtained with $[M+2Trp+Cu-H]^+$ dissociated into $[M+Trp+Cu-H]^+$. The interactions between clopidogrel and *L*-Trp are mainly coordination bonds with Cu(II), hydrogen bonds involving the NH or CO group, and π-π interactions involving the aromatic rings. The significant stereoselectivity may be induced by the larger steric effect of the *R*-clopidogrel phenyl ring, which led to weaker interactions with *L*-Trp. Overall, these results highlighted the potential for chiral discrimination of clopidogrel.

It is noteworthy that when Trp, Tyr and Phe were utilized as CSs for clopidogrel enantiomers, the loss of one or two CSs was found for the trimeric complex ion $[M+2CS+Cu-H]^+$, leading to the product ions of $[M+CS+Cu-H]^+$ and $[M+H]^+$, respectively. This suggested that in the precursor structures, clopidogrel was bound stronger than the two selectors. In contrast, in addition to the loss of CO_2, $[M+Cu-H]^+$ was also observed from $[M+CS+Cu-H]^+$ by losing one chiral selector (Figure 2-25). Such a phenomenon did not occur in ofloxacin or previous studies. Even though the obtained chiral discrimination was not significant enough, it was still worth discussing as it might help to explain the affinity of Cu(II) in complexes[137]. For example, the loss of Tyr from [M+Tyr+Cu−H]+ indicated the higher affinity of clopidogrel towards Cu(II)

than Tyr. However, ofloxacin had a similar affinity towards Cu(II) to Tyr. These might further demonstrate that clopidogrel has a higher affinity towards Cu(II) than ofloxacin.

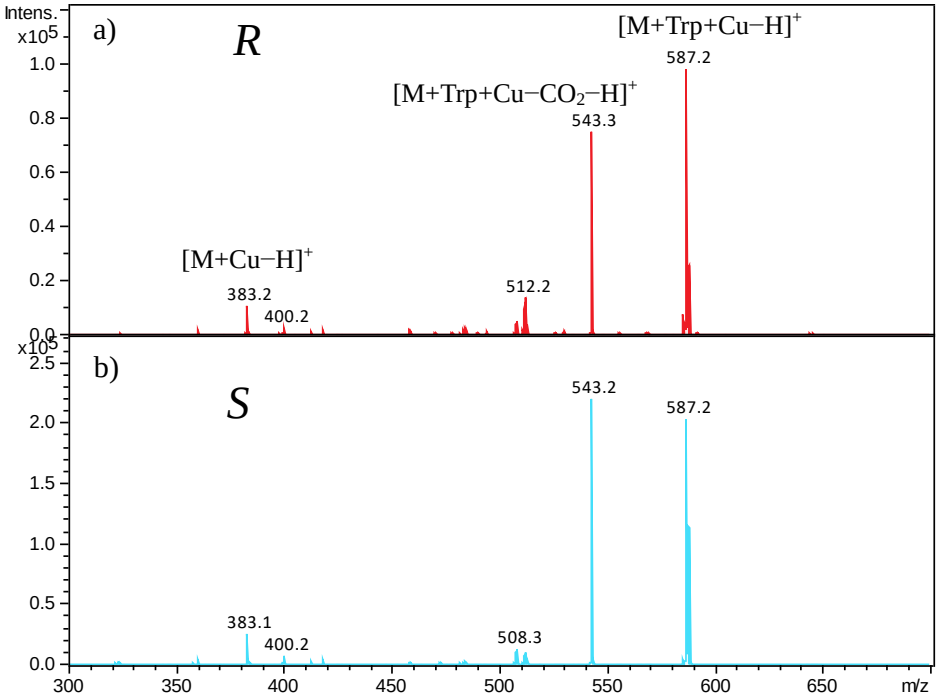

Figure 2-23. MS/MS spectra of *R*/*S*-clopidogrel on $[M+Trp+Cu-H]^+$.

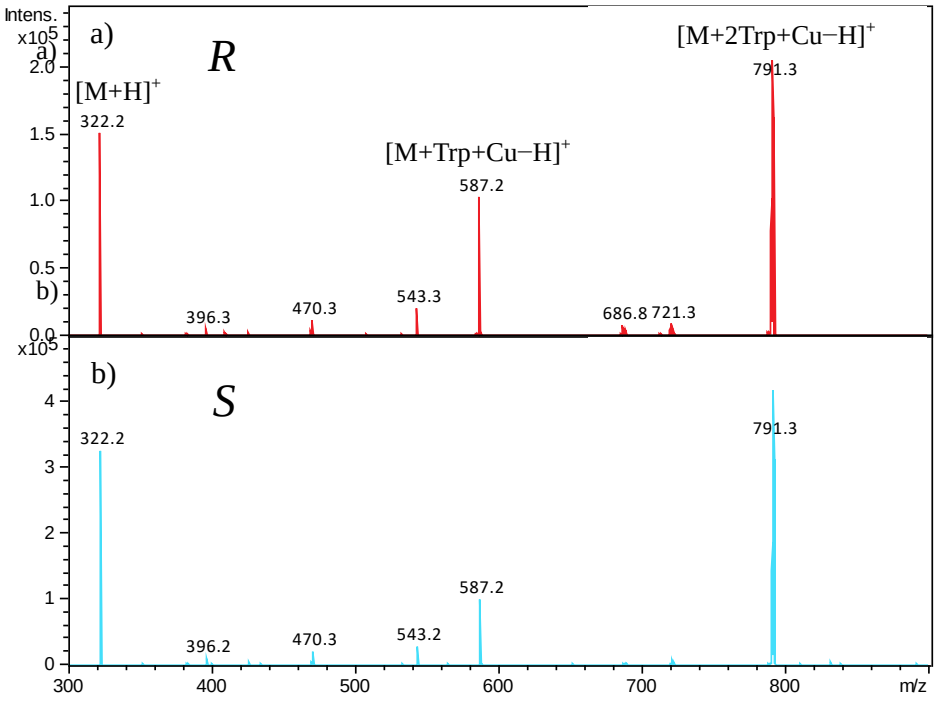

Figure 2-24. MS/MS spectra of *R*/*S*-clopidogrel on $[M+2Trp+Cu-H]^+$.

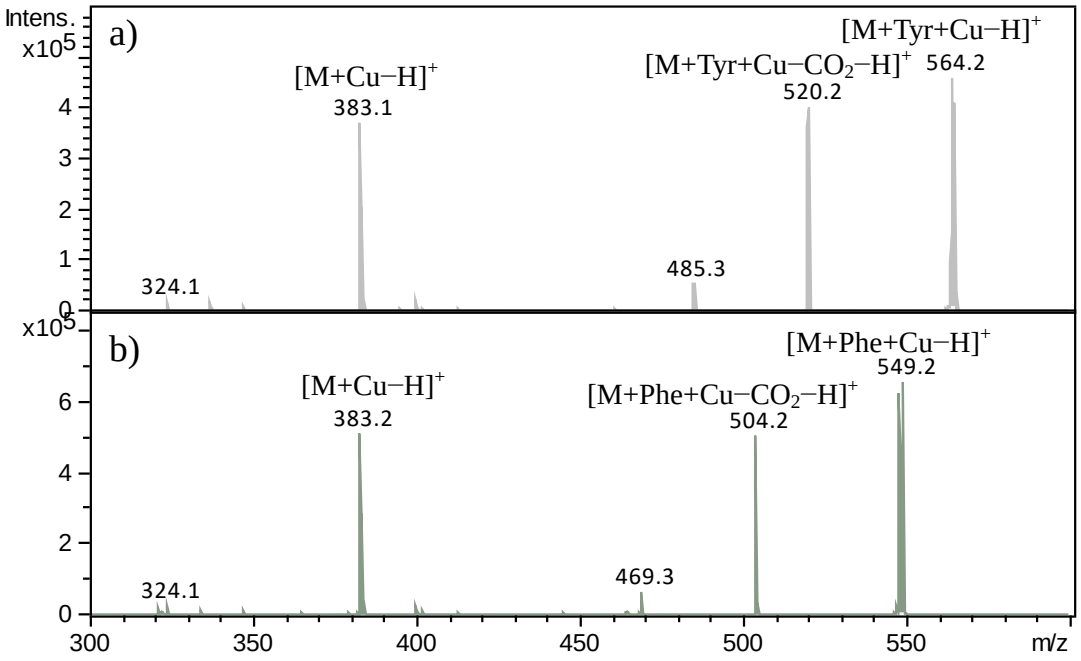

Figure 2-25. MS/MS spectra of *R*-clopidogrel on $[M+CS+Cu-H]^+$ by losing one chiral selector with a) Tyr and b) Phe as CS.

Table 2-5. The CR values of complex ions of clopidogrel and amino acids.

Chiral selector	**Precursor ion**	**Product ion**	**$CR_{R/S}$**
Trp	$[M+CS+Cu-H]^+$	$[M+CS+Cu-CO_2-H]^+$	0.70±0.02
		$[M+Cu-H]^+$	0.87±0.03
	$[M+2CS+Cu-H]^+$	$[M+CS+Cu-H]^+$	2.16±0.04
		$[M+H]^+$	0.92±0.01
Tyr	$[M+CS+Cu-H]^+$	$[M+CS+Cu-CO_2-H]^+$	0.82±0.01
		$[M+Cu-H]^+$	0.93±0.02
	$[M+2CS+Cu-H]^+$	$[M+CS+Cu-H]^+$	1.04±0.31
Phe	$[M+CS+Cu-H]^+$	$[M+CS+Cu-CO_2-H]^+$	0.82±0.03
		$[M+Cu-H]^+$	0.92±0.02
His	$[M+CS+Cu-H]^+$	$[M+CS+Cu-CO_2-H]^+$	0.98±0.04

2.3.5 Chiral recognition of omeprazole

Different from ofloxacin and clopidogrel, it was found that the addition of Cu(II) is not necessary for the formation of complex ions for omeprazole. Some amino acids (*L*-type) that have been widely applied in chiral analysis were chosen as selectors for the recognition of *R/S*-omeprazole, and diastereomers were formed, mostly sodium adduct dimers $[M+CS+Na]^+$, potassium adduct dimers $[M+CS+K]^+$ and trimers $[M+2CS+K]^+$. As no additional sodium ions or potassium ions were introduced into sample solutions, these probably came from the sample itself during the separation process of the racemate using chiral HPLC-MS. Figure 2-26 shows the CID spectra of the two dimers when Phe was utilized as the CS. Interestingly, loss of a Phe from $[M+Phe+Na]^+$ was observed, while for $[M+Phe+K]^+$, only loss of 148 Da was detected, which is neither a selector nor an analyte, indicating the intermolecular binding of $[M+Phe+K]^+$ was stronger than that of $[M+Phe+Na]^+$. According to the literature[138], the lost ion could be part of the omeprazole (Figure 2-27), reflecting that coordination sites of omeprazole in the complex ion may focus on the remaining part. For $[M+2Phe+K]^+$, loss of a Phe or omeprazole was obtained (Figure 2-26c), suggesting the looser binding within trimers than that within dimers. In addition to singly charged complex ions, doubly charged ions of $[2M+CS+Na+H]^{2+}$ were also detected (Figure 2-26d), especially when Trp, Phe, Pro and Tyr were employed as CSs, which contain a part of rigid structures.

The chiral recognition of omeprazole was evaluated by the CR value for all detected cluster ions for comparison. As shown in Table 2-6, among the chiral selectors that were tested, except for Trp, no significant enantioselectivity was obtained for the singly charged ions. Only $[M+Trp+Na]^+$ dissociated into $[M+Na]^+$ was found to have chiral discrimination (Figure 2-28) with a CR value of 1.26 ± 0.03. It's worth noting that

[M+Trp+Na]$^+$ had loose intermolecular binding, but had larger enantioselectivity towards omeprazole enantiomers than the potassium adduct dimers, which might be due to the loss of Trp had a greater influence on the spatial structure than the loss of -$C_8H_8N_2O$. For the doubly charged complexes, more remarkably enantiomeric differences were found with [M+2Phe+K+H]$^{2+}$ and [2M+Tyr+K+H]$^{2+}$, ranging from 0.59 to 0.27.

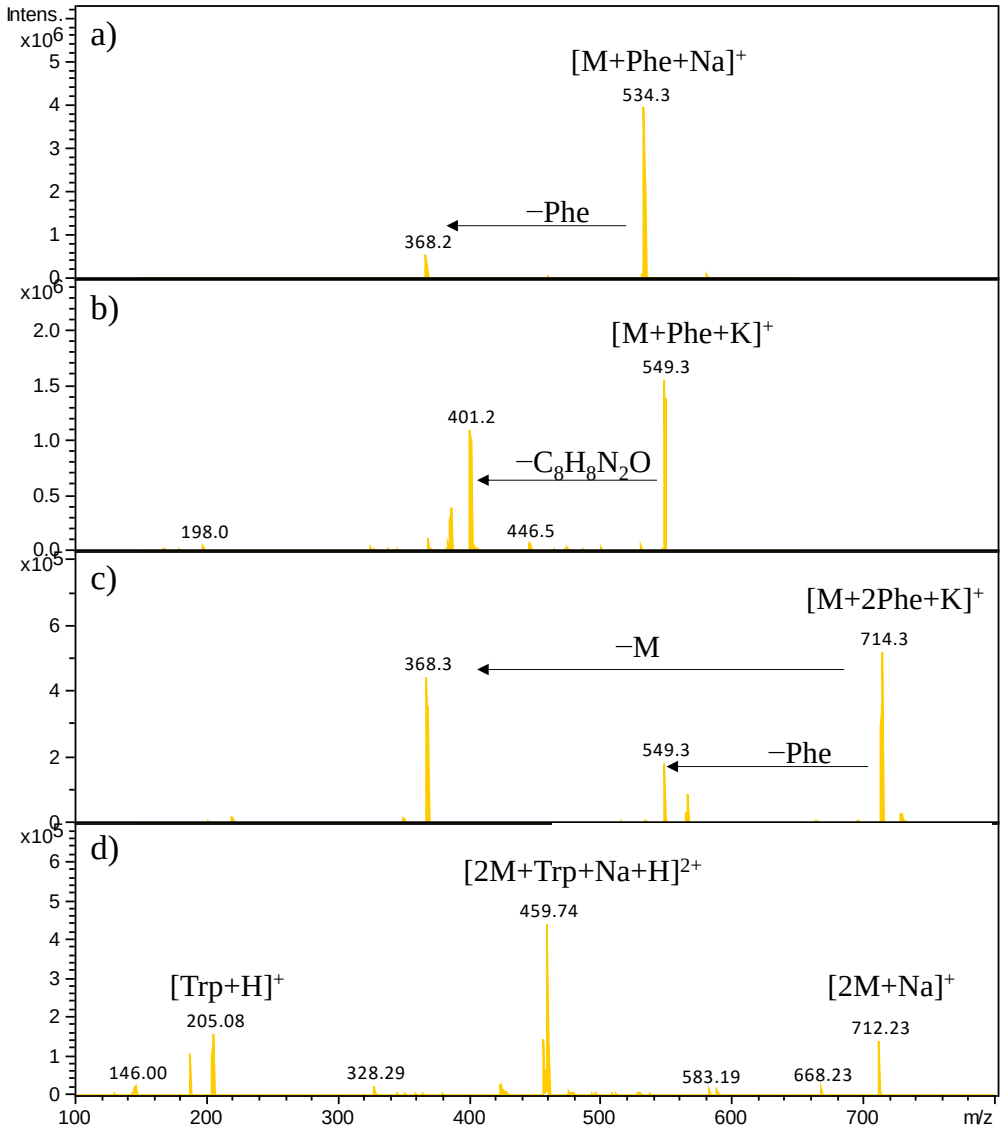

Figure 2-26. MS/MS spectra of omeprazole on the complex ions a) [M+Phe+Na]$^+$, b) [M+Phe+K]$^+$, c) [M+2Phe+K]$^+$, and d) [2M+Trp+Na+H]$^{2+}$.

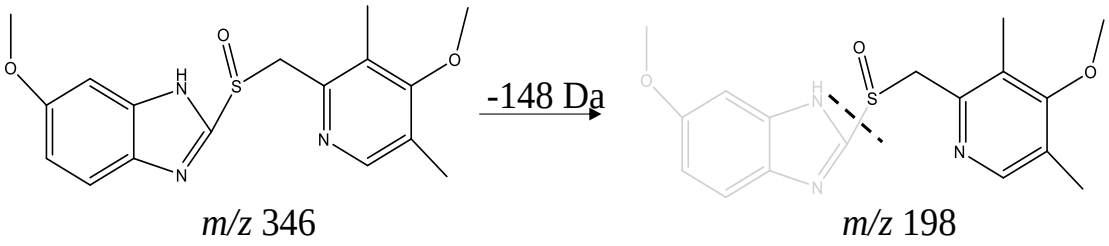

Figure 2-27. The dissociation of omeprazole by loss of 148 Da[138].

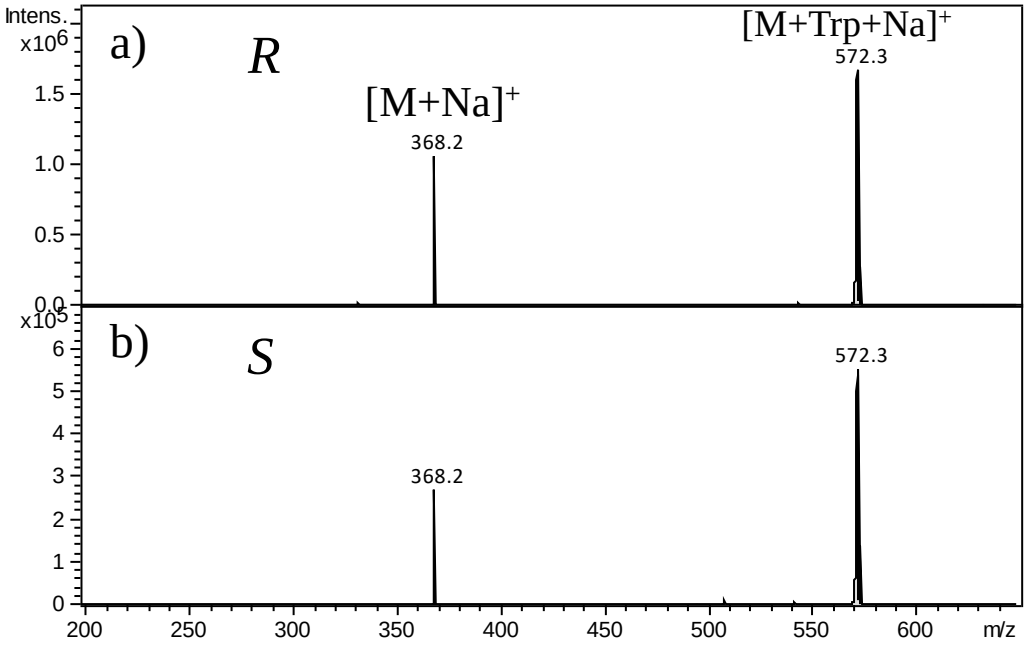

Figure 2-28. MS/MS spectra of *R/S*-omeprazole on $[M+Trp+Na]^+$.

Table 2-6. The CR values of complex ions of omeprazole using different amino acids as chiral selectors without copper-bound.

Chiral selector	Precursor ion	Product ion	CR
Trp	$[M+CS+Na]^+$	$[M+Na]^+$	1.26±0.03
	$[M+CS+K]^+$	$[M+CS+K-C_8H_8N_2O]^+$	0.98±0.01
	$[M+2CS+K]^+$	$[M+CS+K]^+$	0.97±0.01
	$[2M+CS+Na+H]^{2+}$	$[CS+H]^+$	1.16±0.05
		$[2M+Na]^+$	1.06±0.06
Ala	$[M+CS+Na]^+$	$[M+Na]^+$	1.18±0.08
	$[M+CS+K]^+$	$[M+CS+K-C_8H_8N_2O]^+$	1.01±0.01
	$[M+2CS+K]^+$	$[M+CS+K]^+$	0.95±0.03
Phe	$[M+CS+Na]^+$	$[M+Na]^+$	0.91±0.11
	$[M+CS+K]^+$	$[M+CS+K-C_8H_8N_2O]^+$	0.96±0.02
	$[M+2CS+K]^+$	$[M+CS+K]^+$	1.12±0.06
	$[M+2CS+K+H]^{2+}$	$[M+CS+K]^+$	0.27±0.15
		$[CS+H]^+$	0.29±0.15
Pro	$[M+CS+Na]^+$	$[M+Na]^+$	1.04±0.13
	$[M+CS+K]^+$	$[M+CS+K-C_8H_8N_2O]^+$	0.98±0.05
	$[M+2CS+K]^+$	$[M+CS+K]^+$	0.93±0.05
	$[2M+CS+K+H]^{2+}$	$[M+CS+K]^+$	0.96±0.12
		$[2M+K+H]^{2+}$	0.97±0.11
Ser	$[M+CS+Na]^+$	$[M+Na]^+$	0.94±0.09
	$[M+CS+K]^+$	$[M+CS+K-C_8H_8N_2O]^+$	0.93±0.02
	$[M+2CS+K]^+$	$[M+CS+K]^+$	1.06±0.01
Tyr	$[2M+CS+K+H]^{2+}$	$[M+H]^+$	0.50±0.21
		$[M+CS+K]^+$	0.59±0.17

2.3.6 Chiral recognition of bupivacaine

The structure of bupivacaine differs from the previously mentioned chiral drugs and possesses a complex and rigid linear portion. Initial experiments using amino acids or cyclodextrins as chiral selectors did not yield any chiral discrimination and it was difficult to detect complexes. However, an interesting observation was that bupivacaine could be clearly distinguished by self-assembly without the addition of any chiral selectors. The MS/MS spectral results of $[M+H]^+$ and self-assembly dimers $[2M+H]^+$ displayed minimal differences between the two diastereomers, as shown in Figure 2-31 and Figure 2-32, with CR values close to unity. However, for the self-assembly trimers $[3M+H]^+$, loss of bupivacaine was observed with distinct differences in the relative intensity of the product ion *m/z* 577.3 (Figure 2-33), resulting in significant chiral discrimination of bupivacaine with a CR value of 2.50 ± 0.12. One possible explanation of the consequence could be that when the number of assemblies increased, the difference in spatial structures between the two diastereomers also increased, which led to different dissociation patterns of $[3M+H]^+$.

In addition, Ieritano, Christian, et al.[139] found the phenomenon of protonation-induced chirality when investigating verapamil, whereby the tertiary amine was bound to three different substituents, and the protonation would induce an extra chiral center at the tertiary amine, transferring the enantiomers to diastereomers as illustrated in Figure 2-29. This additional chiral center induced by protonation allowed for differentiation of the enantiomers using ion mobility mass spectrometry, due to the different structures of the two diastereomers resulted in different mobility in the gas phase. Similar to verapamil, bupivacaine also features a tertiary amine connected to three different substituents, and we hypothesized that the protonation of bupivacaine might also

generate extra chiral centers. For example, the *R*-bupivacaine is protonated to form (*R*, *R*) and (*S*, *S*) diastereomers (Figure 2-30). This could potentially facilitate chiral discrimination using ion mobility mass spectrometry. Although direct analysis of two protonated enantiomers by ion trap mass spectrometry without separation is still not possible, the introduction of protonation could offer more chiral centers for complex ion formation, for example, four chiral centers for $[3M+H]^+$, (*R*, *R*, *R*, *R*) and (*R*, *R*, *R*, *S*), thereby improving chiral recognition.

To validate the hypothesis of larger spatial differences or of the *N*-protonation induced chiral center that led to the differentiation of bupivacaine, further confirmation by using IM-MS, standard Gibbs energies, computational model and Gaussian calculation is necessary. More compounds showing similar chemical structures with a tertiary amine, e.g., ofloxacin and clopidogrel, will be studied to make a systematic study using both MS/MS and IM-MS in our future study.

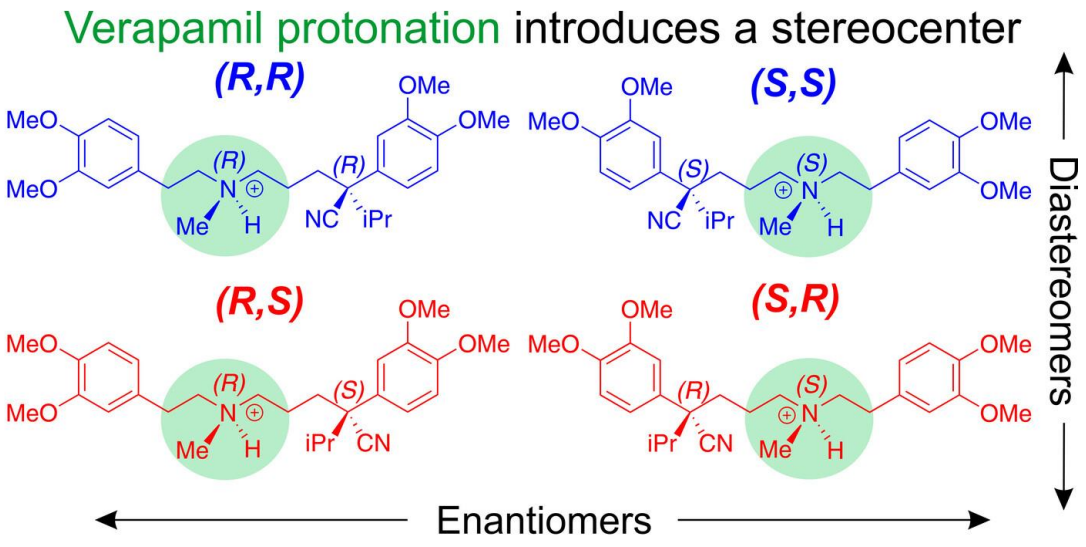

Figure 2-29. The protonation of *R/S*-verapamil at the tertiary amine[139].

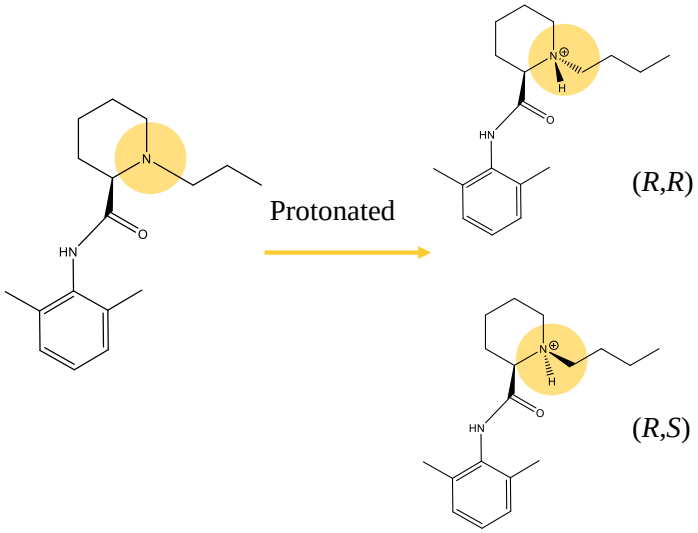

Figure 2-30. The protonation of *R/S*-bupivacaine at the tertiary amine.

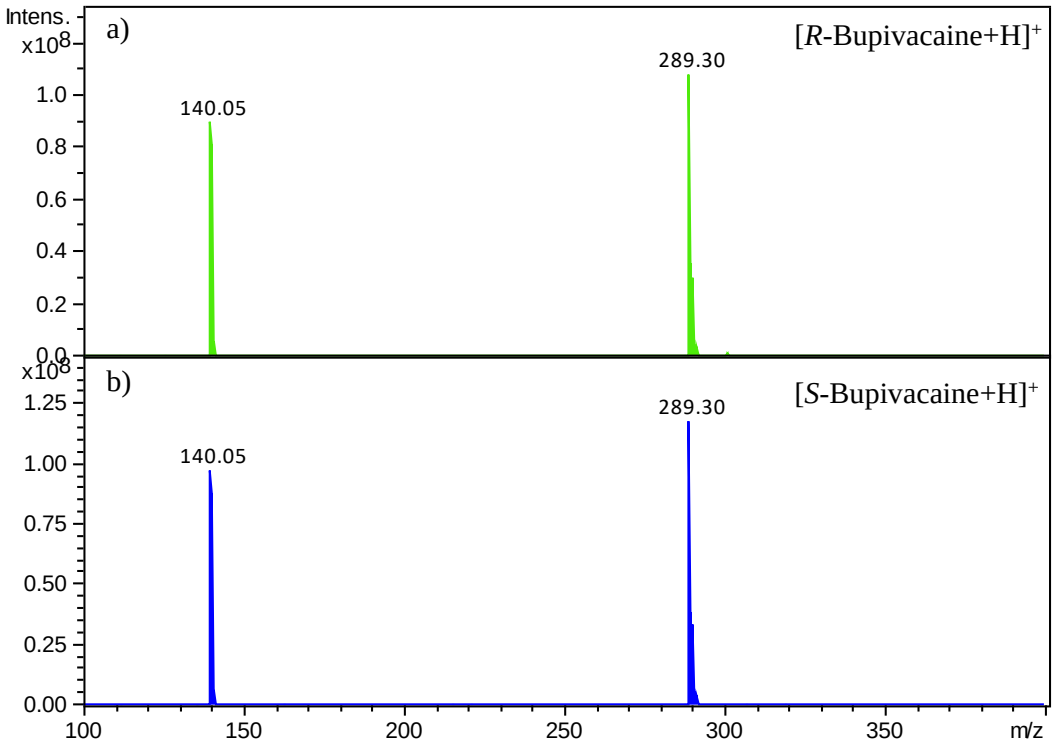

Figure 2-31. MS/MS spectra of [*R/S*-bupivacaine+H]$^+$.

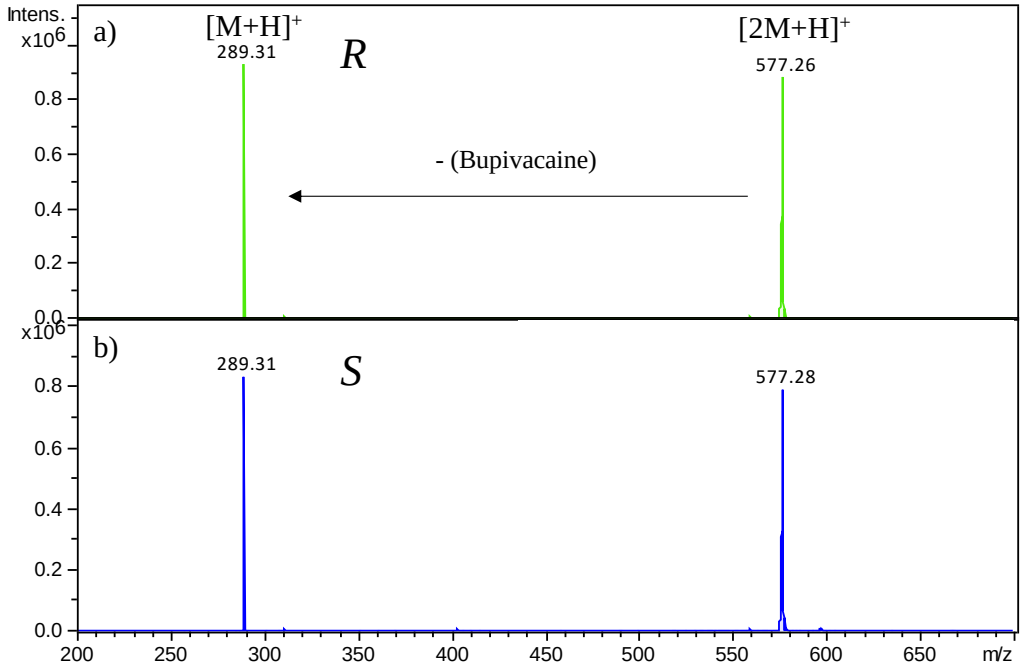

Figure 2-32. MS/MS spectra of *R*/*S*-clopidogrel on $[2M+H]^+$.

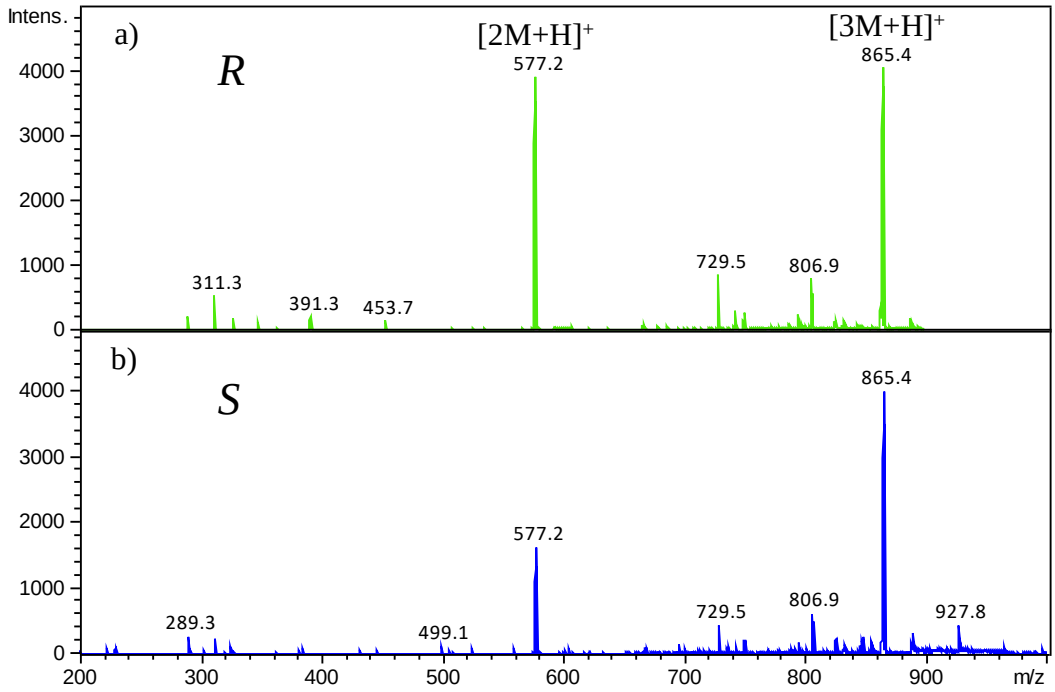

Figure 2-33. MS/MS spectra of *R*/*S*-clopidogrel on $[3M+H]^+$.

2.4 Conclusions

The analysis of chirality in drugs is crucial in pharmaceutical development, and it may also help to explain the mechanisms of biological activities of chiral drugs in the biological environment. In this chapter, tandem mass spectrometry was employed to analyze three drugs by introducing various chiral selectors and metal ions to form complexes. Cu(II) showed the best performance as it helped the formation of a wider range of diastereomeric ions. The selection of chiral selectors depended on the structure of chiral drugs. For ofloxacin, chiral recognition was achieved with Pro and Tyr as chiral selectors, and the most significant result was obtained when $[M+2Tyr+Cu-H]^+$ was dissociated into $[M+Tyr+Cu-H]^+$ with a CR value of 0.85 ± 0.02. Based on this, a standard calibration curve for quantifying enantiomeric purities of ofloxacin was established with an excellent linear coefficient of 0.9897. In the case of clopidogrel, chiral selectors that resulted in chiral recognition were different from ofloxacin, which were Trp, Tyr and Phe. This is mainly due to its more dimensional 3D structure, which facilitated π-π stackings and therefore improved chiral analysis. A significant CR value of 2.16 ± 0.04 was obtained when the timers $[M+2Trp+Cu-H]^+$ dissociated into $[M+Trp+Cu-H]^+$. For omeprazole, various complexes, including singly charged ions and doubly charged ions, were observed even without Cu(II) ions. An outstanding CR value of 0.27 ± 0.15 was obtained by dissociating $[M+2CS+K+H]^{2+}$ into $[M+CS+K]^+$. Bupivacaine exhibited a completely different phenomenon. Without any chiral selectors, bupivacaine enantiomers were well discriminated by the self-assembly trimers $[3M+H]^+$ in MS/MS, with a significant CR value of 2.50 ± 0.12. We hypothesized that either the larger spatial differences in higher assembly diastereomeric ions or the protonation at the tertiary amine inducing an additional chiral center led to the chiral analysis of bupivacaine. We will take insights into this in the following study.

This work provided a unique insight into the chiral analysis of drugs with different structures. The MS/MS approach proved to be effective in differentiating all the tested drugs, and the method applied was simple, straightforward and rapid. This MS/MS-based method can apply to the differentiation of other chiral compounds as well. Further confirmation with the help of standard Gibbs energies, computational model and Gaussian calculation is necessary to better understand the structure of these complexes.

Chapter 3. A Systematical Study of Chiral Analysis-Omeprazole as An Example

3.1 Introduction

The previous results in Chapter 2 indicated that the chiral recognition of drugs could be achieved using our method based on MS/MS. In addition to simply achieving the chiral discrimination, a systematical study that can provide general instructions for chiral analysis is an important issue. For example, the selection of chiral selectors for different types of chiral compounds or a universal kind of selectors that can be applied to most chiral compounds.

Omeprazole is a chiral drug with a complex chemical structure that has been rarely studied. According to Chapter 2, among the four drugs, more types of diastereomeric complexes containing omeprazole could be detected, and the best chiral recognition result was obtained as 0.27 ± 0.15. Herein, it was employed as a prime example. To conduct a comprehensive investigation into chiral effects and find out general principles, we initiated our research with amino acids due to their low cost and various structures that are easy to modify. We then explored the use of both single amino acids and combinations of two amino acids, as well as peptides, as chiral selectors, with or without the addition of copper ions. The chiral environment created by these selectors varied, leading to distinct chiral effects in terms of recognition. Peptides, in particular, have been little reported as selectors for chiral analysis, and we believe that peptides hold immense potential due to their ability to be designed in diverse configurations, enabling them to accommodate different types of chiral compounds. The strategy of using peptides as chiral selectors was extended to the analysis of other chiral drugs.

3.2 Experimental

3.2.1 Chemicals

Methanol (HPLC grade) was obtained from Anaqua Chemical Supply (Houston, USA). Milli-Q water was produced from a Milli-Q water purification system (Millipore, Bedford, MA, USA). *L*-Amino acids (proline, tyrosine, threonine, and phenylalanine) were purchased from Macklin (Shanghai, China). *L*-Amino acids (leucine, tryptophan, histidine, and alanine), and the metal salt of copper(II) nitrate were purchased from Sigma-Aldrich (St. Louis, USA). *L*-Dipeptides (Pro-Ala, Trp-Ala, Phe-Ala, Glu-Ala, His-Ala, Thr-Ala, Leu-Ala, His-Ser, His-Phe, Gly-Phe, Gly-Pro, Gly-Ala, Gly-Glu, Gly-Asp and Pro-Gly) were purchased from Sigma-Aldrich (St. Louis, USA).

3.2.2 Sample preparation and mass spectrometry

This was just the same as described in Chapter 2.

3.3 Results and discussion

3.3.1 One amino acid without the copper-bound

This part of the study has been discussed in Chapter 2. Overall, only Trp was found to be an ideal chiral selector for the discrimination of omeprazole enantiomers.

3.3.2 One amino acid with the copper-bound

In the absence of copper ions in the solution, some amino acids have demonstrated optimal chiral selectivity for omeprazole. Metal ions, such as Ni(II), Co(II), Mg(II), Zn(II) and Cu(II), have been recognized for their great impact on chiral analysis because they can enhance interactions within complexes. Given the superior performance of Cu(II) compared to other metal ions[113], copper ions were also applied in this study for

comparison.

When amino acids e.g., Ser and Ala, were used as selectors, no copper-bound diastereomers containing the selector and omeprazole were observed. However, when Trp, Phe and Pro were utilized, some doubly charged copper-bound cluster ions, $[2M+CS+Cu+Na-H]^{2+}$, $[2M+2CS+Cu+K-H]^{2+}$, $[M+2CS+Cu+K-H]^{2+}$, and $[3M+2CS+Cu+K-H]^{2+}$ were detected. This could be attributed to the presence of a rigid ring in the side chain of these three amino acids. Both Trp and Phe possess aromatic rings that can engage in strong π-π stacking interactions with omeprazole. On the other hand, Pro and Trp exhibit an imidazole ring and a pyrrolidine loop, which can form robust coordination with copper ions, detailed structural information needs to be further confirmed.

A typical CID spectrum of these doubly charged copper-containing ions was illustrated in Figure 3-1, revealing the loss of various moieties and the generation of multiple product ions. These product ions could be used for the evaluation of CR values. As displayed in Table 3-1, compared with amino acids without copper-bound, here, enantioselectivity was only observed with Trp, and no chiral discrimination was caused by Pro or Phe. This further confirmed the outstanding ability of Trp to achieve chiral recognition of omeprazole. The most significant finding was the dissociation of $[2M+2Trp+Cu+K-H]^{2+}$, leading to the formation of $[M+2Trp+Cu+K-2H]^{+}$, resulting in a CR value of 0.41 ± 0.07. It might be due to the complicated spatial arrangement of $[2M+2Trp+Cu+K-H]^{2+}$ so that when the chirality of omeprazole changed, the induced chiral effect was substantial enough for the chiral discrimination.

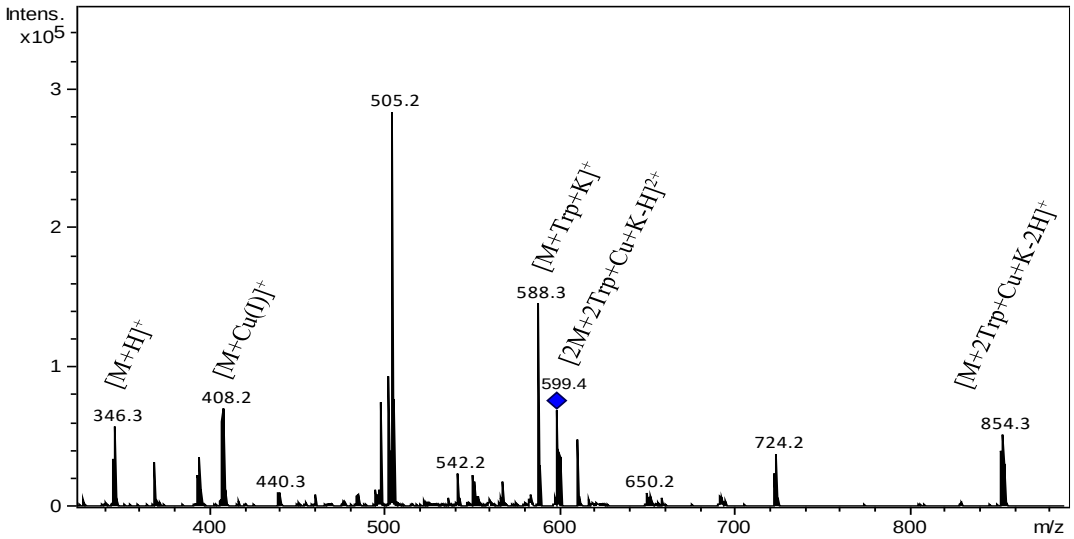

Figure 3-1. MS/MS spectra of omeprazole on $[2M+2Trp+Cu+K-H]^{2+}$.

Table 3-1. The significant CR values of complex ions of omeprazole using different amino acids as chiral selectors with copper-bound.

Chiral selector	Precursor ion	Product ion	CR
Trp	$[M+3CS+Cu+K-H]^{2+}$	$[M+H]^+$	1.11 ± 0.02
		$[3CS+Cu+K-2H]^+$	1.11 ± 0.02
	$[2M+2CS+Cu+K-H]^{2+}$	$[M+H]^+$	0.46 ± 0.09
		$[M+CS+K]^+$	0.60 ± 0.10
		$[M+CS+Cu-H]^+$	0.58 ± 0.17
		$[M+2CS+Cu+K-2H]^+$	0.41 ± 0.07
	$[3M+2CS+Cu+K-H]^{2+}$	$[M+H]^+$	1.21 ± 0.11
		$[2M+2CS+Cu+K-2H]^+$	1.31 ± 0.12
Phe	$[2M+CS+Cu+Na-H]^{2+}$	$[M+H]^+$	1.07 ± 0.13
	$[2M+2CS+Cu+K-H]^{2+}$	$[2M+CS+Cu+K-H]^{2+}$	0.81 ± 0.13
		$[M+CS+K]^+$	0.83 ± 0.10
		$[M+CS+Cu-H]^+$	1.46 ± 0.47

3.3.3 Combination of two amino acids as the chiral selectors without copper-bound

The selection of chiral selectors towards omeprazole using a single amino acid was very limited. Systematical studies involving two amino acids have not been reported, and we assumed that combining different kinds of amino acids may create a completely different chiral environment, leading to enhanced chiral effects and improved chiral discrimination.

In this study, the combination of two amino acids as selectors was initially examined without adding any copper ions. As summarized in Table 3-2, three sets of combinations of two amino acids were tested, with one amino acid fixed (histidine, alanine, or phenylalanine) and the other changed. The selection of the other amino acids includes those with linear or rigid side chains. In all combinations, potassium adduct dimers $[M+CS1+CS2+K]^+$ could be detected, except for His+Phe and His+Tyr (the intensity of the cluster ion was low and unstable). When applying the dissociation energy, the loss of amino acids rather than omeprazole was obtained, illustrating that omeprazole has a stronger binding than the selectors within the cluster.

Notably, when His was fixed, the loss of another amino acid was always observed (Figure 3-2). Even in the case where both amino acids were dissociated, for example, when $[M+His+Ser+K]^+$ was dissociated to $[M+His+K]^+$ and $[M+Ser+K]^+$, the intensity of the latter was much higher (Figure 3-3a). These results indicated that His was more stable against dissociation compared to the other investigated amino acids, which was likely attributed to the imidazole ring in the side chain of histidine that provides the strong coordination site. On the other hand, when Ala was fixed, the loss of Ala was

consistently observed. Similarly, when $[M+Ala+Leu+K]^+$ was dissociated to $[M+Ala+K]^+$ and $[M+Leu+K]^+$, the intensity of the former was much higher (Figure 3-3b), implying that Ala was easier to dissociate than the others. However, if fixing Phe, the loss of amino acid depended. For example, Ala, Ser, Leu and Pro were lost, but Thr, Trp and Tyr were left (Figure 3-4). The results demonstrated different binding affinities of two amino acids in the precursor ion. Based on these findings, a possible order of binding affinity of amino acids towards omeprazole-containing potassium adduct dimers may be derived: His > Thr/Trp/Tyr > Phe > Ser/Leu/Pro > Ala, which could provide a strategy for selecting the combinations of two amino acids as chiral selectors in this study. The chiral recognition results were then summarized in Table 3-2, as shown, only four combinations of two amino acids resulted in significant discrimination of omeprazole: His+Ala, His+Leu, His+Thr and Phe+Trp (highest+lowest, or two higher ones). As previously mentioned, His alone showed no enantioselectivity towards omeprazole. However, when together with another AA, e.g., Ala, Leu and Thr, chiral analysis of omeprazole could be achieved. This is possibly due to the more side chains that provide binding sites, as well as the specific chiral environment. The combination of two amino acids as chiral selectors demonstrated the possibility for the analysis of chiral compounds.

To further investigate the dissociation process, MS^3 was performed based on the MS/MS consequences (Figure 3-5). Take His+Ala as an example, the product ion of $[M+His+K]^+$ from $[M+His+Ala+K]^+$ was isolated and dissociated in the IT-MS, which then led to the ion of *m/z* 391.2 by losing 148Da, consistent with the aforementioned results with one amino acid as the CS. A possible explanation could be that after losing an amino acid, the rest part of the original trimers would reorganize in structure, so as

to be similar to the dimers. A study to have a deep examination will be done in the future.

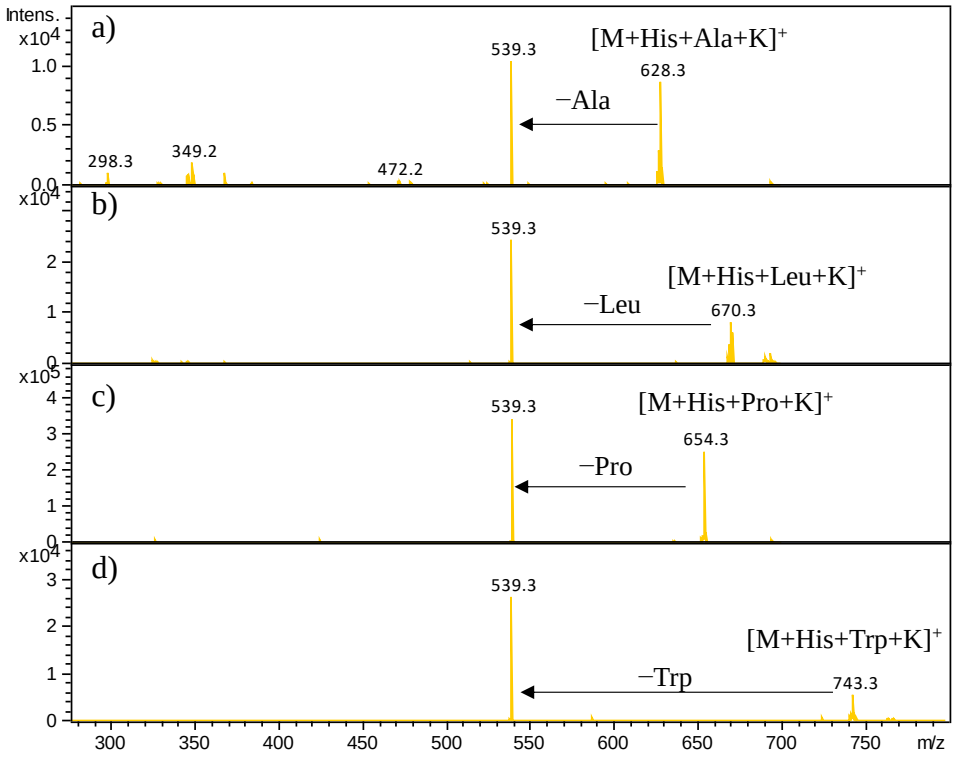

Figure 3-2. MS/MS spectral results of omeprazole on a) $[M+His+Ala+K]^+$, b) $[M+His+Leu+K]^+$, c) $[M+His+Pro+K]^+$and d) $[M+Ala+Trp+K]^+$.

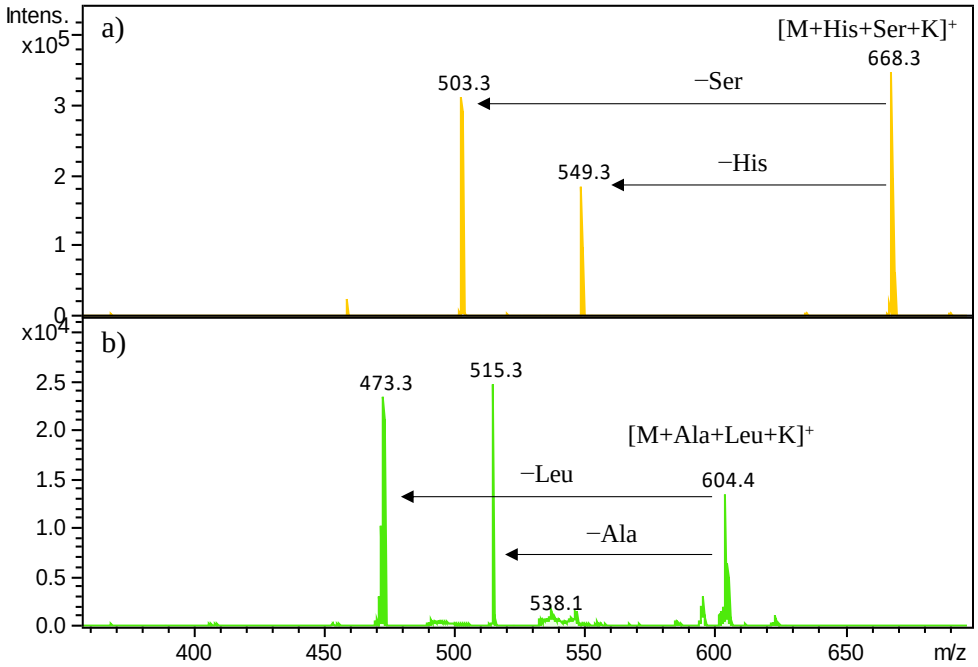

Figure 3-3. MS/MS spectral results of omeprazole on a) $[M+His+Ser+K]^+$ and b) $[M+Ala+Leu+K]^+$.

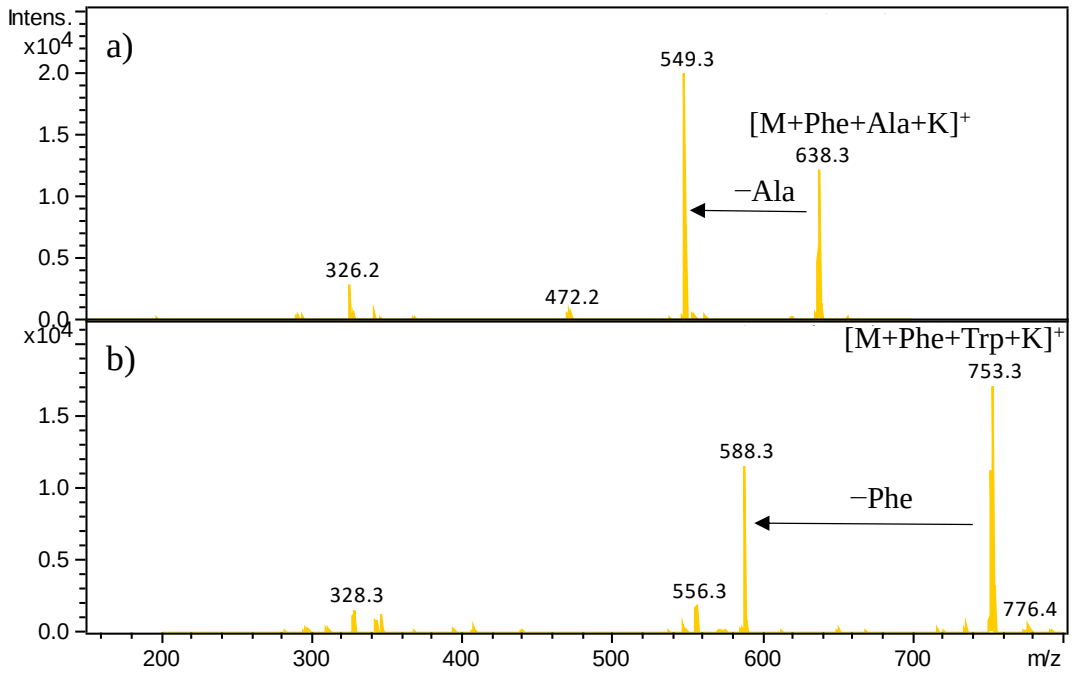

Figure 3-4. MS/MS spectral results of omeprazole on a) $[M+Phe+Ala+K]^+$ and b) $[M+Phe+Trp+K]^+$.

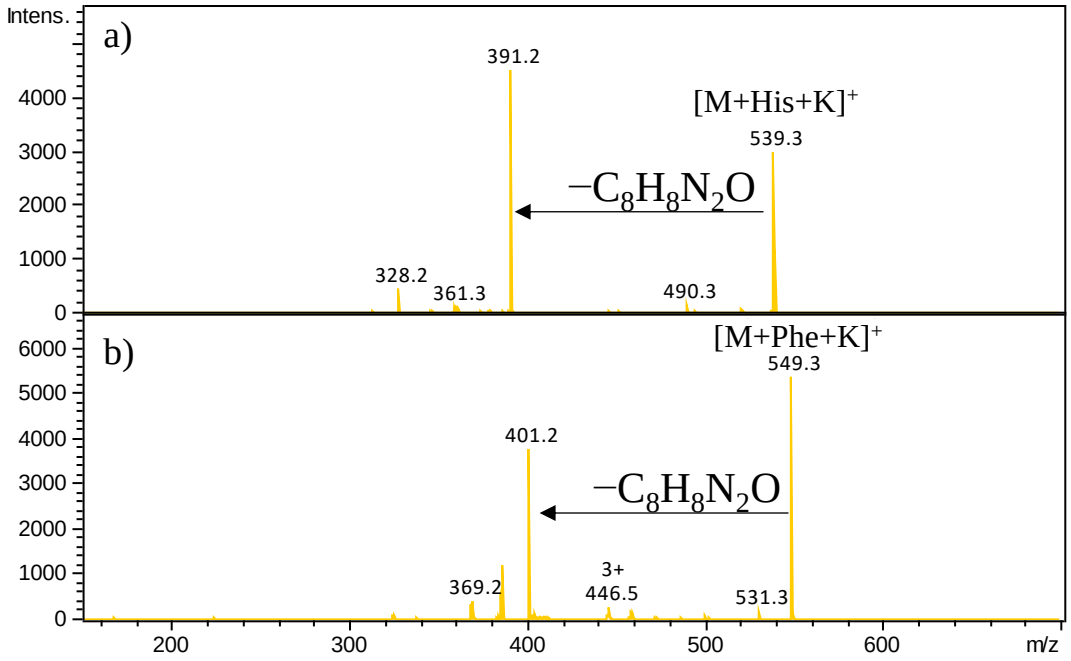

Figure 3-5. MS^3 spectral results of omeprazole on the product ions a) $[M+His+K]^+$ and b) $[M+Phe+K]^+$ obtained from MS^2.

Table 3-2. The CR values of complex ions $[M+CS1+CS2+K]^+$ of omeprazole using different combinations of two amino acids as two chiral selectors.

Two amino acids	Precursor ion	Product ion	CR
His+Ser	$[M+His+Ser+K]^+$	$[M+His+K]^+$	1.06±0.04
		$[M+Ser+K]^+$	0.94±0.12
His+Ala	$[M+His+Ala+K]^+$	$[M+His+K]^+$	1.51±0.08
His+Leu	$[M+His+Leu+K]^+$	$[M+His+K]^+$	0.67±0.04
His+Thr	$[M+His+Thr+K]^+$	$[M+His+K]^+$	1.17±0.01
His+Trp	$[M+His+Trp+K]^+$	$[M+His+K]^+$	1.03±0.04
His+Pro	$[M+His+Pro+K]^+$	$[M+His+K]^+$	0.91±0.03
His+Phe	NA	NA	NA
His+Tyr	NA	NA	NA
Ala+Ser	$[M+Ala+Ser+K]^+$	$[M+Ser+K]^+$	1.02±0.02
Ala+Leu	$[M+Ala+Leu+K]^+$	$[M+Leu+K]^+$	1.07±0.07
		$[M+Ala+K]^+$	1.04±0.05
Ala+Thr	$[M+Ala+Thr+K]^+$	$[M+Thr+K]^+$	1.08±0.04
Ala+Tyr	$[M+Ala+Tyr+K]^+$	$[M+Tyr+K]^+$	1.01±0.03
Ala+Pro	$[M+Ala+Pro+K]^+$	$[M+Pro+K]^+$	1.12±0.09
		$[M+Ala+K]^+$	1.16±0.07
Ala+His	$[M+Ala+His+K]^+$	$[M+His+K]^+$	1.51±0.08
Ala+Phe	$[M+Ala+Phe+K]^+$	$[M+Phe+K]^+$	1.17±0.07
Phe+Ala	$[M+Phe+Ala+K]^+$	$[M+Phe+K]^+$	1.17±0.07
Phe+Thr	$[M+Phe+Thr+K]^+$	$[M+Phe+K]^+$	1.26±0.03
		$[M+Thr+K]^+$	1.26±0.03
Phe+Ser	$[M+Phe+Ser+K]^+$	$[M+Phe+K]^+$	1.02±0.05
		$[M+Ser+K]^+$	1.06±0.01
Phe+Leu	$[M+Phe+Leu+K]^+$	$[M+Phe+K]^+$	1.02±0.01
Phe+Trp	$[M+Phe+Trp+K]^+$	$[M+Trp+K]^+$	1.53±0.07
Phe+Pro	$[M+Phe+Pro+K]^+$	$[M+Phe+K]^+$	0.94±0.01
Phe+Tyr	$[M+Phe+Tyr+K]^+$	$[M+Tyr+K]^+$	1.02±0.09

3.3.4 Combination of two amino acids as the chiral selectors with copper-bound

Again, Cu(II) was added to the mixture to test the coordination abilities of two amino acids as selectors. When combinations of two amino acids were applied, no copper-bound complex ions containing two AAs and omeprazole were observed for most cases. Diastereomers of $[CS1+CS2+Cu-H]^+$ tended to be detected, suggesting that Cu(II) was easier to coordinate with amino acids than with omeprazole. When Trp+Pro, Phe+His, and Phe+Trp were investigated, copper-bound trimers $[M+CS1+CS2+Cu-H]^+$ were detected as shown in Figure 3-6, possibly due to strong π-π interactions between omeprazole and these amino acids. Under CID, the corresponding product ions could be formed by losing either CS1 or CS2. Figure 3-6 shows an example of a CID spectrum of $[M+Phe+Trp+Cu-H]^+$, with the loss of Phe and Trp to form $[M+Trp+Cu-H]^+$ and $[M+Phe+Cu-H]^+$, respectively. However, there were large variations in the relative intensity of the MS/MS spectra (Figure 3-7), reflecting that the complex ions were unstable and prone to dissociation because of the loose intermolecular binding, resulting in no significant chiral discrimination results.

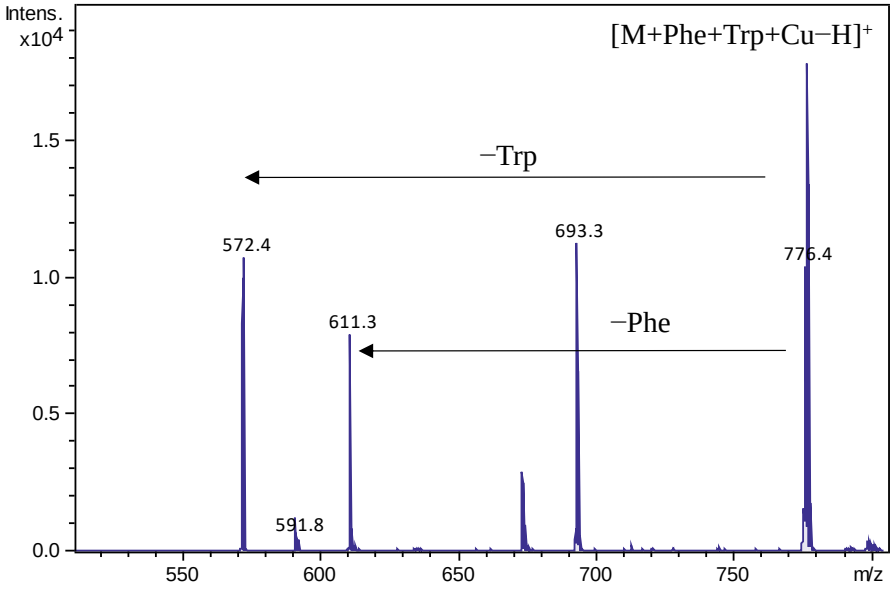

Figure 3-6. A MS/MS spectrum of omeprazole on $[M+Phe+Trp+Cu-H]^+$.

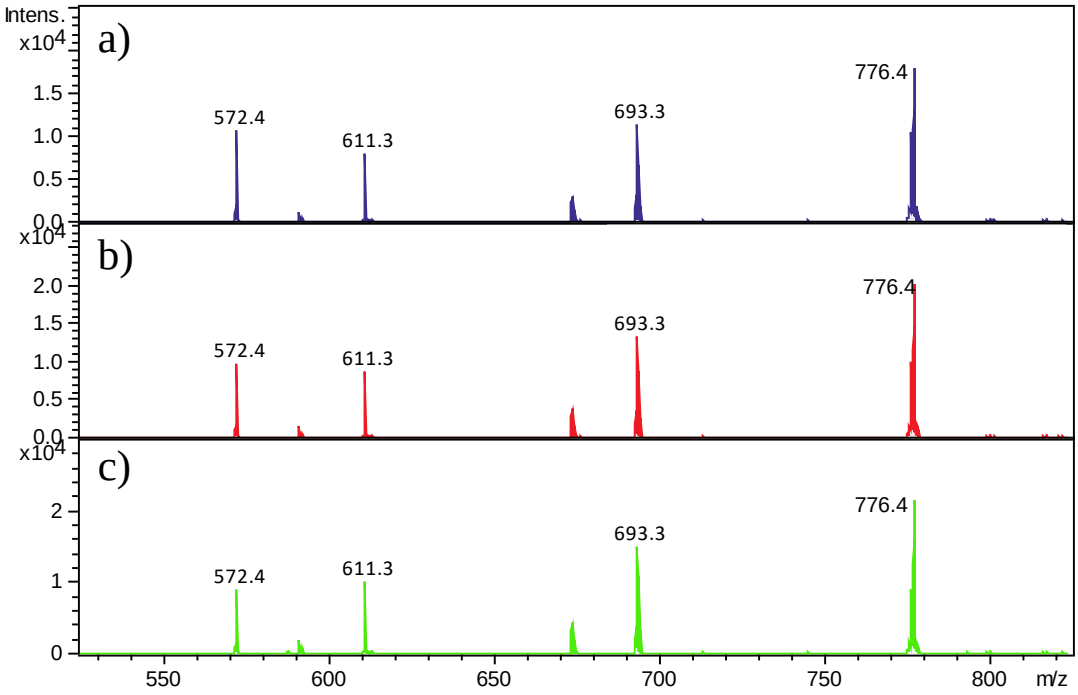

Figure 3-7. Three replicates of MS/MS spectra of $[M+Phe+Trp+Cu-H]^+$.

Table 3-3. The CR values of complex ions of omeprazole using different combinations of two amino acids as two chiral selectors with copper-bound.

Two amino acids	**Precursor ion**	**Product ion**	**CR**
Trp+Pro	$[M+Trp+Pro+Cu-H]^+$	$[M+Trp+Cu-H]^+$	1.20±0.14
Phe+His	$[M+Phe+His+Cu-H]^+$	$[M+His+Cu-H]^+$	0.86±0.09
Phe+Trp	$[M+Phe+Trp+Cu-H]^+$	$[M+Trp+Cu-H]^+$	0.44±0.17
	$[M+Phe+Trp+Cu-H]^+$	$[M+Phe+Cu-H]^+$	0.93±0.03

3.3.5 Peptides as chiral selectors without copper-bound

Experimentally, the above results have demonstrated that two amino acids as chiral selectors are better than one amino acid as one chiral selector, which could be a possible strategy for the differentiation of chiral compounds. Still, the choice is very limited, and among the combinations, only four of them allowed the identification of omeprazole enantiomers. Based on the idea of using two separate amino acids, we hypothesized that the linked amino acids may provide a further enhanced chiral effect. Compared with two separated compounds, the linkage between two AAs by peptide bonds makes the structure more compact, which may further enhance the intermolecular binding of complex ions. Thus, peptides were investigated in this study.

The main advantage of peptides is that they are robust and versatile, then can be easily synthesized and designed by selecting different types of amino acids, with various structures, and can be modified at different residues. Except for as an individual chiral selector used in MS/MS, peptides can also be easily attached to the LC column, expanding the designation of chiral columns. Unlike two chiral amino acids, which have four different types of combinations, CS1 (*L*) + CS2 (*L*), CS1 (*D*) + CS2 (*D*), CS1 (*L*) + CS2 (*D*), and CS1 (*D*) + CS2 (*L*), for a dipeptide, there can be eight possibilities, as the order of amino acids can change as well (Figure 3-8). We first have insights into *L*-*L* dipeptides.

For comparison, a series of dipeptides were studied with one of the amino acids fixed as Ala: Pro-Ala, Trp-Ala, Phe-Ala, His-Ala, Thr-Ala, Glu-Ala and Arg-Ala. The structures of the dipeptides are displayed in Figure 3-9. Interestingly, for each dipeptide, more diastereomers could be detected than using one or two amino acids, both singly

and doubly charged ions, such as $[M+CS+Na]^+$, $[M+CS+K]^+$, $[M+2CS+K]^+$, $[2M+CS+K]^+$, $[M+CS+K+H]^{2+}$ and $[M+CS+Na+H]^{2+}$. The most observed one was the doubly charged potassium adduct dimer $[M+CS+K+H]^{2+}$, the most observed product of which was $[M+H]^+$. Figure 3-10 shows the MS/MS spectra of $[M+CS+K+H]^{2+}$ with different dipeptides as CSs. The results confirm that the two enantiomers were clearly distinguished using peptides as chiral selectors. As detailed in Table 3-4, for Pro-Ala, Trp-Ala, Phe-Ala and Glu-Ala, enantioselectivity was obtained with CR values ranging from 1.24 ± 0.04 to 0.33 ± 0.04, however, no significant consequences were achieved when using combinations of two amino acids Pro+Ala, Trp+Ala and Phe+Ala. Though for His-Ala, Thr-Ala and Arg-Ala, their corresponding CR values for $[M+H]^+$ were almost close to 1.00, they can still discriminate omeprazole enantiomers by $[M+CS+K]^+$ or $[M+CS+Na]^+$. According to the experimental results, dipeptides served as ideal chiral selectors toward omeprazole when looking into other diastereomeric complex ions. For example, a clear difference was obtained between two enantiomers with $[M+His\text{-}Ala+Na]^+$ dissociated to $[M+Na]^+$. For the above six dipeptides, there were always certain complex ions that could be used for the chiral discrimination of omeprazole. The most discriminative result was obtained with *L*-Trp-*L*-Ala as the chiral selector, which has various sites for hydrogen bonds, a side chain indole for π interactions and a flexible alanine that can adjust to analytes. Due to the different spatial arrangements of the phenyl ring of the analyte, the interactions between the dipeptide and two omeprazole enantiomers could be significantly influenced.

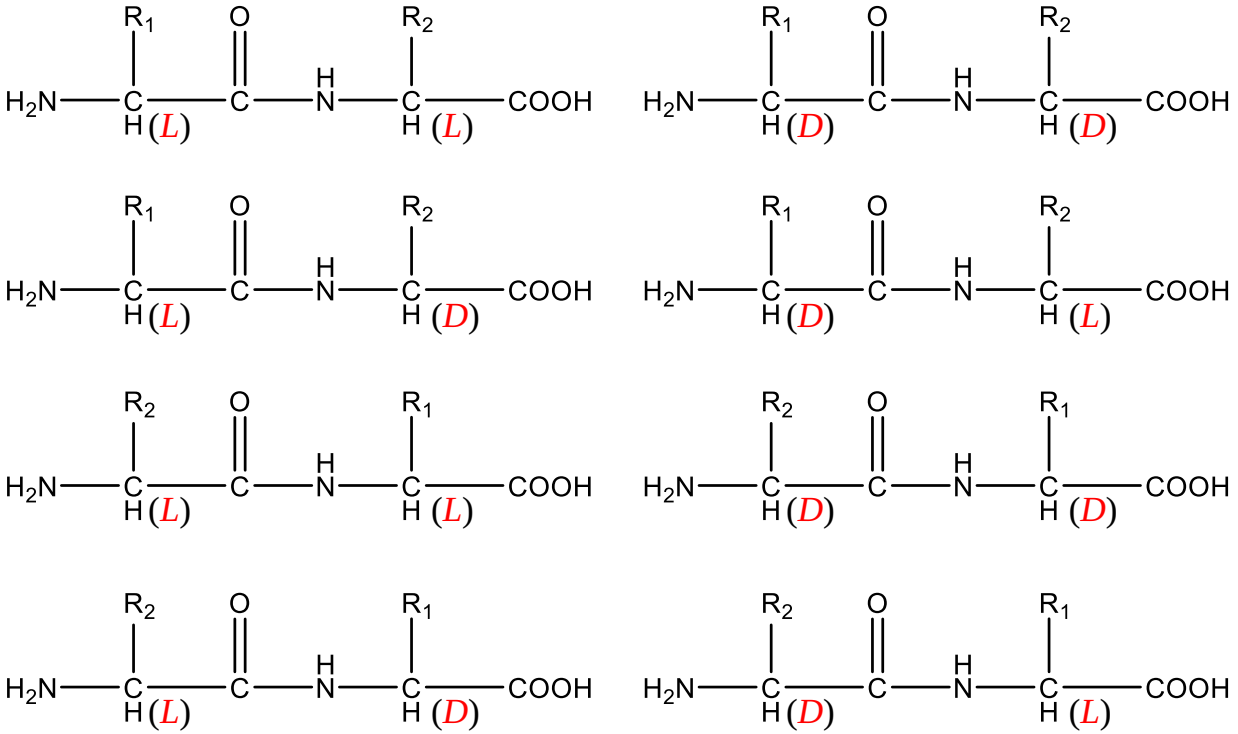

Figure 3-8. Eight possibilities for designing a dipeptide.

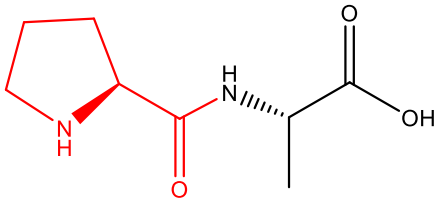

L-Pro-*L*-Ala

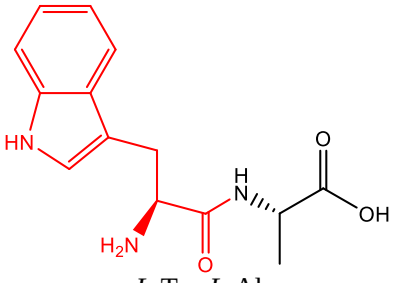

L-Trp-*L*-Ala

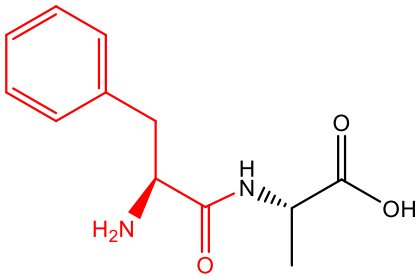

L-Phe-*L*-Ala

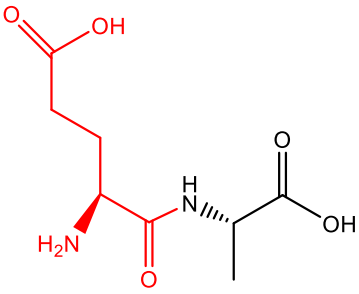

L-Glu-*L*-Ala

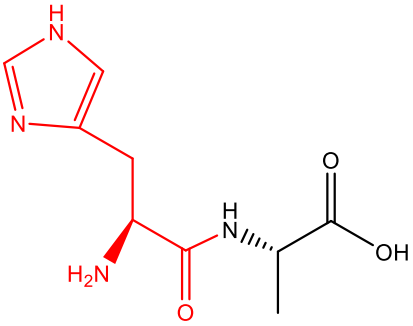

L-His-*L*-Ala

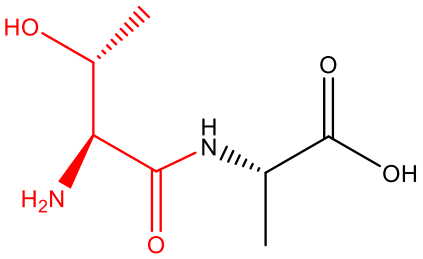

L-Thr-*L*-Ala

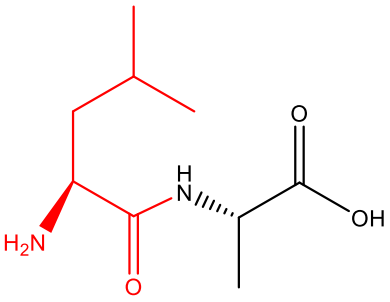

L-Leu-*L*-Ala

Figure 3-9. The structure of Pro-Ala, Trp-Ala, Phe-Ala, His-Ala, Thr-Ala, Glu-Ala and Arg-Ala.

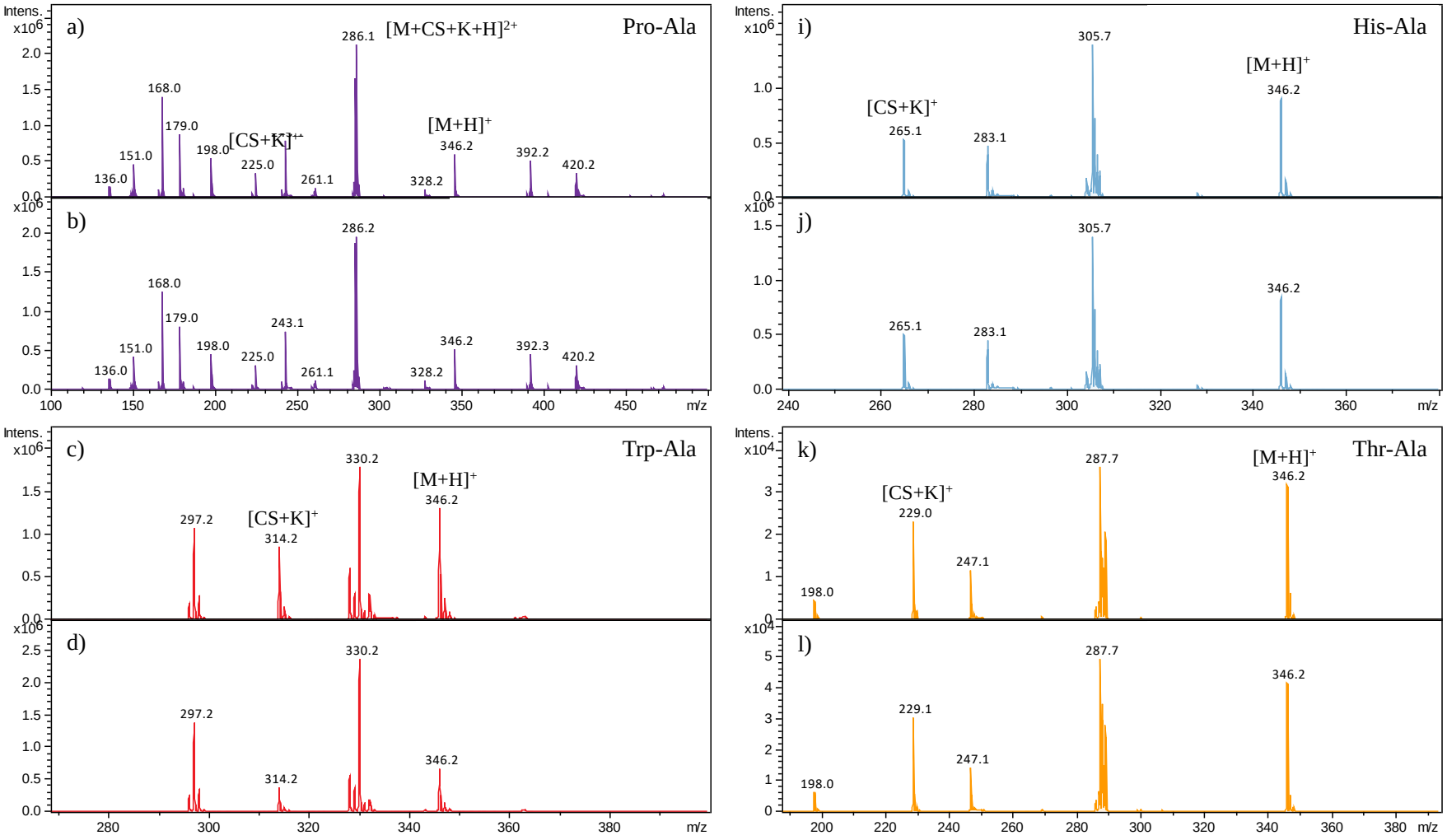

Figure 3-10. MS/MS spectra of *R/S*-omeprazole on $[M+CS+K+H]^{2+}$ with different amino acids as chiral selectors. (To be continued)

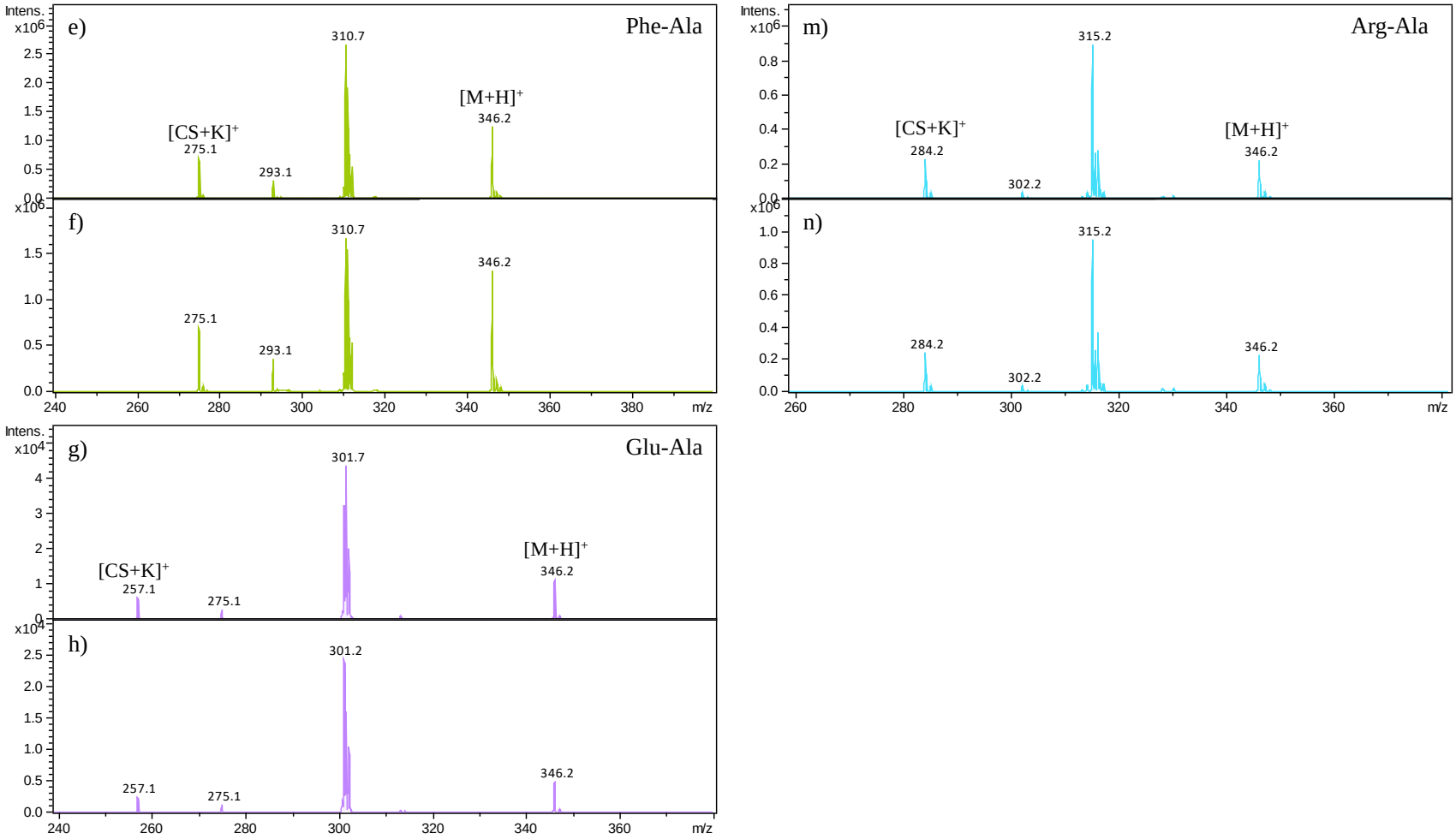

Figure 3-11-continued. MS/MS spectra of *R/S*-omeprazole on $[M+CS+K+H]^{2+}$ with different amino acids as chiral selectors.

Table 3-4. MS/MS results of the diastereomeric complex ions of omeprazole using dipeptides as chiral selectors with Ala fixed.

Dipeptides	Precursor ion	Product ion	CR
Pro-Ala	$[M+CS+K+H]^{2+}$	$[M+H]^{+}$	1.24±0.04
Trp-Ala	$[M+CS+K+H]^{2+}$	$[M+H]^{+}$	0.33±0.04
	$[M+2CS+K+H]^{2+}$	$[M+CS+K+H]^{2+}$	1.18±0.02
Phe-Ala	$[M+CS+K+H]^{2+}$	$[M+H]^{+}$	0.60±0.01
His-Ala	$[M+CS+K+H]^{2+}$	$[M+H]^{+}$	1.06±0.01
	$[M+CS+Na]^{+}$	$[CS+Na]^{+}$	1.22±0.03
	$[M+CS+Na]^{+}$	$[M+Na]^{+}$	1.46±0.05
Thr-Ala	$[M+CS+K+H]^{2+}$	$[M+H]^{+}$	1.07±0.05
	$[M+CS+K]^{+}$	$[M+K]^{+}$	0.18±0.02
	$[2M+CS+K]^{+}$	$[M+CS+K]^{+}$	1.32±0.03
	$[M+CS+K]^{+}$	$[M+CS+K-C_8H_8N_2O]^{+}$	0.18±0.02
Arg-Ala	$[M+CS+K+H]^{2+}$	$[M+H]^{+}$	1.02±0.01
	$[M+CS+K]^{+}$	$[M+CS+K-C_8H_8N_2O]^{+}$	1.13±0.02
Glu-Ala	$[M+CS+K+H]^{2+}$	$[M+H]^{+}$	1.93±0.18
	$[M+CS+K+H]^{2+}$	$[CS+Na]^{+}$	1.35±0.30
	$[M+CS+K]^{+}$	$[M+K]^{+}$	0.43±0.06
	$[2M+CS+Na]^{+}$	$[M+Na]^{+}$	1.65±0.08

The same measurements were performed with another set of dipeptides containing His applied as chiral selectors, consisting of His-Ser, His-Phe and His-Ala, and the corresponding structures were exhibited in Figure 3-11. Numerous diastereomers were formed as summarized in Table 3-5, most of which were sodium or potassium adduct dimers and trimers. Compared with Ala-based peptides, using His-based peptides tends to form more singly charged ions. When dissociated, loss of dipeptide or omeprazole was observed. The most chiral discrimination of using each dipeptide was obtained with $[M+2His\text{-}Ser+K]^+$ dissociated into $[2His\text{-}Ser+K]^+$ (CR=0.75 $\pm$ 0.02), $[M+2His\text{-}Phe+K]^+$ dissociated into $[2His\text{-}Ser+K]^+$ (CR=1.32 $\pm$ 0.08), and $[M+His\text{-}Ala+Na]^+$ dissociated into $[His\text{-}Ala+Na]^+$ (CR=1.46$\pm$0.05). The results demonstrated that the loss of omeprazole had a greater impact on the chiral structure of ions.

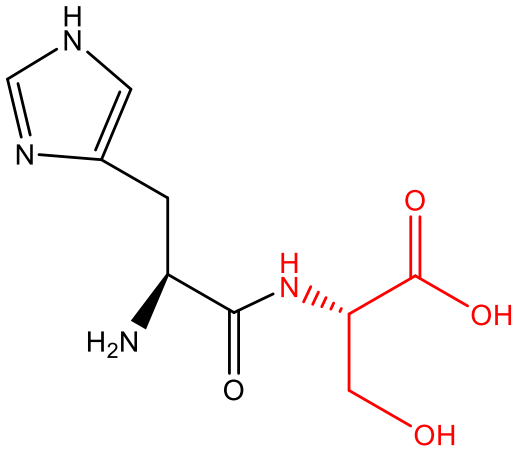

L-His-*L*-Ser

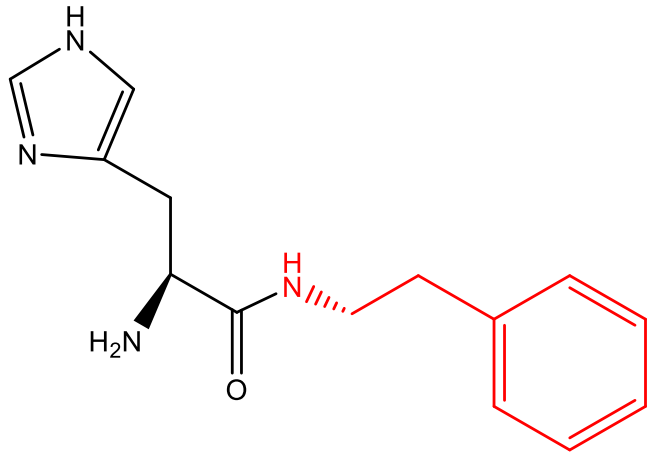

L-His-*L*-Phe

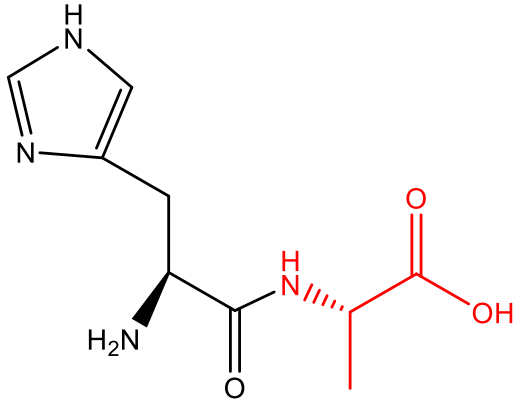

L-His-*L*-Ala

Figure 3-11. The structure of His-Ser, His-Phe and His-Ala.

Table 3-5. The CR values of complex ions of omeprazole using dipeptides as chiral selectors with His fixed.

Dipeptides	Precursor ion	Product ion	CR
His-Ser	$[M+CS+H]^+$	$[M+H]^+$	0.98±0.03
		$[CS+H]^+$	0.97±0.04
	$[M+CS+Na]^+$	$[M+Na]^+$	0.91±0.07
		$[CS+Na]^+$	0.90±0.05
	$[M+CS+K]^+$	$[M+K]^+$	0.81±0.18
		$[CS+K]^+$	0.79±0.17
		$[M+CS+K-C_8H_8N_2O]^+$	0.85±0.02
	$[M+2CS+K]^+$	$[2CS+K]^+$	0.75±0.02
	$[2M+CS+Na]^+$	$[M+CS+Na]^+$	0.95±0.03
	$[2M+CS+K]^+$	$[M+CS+K]^+$	1.02±0.02
His-Phe	$[M+CS+H]^+$	$[M+H]^+$	1.06±0.01
		$[CS+H]^+$	1.08±0.03
	$[M+CS+Na]^+$	$[M+Na]^+$	1.22±0.05
		$[CS+Na]^+$	1.13±0.06
	$[M+CS+K]^+$	$[CS+K]^+$	1.36±0.15
	$[M+2CS+K]^+$	$[2CS+K]^+$	1.32±0.08
	$[2M+CS+K]^+$	$[M+CS+K]^+$	1.03±0.01
His-Ala	$[M+CS+K+H]^{2+}$	$[CS+K]^+$	1.04±0.04
		$[M+H]^+$	1.06±0.01
	$[M+CS+Na]^+$	$[CS+Na]^+$	1.22±0.03
		$[M+Na]^+$	1.46±0.05
	$[M+CS+K]^+$	$[M+CS+K-C_8H_8N_2O]^+$	1.05±0.04
	$[2M+CS+K]^+$	$[M+CS+K]^+$	0.91±0.08
His-Ser	$[M+CS+H]^+$	$[M+H]^+$	0.98±0.03

For the comparison of two amino acids and dipeptides, take the potassium adduct ion as an example, $[M+His+Ser+K]^+$ tended to lose one or two amino acids, with no loss of the analyte. While for $[M+His-Ser+K]^+$, loss of His-Ser or omeprazole is all possible. In addition, when two amino acids His+Ser were utilized as chiral selectors, no chiral recognition was found. However, omeprazole enantiomers were sufficiently distinguished using the dipeptide His-Ser. It is speculated that the discrimination may correspond to the specific structure of complexes. Two amino acids could provide multiple binding sites and interactions, but the intermolecular binding using two separate AAs is loose. When they are linked by a peptide bond, the structure is more rigid, thus creating enhanced chiral effects. The above results confirm the superiority of dipeptides in chiral analysis of omeprazole. Further confirmation will be done to better understand the structure of these complexes, with the help of standard Gibbs energies, computational model and Gaussian calculation.

3.3.6 Peptides as the chiral selectors with copper-bound

Nearly no copper-bound complex ions containing both omeprazole and dipeptides were observed, which might be due to their lower interaction with copper.

3.3.7 Peptides with one chiral center as chiral selectors

All of the dipeptides mentioned above possess two chiral centers. Among 20 common amino acids, glycine stands out as the only one without chirality. To further explore the capabilities of dipeptides with a single chiral center, Gly-Phe, Gly-Pro, Gly-Leu, Gly-Ala, Gly-Glu, and Gly-Asp were examined, the structures of which were exhibited in Figure 3-12. Gly-Phe and Gly-Pro have rigid rings in their side chains, while Gly-Leu, Gly-Ala, Gly-Glu and Gly-Asp differ in terms of side chain length and functional group. The results, summarized in Table 3-6, showed that despite having only one chiral center, the identification of the absolute configuration of omeprazole still could be realized with all these dipeptides. Additionally, most of the detected complex ions were singly charged dimers and trimers, except for Gly-Pro and Gly-Leu, protonated doubly charged dimers $[M+CS+K+H]^{2+}$ were observed. Significant chiral recognition was obtained using these six dipeptides as chiral selectors, yielding CR values ranging from 0.85 ± 0.02 to 0.44 ± 0.07. The most distinct one was obtained by $[M+Gly\text{-}Pro+K+H]^{2+}$ dissociated into $[Gly\text{-}Pro+H]^{+}$ (CR value 0.44 ± 0.07).

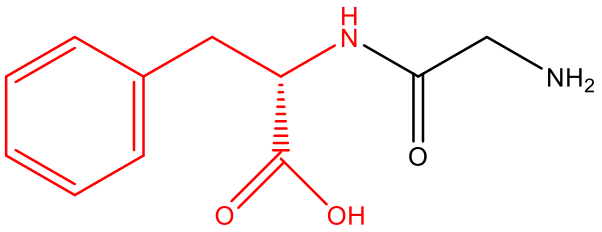

Gly-*L*-Phe

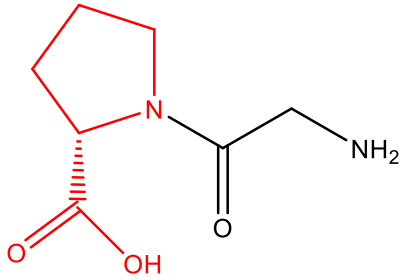

Gly-*L*-Pro

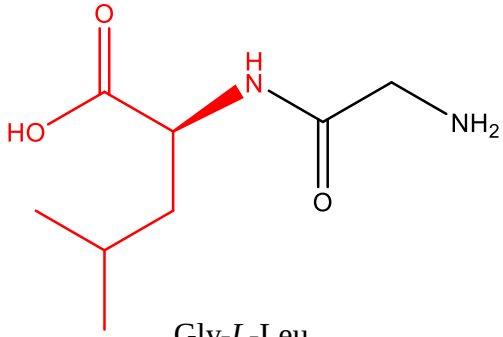

Gly-*L*-Leu

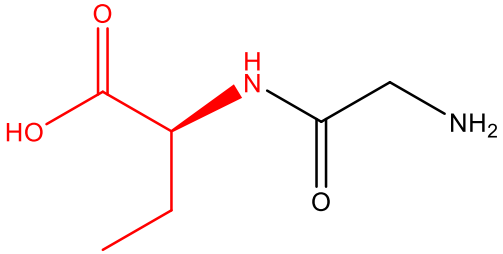

Gly-*L*-Ala

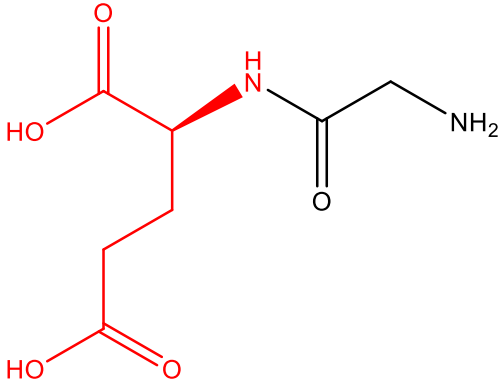

Gly-*L*-Glu

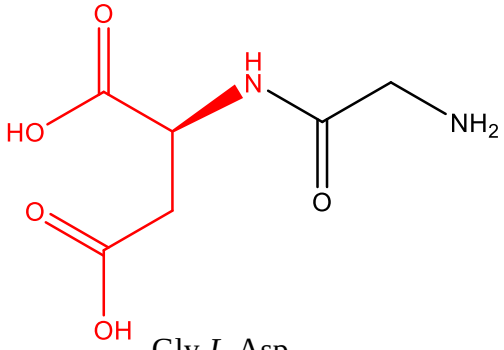

Gly-*L*-Asp

Figure 3-12. The structure of Gly-Phe, Gly-Pro, Gly-Leu, Gly-Ala, Gly-Glu, and Gly-Asp.

Table 3-6. The CR values of complex ions of omeprazole using dipeptides as chiral selectors with Gly fixed.

Dipeptides	**Precursor ion**	**Product ion**	**CR**
Gly-Phe	$[M+2CS+Na]^+$	$[M+CS+Na]^+$	1.84±0.18
Gly-Pro	$[M+CS+K+H]^{2+}$	$[M+H]^+$	0.81±0.02
		$[CS+H]^+$	0.44±0.07
	$[M+CS+K]^+$	$[M+H]^+$	1.38±0.07
Gly-Leu	$[M+CS+K+H]^{2+}$	$[CS+H]^+$	0.79±0.06
	$[M+CS+K]^+$	$[M+K]^+$	0.70±0.15
	$[M+2CS+K]^+$	$[M+H]^+$	1.68±0.17
	$[2M+CS+Na]^+$	$[2M+Na]^+$	1.02±0.04
	$[2M+CS+K]^+$	$[2M+K]^+$	1.12±0.01
Gly-Ala	$[M+CS+Na]^+$	$[M+Na]^+$	0.89±0.02
	$[M+CS+K]^+$	$[M+H]^+$	1.73±0.12
Gly-Glu	$[M+CS+Na]^+$	$[M+Na]^+$	0.87±0.02
	$[2M+CS+Na]^+$	$[2M+Na]^+$	0.55±0.10
Gly-Asp	$[2M+CS+K]^+$	$[M+CS+K]^+$	1.14±0.02

3.3.8 Peptides with different orders of amino acids as chiral selectors

As mentioned in Figure 4-11, the order of AAs can vary even when synthesized from the same components. Here, we simply take two dipeptides Gly-Pro and Pro-Gly as an example to investigate whether the order would have a great impact on the chiral discrimination. Figure 3-13 shows the structures of two dipeptides, with Gly-Pro being more cyclic and Pro-Gly being more linear. The chiral recognition ability of them towards omeprazole enantiomers was then evaluated as shown in Table 3-7. Interestingly, under the same dissociation path, the obtained CR values were very different. When Gly-Pro was used as the selector, there was no difference observed from $[M+CS+K+H]^{2+}$ to $[M+H]^{+}$, and from $[M+CS+K]^{+}$ to $[M+H]^{+}$. However, better chiral analysis was achieved using Pro-Gly as the selector. On the other hand, Gly-Pro performed better for $[M+CS+K]^{+}$ to $[M+K]^{+}$, with less standard deviation. The CR value obtained from $[M+CS+K]^{+}$ to $[M+H]^{+}$ using Gly-Pro is smaller than 1.0, while that using Pro-Gly is larger than 1.0, suggesting the different preference of cluster ions for the homochiral or heterochiral (Figure 3-14). These results highlight the importance of the order of AAs in peptides, which has a great impact on the spatial structure. However, enantioselectivity still could be achieved with all dipeptides used, indicating the strong chiral discrimination ability of peptides as chiral selectors.

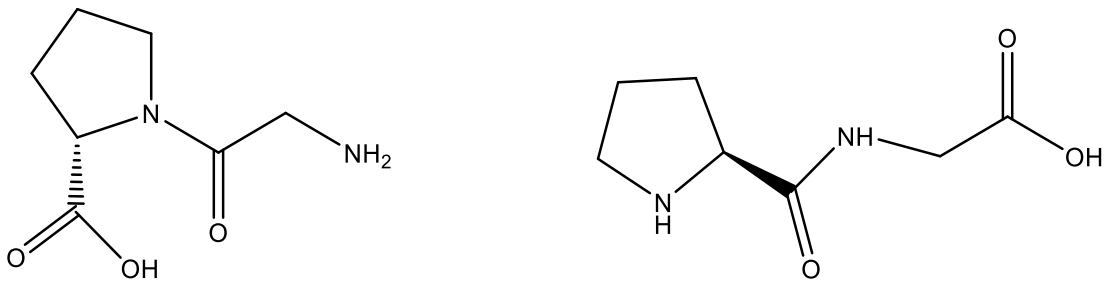

Gly-*L*-Pro *L*-Pro-Gly

Figure 3-13. Structures of Gly-Pro and Pro-Gly.

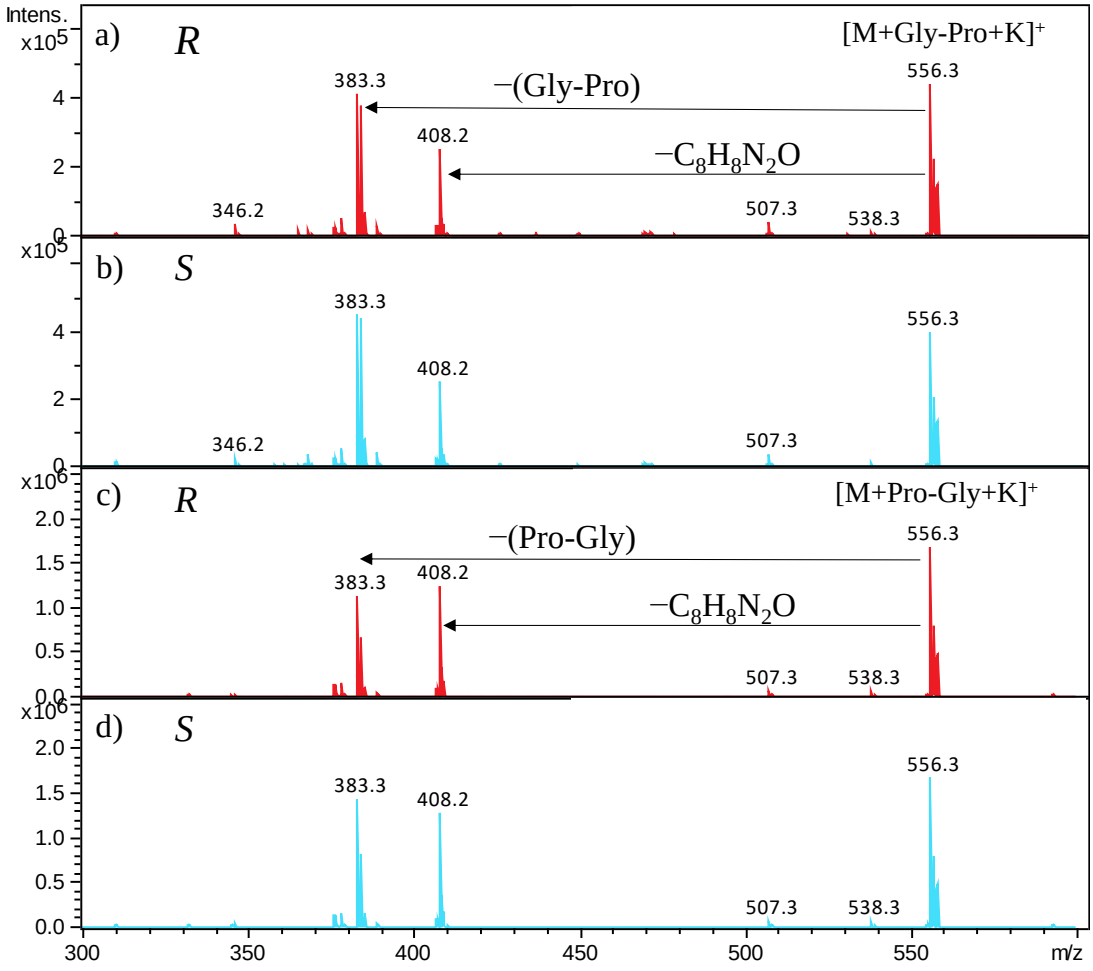

Figure 3-14. MS/MS spectra of *R/S*-omeprazole on a-b) $[M+Gly-Pro+K]^+$ and c-d) $[M+Pro-Gly+K]^+$ under the same collision-induced dissociation energy.

Table 3-7. The CR values of complex ions of omeprazole using Gly-Pro and Pro-Gly as chiral selectors.

Dipeptides	**Precursor ion**	**Product ion**	**CR**
Gly-Pro	$[M+CS+K+H]^{2+}$	$[CS+H]^{+}$	0.79 ± 0.06
		$[M+H]^{+}$	1.02 ± 0.02
	$[M+CS+K]^{+}$	$[M+K]^{+}$	0.80 ± 0.01
		$[M+H]^{+}$	0.82 ± 0.06
Pro-Gly	$[M+CS+K+H]^{2+}$	$[CS+H]^{+}$	0.44 ± 0.07
		$[M+H]^{+}$	0.81 ± 0.02
	$[M+CS+K]^{+}$	$[M+K]^{+}$	0.76 ± 0.07
		$[M+H]^{+}$	1.38 ± 0.07

3.3.9 Performance of the peptide approach using Orbitrap MS

To verify the peptide-based approach for the analysis of chiral compounds, in addition to the ion trap MS, we also tried to perform similar experiments on the Orbitrap Exploris 120 mass spectrometer (Thermo Fisher Scientific, Waltham, MA, USA). The ESI+ conditions were optimized in terms of spray voltage (3600 V), ion transfer tube temperature (200 ℃), sheath gas (25 Arb), aux gas (5 Arb) and vaporizer temperature (200 ℃). Gas-phase complex ions were generated by electrospraying.

Considering the influence of the mobile phase that would dilute sample solutions, samples were prepared at a concentration of 100 μM for both omeprazole and chiral selectors in 50% methanol. Three replicates were performed for each sample.

To improve the efficiency, an autosampler of UltiMate 3000 UPLC (Thermo Fisher Scientific, Waltham, MA, USA) was applied rather than injection by hand. As no column for separation is needed, direct infusion was employed. The injected sample volume is 20 μL. The mobile phase consisted of 50% eluent A methanol and 50% B water. A flow rate of 0.1 mL min^{-1} was used for the 3-minute elution. Accurate MS/MS spectra were acquired in the mass range of *m/z* 300-1000 with an isolation window of 2 Da and a resolution of 120000 FWHM (full width at half maximum). The HCD collision energies (%) depended on the relative intensity of product ions to precursor ions. The acquired spectra were processed by the software of FreeStyle (Thermo Fisher Scientific, Waltham, MA, USA).

Dipeptides of Pro-Ala, Thr-Ala, Phe-Ala, His-Ala, His-Phe, His-Ser, His-Gly, Gly-Phe, Gly-Leu, Gly-Glu, Gly-Pro were studied. An example of MS/MS spectra of the complex ion $[M+CS+K]^+$ using Pro-Ala as the chiral selector is shown in Figure 3-15. As displayed, two diastereomers could be clearly distinguished by the difference in the relative intensity of product ions $[Pro\text{-}Ala+H]^+$ and $[M+K]^+$, the corresponding CR values were 0.47 ± 0.02 and 1.43 ± 0.06, respectively. The cluster ions that led to significant recognition of the chiral drug were summarized in Table 3-8. When compared with results obtained from IT-MS, inconsistent CR values were observed, apart from this, the dipeptides Thr-Ala and His-Ala didn't show any enantioselectivity towards the drug in this study. A possible explanation could be that different types of dissociation energies were applied in two MS techniques, which contributed to different MS/MS spectral patterns. The IT-MS tends to be gentler on complex ions. Even so, the strategy of employing dipeptides as chiral selectors is still feasible. Given that with the help of the UPLC autosampler, both labor intensity and sampling time decreased, the application of UPLC-Orbitrap 120 MS in this study is worth considering. Further optimization will be performed.

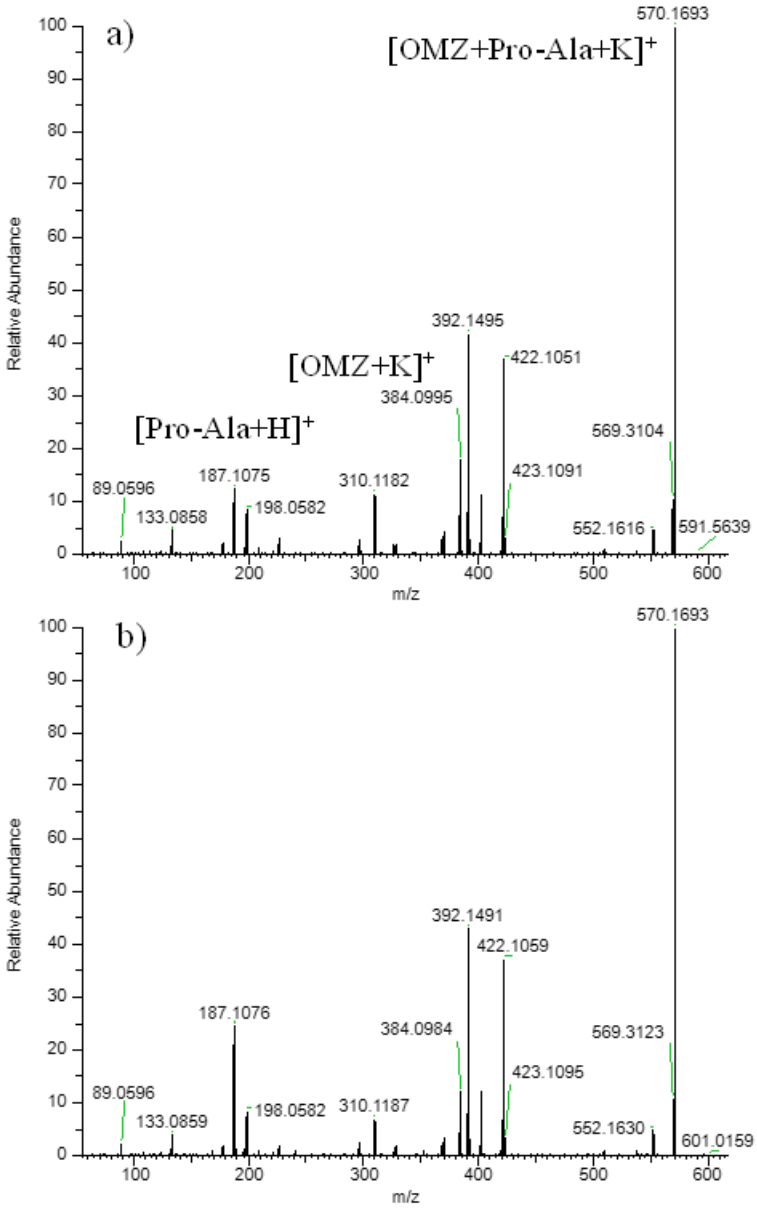

Figure 3-15. MS/MS spectra of [*R/S*-omeprazole+Pro-Ala+K]$^+$.

Table 3-8. The CR values of complex ions of omeprazole using various dipeptides as chiral selectors based on orbitrap consequences.

Dipeptides	Precursor ion	Product ion	CR
Gly-Pro	$[M+2CS+Na]^+$	$[M+Na]^+$	0.06±0.03
Gly-Leu	$[M+CS+K]^+$	$[M+K]^+$	0.23±0.01
	$[M+CS+Na]^+$	$[M+Na]^+$	1.17±0.03
	$[M+2CS+K]^+$	$[M+CS+K]^+$	3.75±0.47
	$[M+2CS+Na]^+$	$[M+CS+Na]^+$	2.07±0.26
Gly-Glu	$[M+CS+K]^+$	$[M+K]^+$	0.19±0.13
Gly-Phe	$[M+CS+K]^+$	$[M+K]^+$	0.60±0.03
	$[M+CS+Na]^+$	$[M+Na]^+$	1.20±0.02
	$[2M+CS+K]^+$	$[M+CS+K]^+$	3.19±0.33
Pro-Ala	$[M+CS+K]^+$	$[M+K]^+$	1.43±0.06
	$[M+CS+K]^+$	$[CS+H]^+$	0.47±0.02
	$[M+2CS+K]^+$	$[M+CS+K]^+$	1.20±0.02
	$[M+2CS+K]^+$	$[M+H]^+$	1.96±0.02
	$[2M+CS+K]^+$	$[M+CS+K]^+$	1.12±0.03
Phe-Ala	$[2M+CS+K]^+$	$[M+CS+K]^+$	1.15±0.02
	$[2M+CS+K]^+$	$[2M+K]^+$	1.14±0.02
His-Ala	$[M+2CS+K]^+$	$[2CS+K]^+$	0.54±0.13
	$[2M+CS+H]^+$	$[M+H]^+$	0.22±0.20
His-Ser	$[M+CS+K]^+$	$[CS+K]^+$	0.21±0.08
His-Gly	$[M+CS+K]^+$	$[CS+K]^+$	2.02±0.13
	$[M+2CS+H]^+$	$[M+CS+H]^+$	1.18±0.03

3.3.10 Extension of dipeptides to the chiral recognition of clopidogrel

Dipeptides have proven to be ideal chiral selectors for omeprazole. In order to investigate the versatility of dipeptides, we have also extended the application to another chiral drug, clopidogrel (Clo). Different from omeprazole, nearly no doubly charged complexes were detected or dissociated. The most observed ions were singly charged dimers and trimers, including $[M+CS+K]^+$, $[M+CS+Na]^+$, $[M+CS+H]^+$, $[M+2CS+K]^+$, and $[M+2CS+Na]^+$. Dipeptides mentioned previously were applied here for the recognition of clopidogrel. Figure 3-16 displayed an example of MS/MS spectral results using Phe-Ala as the chiral selector, and significant differences in dissociated patterns could be observed between dimers $[M+Phe\text{-}Ala+Na]^+$ of two clopidogrel diastereomers by losing an analyte to form $[Phe\text{-}Ala+Na]^+$ (*m/z* 259.2), with a CR value of 0.54 ± 0.10. Chiral recognition of clopidogrel could be achieved with all dipeptides tested. A summary of chiral discrimination results was shown in Table 3-10 and Table 3-11.

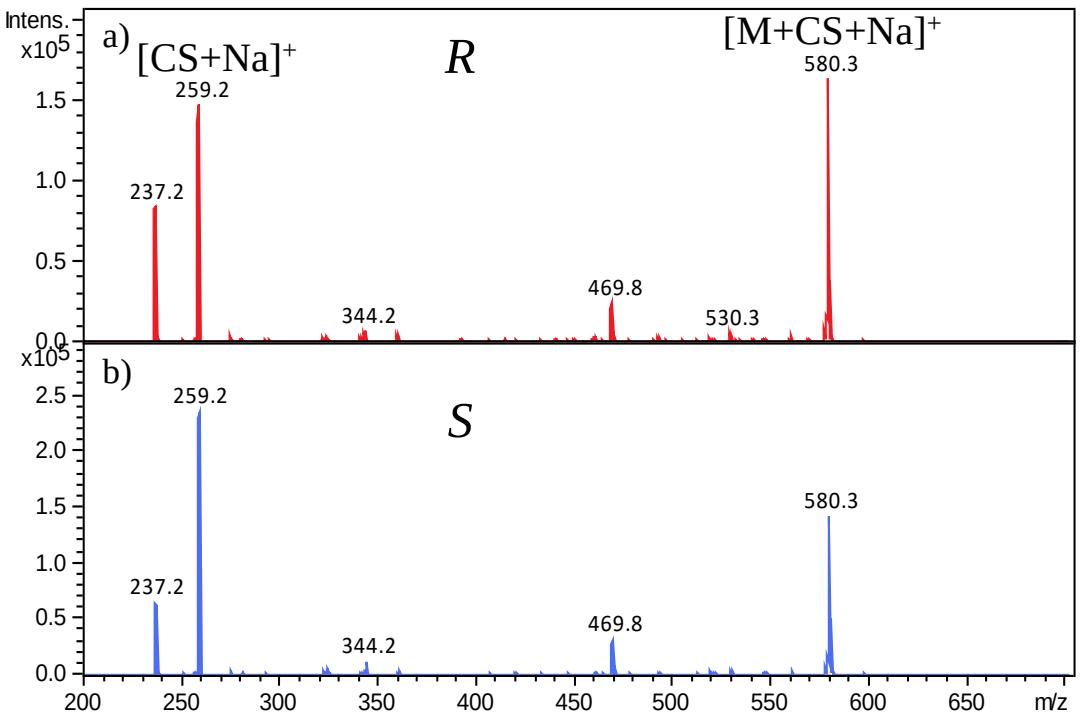

Figure 3-16. MS/MS spectra of *R*/*S*-clopidogrel on $[M+CS+Na]^+$ with Pro-Ala as the chiral selector.

Table 3-9. The CR values of complex ions of clopidogrel using dipeptides as chiral selectors with His fixed.

Dipeptides	**Precursor ion**	**Product ion**	**CR**
His-Ser	$[M+CS+Na]^+$	$[CS+Na]^+$	0.47±0.04
His-Phe	$[M+CS+Na]^+$	$[CS+Na]^+$	0.77±0.04
	$[M+CS+K]^+$	$[CS+K]^+$	0.72±0.04
	$[2M+CS+Na]^+$	$[2M+Na]^+$	0.55±0.07
	$[2M+CS+K]^+$	$[2M+K]^+$	1.14±0.01
His-Ala	$[M+2CS+Na]^+$	Unknown	0.27±0.02

Table 3-10. The CR values of complex ions of clopidogrel using dipeptides as chiral selectors with Ala fixed.

Dipeptides	**Precursor ion**	**Product ion**	**CR**
Trp-Ala	$[M+CS+Na]^+$	$[CS+Na]^+$	0.84±0.03
	$[M+CS+K]^+$	$[CS+K]^+$	0.50±0.05
Phe-Ala	$[M+CS+H]^+$	$[M+H]^+$	0.68±0.03
	$[M+CS+Na]^+$	$[CS+Na]^+$	0.54±0.10
		$[CS+H]^+$	0.54±0.07
	$[M+CS+K]^+$	$[CS+K]^+$	0.80±0.02
	$[M+2CS+K]^+$	$[2CS+K]^+$	0.50±0.07
Pro-Ala	$[M+CS+K]^+$	$[CS+K]^+$	3.60±0.70
	$[M+2CS+K]^+$	$[2CS+K]^+$	0.80±0.05
Thr-Ala	$[M+CS+H]^+$	$[M+H]^+$	0.67±0.04
	$[M+CS+K]^+$	$[CS+K]^+$	1.21±0.04
	$[M+2CS+K]^+$	$[2CS+K]^+$	0.48±0.08
His-Ala	$[M+2CS+Na]^+$	Unknown	0.27±0.02
Glu-Ala	$[M+CS+K]^+$	$[M+H]^+$	0.74±0.03

Table 3-11. The CR values of complex ions of clopidogrel using dipeptides as chiral selectors with Gly fixed.

Dipeptides	Precursor ion	Product ion	CR
Gly-Glu	$[M+CS+Na]^+$	$[CS+Na]^+$	0.73±0.03
	$[M+2CS+K]^+$	$[2CS+K]^+$	0.47±0.09
Gly-Phe	$[M+2CS+Na]^+$	$[2CS+Na]^+$	0.26±0.04
	$[M+2CS+K]^+$	$[2CS+K]^+$	1.34±0.05
		$[M+CS+K]^+$	1.56±0.06
	$[2M+CS+Na]^+$	$[M+CS+Na]^+$	0.43±0.06
	$[2M+CS+K]^+$	$[M+CS+K]^+$	0.79±0.02
Gly-Asp	$[M+2CS+Na]^+$	$[2CS+Na]^+$	0.63±0.07
	$[M+2CS+K]^+$	$[2CS+K]^+$	0.42±0.06
Gly-Ala	$[M+2CS+Na]^+$	$[2CS+Na]^+$	0.54±0.09
	$[M+2CS+K]^+$	$[2CS+K]^+$	0.70±0.05
		$[M+CS+K]^+$	0.73±0.05
	$[2M+CS+K]^+$	$[M+CS+K]^+$	0.44±0.06
Gly-Pro	$[M+CS+H]^+$	$[M+H]^+$	1.25±0.05
	$[M+CS+K]^+$	$[CS+K]^+$	1.19±0.03
	$[M+2CS+Na]^+$	$[2CS+Na]^+$	0.79±0.02
	$[M+2CS+K]+$	$[2CS+K]^+$	0.90±0.02
	$[2M+CS+Na]^+$	$[M+CS+Na]^+$	0.66±0.09

Interestingly, dissociation patterns were very different between complex ions containing omeprazole and clopidogrel. These results demonstrated the affinity of peptides and chiral drugs towards sodium ion or potassium ion. Some comparison results were exhibited in Figure 3-17 and Figure 3-18, as shown, with the same peptides (Phe-Ala, Pro-Ala and Thr-Ala), loss of a peptide occurred in $[omeprazole+CS+Na]^+$, while $[omeprazole+CS+K]^+$ tended to lose 148 Da, indicating that omeprazole may have higher affinity towards Na^+ than these peptides, but lower affinity towards K^+. Clopidogrel is another thing, as for both $[clopidogrel+CS+Na]^+$ and $[clopidogrel+CS+K]^+$, dissociation of Clopidogrel was easier than that of peptides, illustrating the lower affinity of Clo towards Na^+ and K^+. These observations may be related to the structure of complex ions, further investigations will be done to have a deep understanding of the role of dipeptides in the recognition of different chiral compounds.

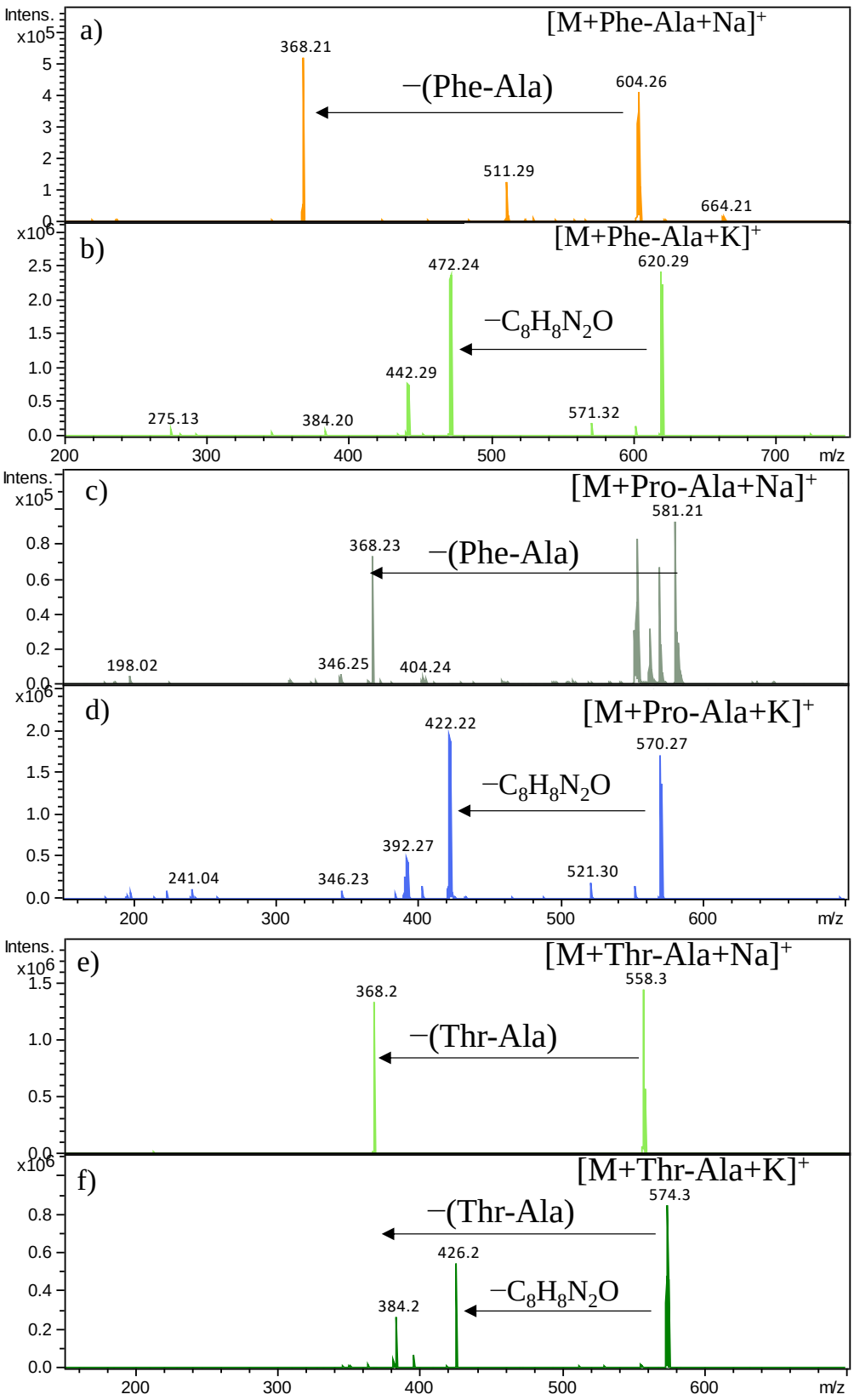

Figure 3-17. MS/MS spectra of omeprazole on $[M+CS+Na]^+$ (top) and $[M+CS+K]^+$ (bottom) with different dipeptides as chiral selectors.

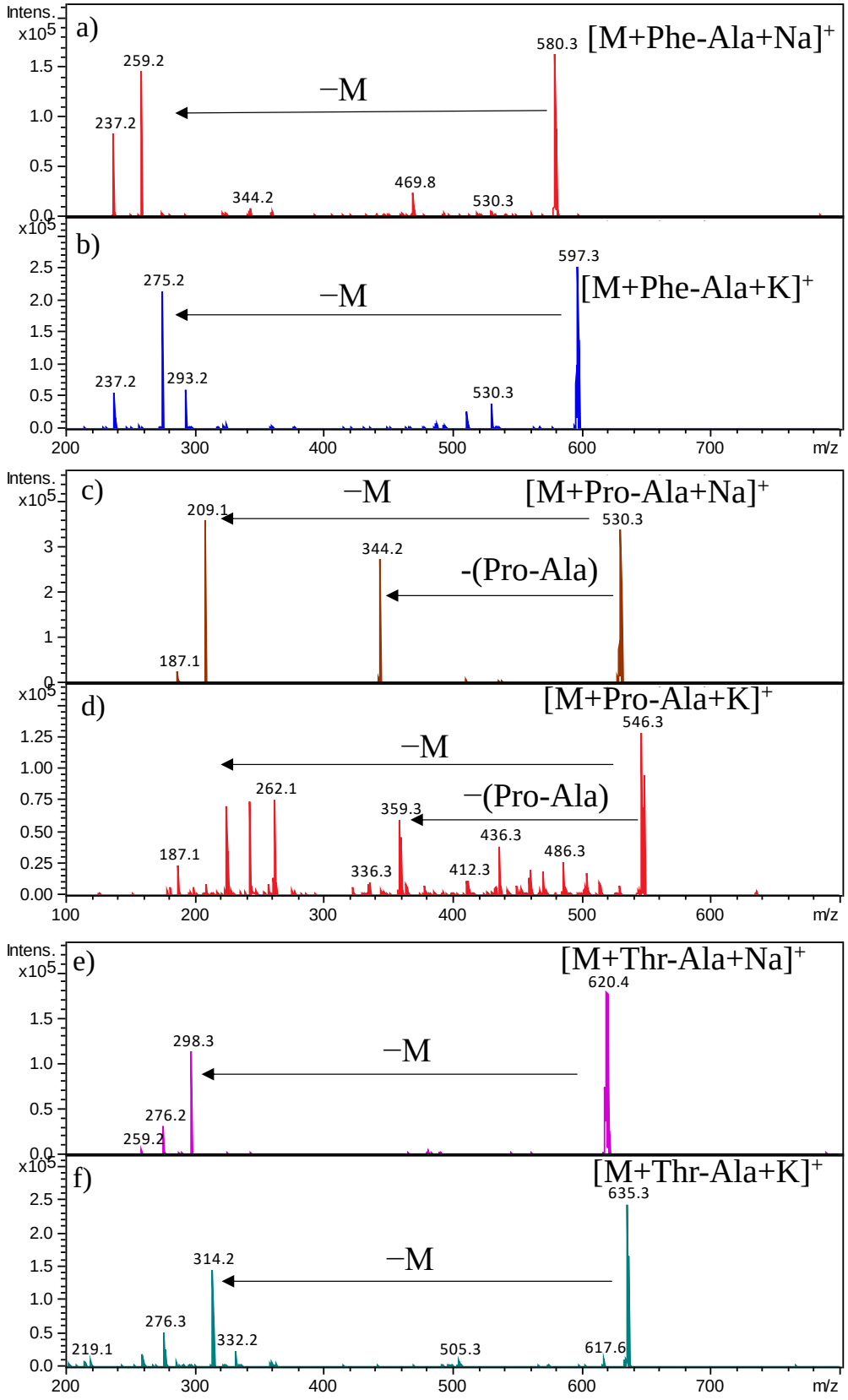

Figure 3-18. MS/MS spectra of clopidogrel on $[M+CS+Na]^+$ (top) and $[M+CS+K]^+$ (bottom) with different dipeptides as chiral selectors.

To compare the ability of peptides in chiral analysis to that of amino acids, combinations of two amino acids were investigated as well. In contrast to peptides, no higher assembly of complex ions was observed, and only those containing one analyte, one CS1 and one CS2 were detected, most were $[M+CS1+CS2+K]^+$. $[M+CS1+CS2+H]^+$ and $[M+CS1+CS2+Na]^+$. The latter two had low intensity or were unstable under the dissociating energy. Similar to omeprazole, the order of binding affinity of amino acids towards the clopidogrel-containing ions may be concluded. As shown in Figure 3-19, when one of the amino acids was fixed as Ala, the dissociation of Ala was easier than the analyte or the other AA. Even the loss of Trp was observed in Figure 3-19a, the intensity of Ala was higher than that of Trp. An exception was Pro, which was easier to dissociate from complexes than Ala. In contrast to Ala, when His was fixed, the loss of the other AA was observed (Figure 3-20), indicating that His has a higher binding affinity towards the complex ion. A more detailed order will be derived with more combinations of two amino acids investigated.

When looking deeply into the recognition results as shown in Table 3-12, it could be observed that among all combinations tested, only two showed enantioselectivity towards clopidogrel, Trp+Ala and Glu+Ala. This is consistent with the previous results for omeprazole, strengthening the priority of peptides over two separated amino acids in the analysis of the chiral drug.

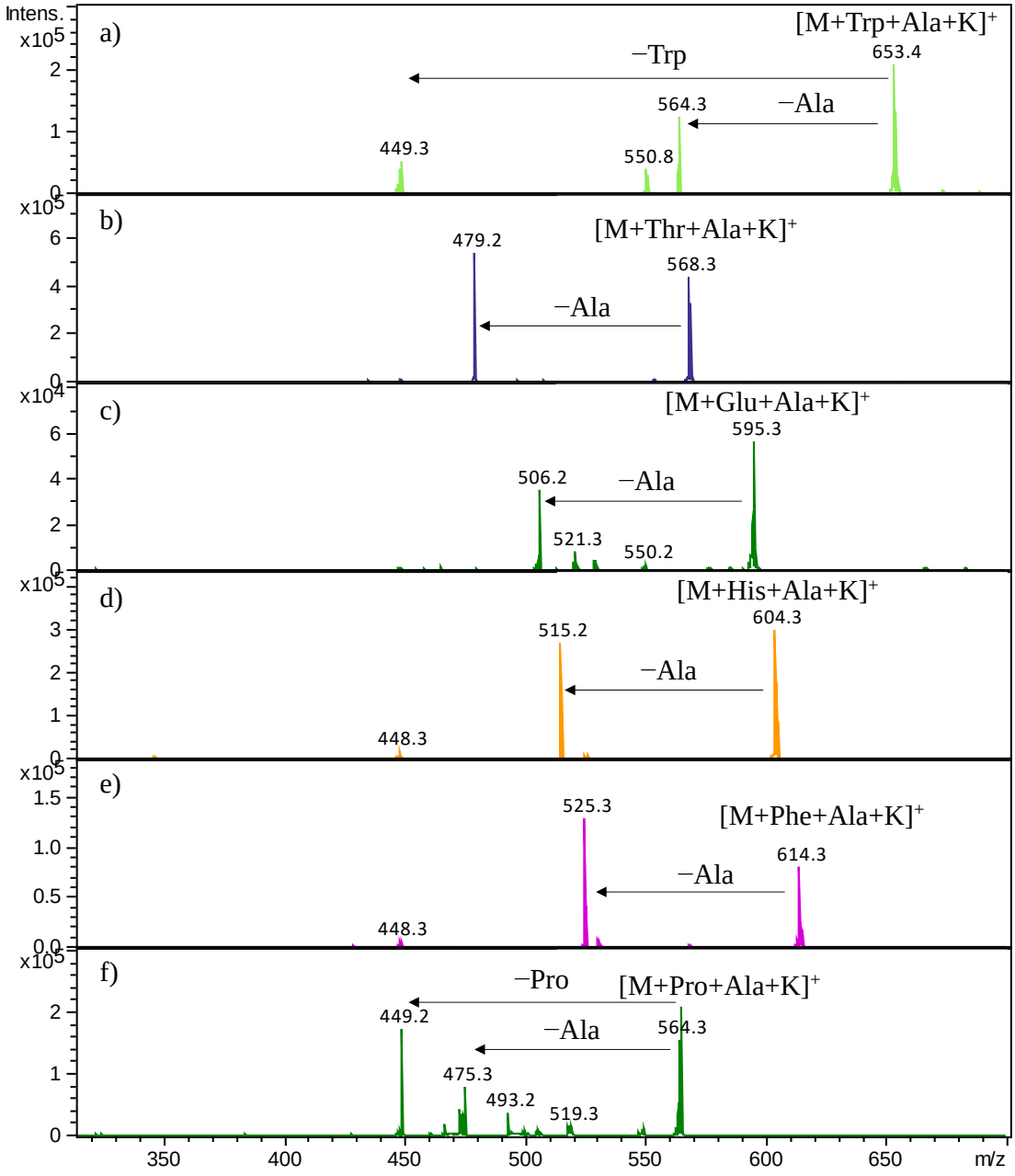

Figure 3-19. MS/MS spectra of clopidogrel on $[M+CS1+CS2+K]^+$ with different combinations of two amino acids as chiral selectors with Ala fixed.

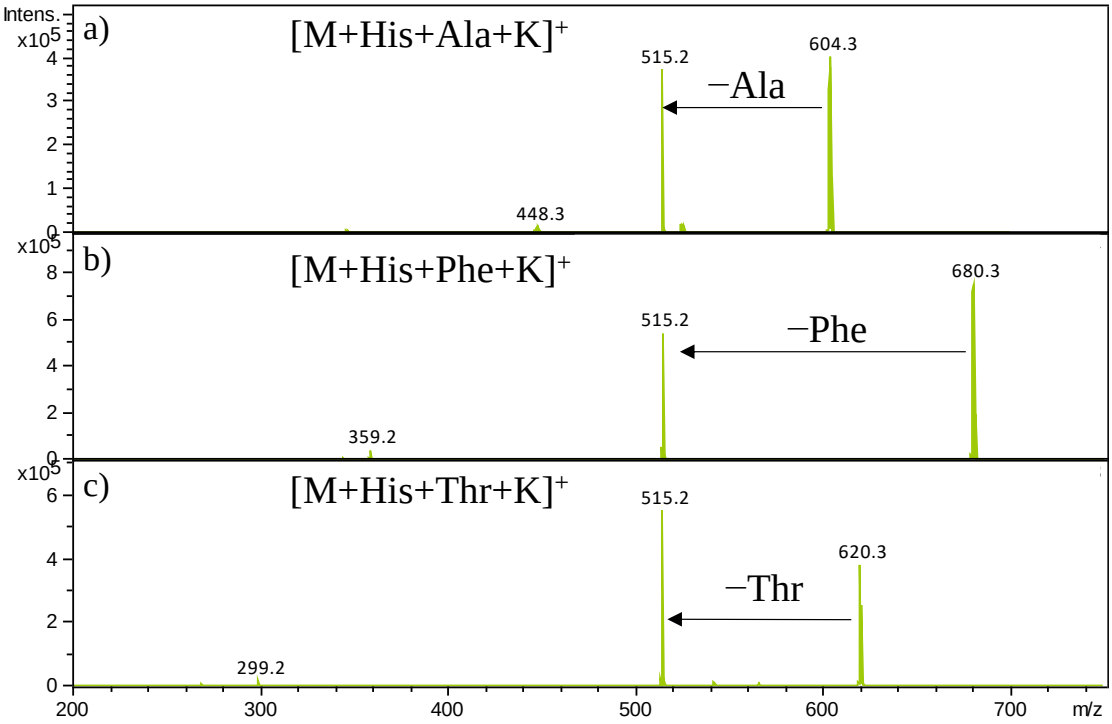

Figure 3-20. MS/MS spectra of clopidogrel on $[M+CS1+CS+K]^+$ with different combinations of two amino acids as chiral selectors with His fixed.

Table 3-12. The CR values of complex ions of clopidogrel using two amino acids as chiral selectors.

Two amino acids	Precursor ion	Product ion	CR
Trp+Ala	$[M+Trp+Ala+Na]^+$	$[M+Ala+Na]^+$	1.01±0.03
	$[M+Trp+Ala+K]^+$	$[M+Trp+K]^+$	0.54±0.06
	$[M+Trp+Ala+K]^+$	$[M+Ala+K]^+$	1.12±0.04
Thr+Ala	$[M+Thr+Ala+K]^+$	$[M+Thr+K]^+$	1.04±0.01
Glu+Ala	$[M+Glu+Ala+K]^+$	$[M+Glu+K]^+$	0.69±0.03
Phe+Ala	$[M+Phe+Ala+Na]^+$	$[M+Ala+Na]^+$	1.16±0.08
	$[M+Phe+Ala+K]^+$	$[M+Ala+K]^+$	0.83±0.05
Pro+Ala	$[M+Pro+Ala+H]^+$	$[M+Ala+H]^+$	1.02±0.20
	$[M+Pro+Ala+Na]^+$	$[M+Ala+Na]^+$	0.91±0.06
	$[M+Pro+Ala+K]^+$	$[M+Ala+K]^+$	0.97±0.03
	$[M+Pro+Ala+K]^+$	$[M+Pro+K]^+$	0.99±0.03
His+Ala	$[M+His+Ala+K]^+$	$[M+His+K]^+$	1.02±0.02
His+Phe	$[M+His+Phe+K]^+$	$[M+His+K]^+$	1.01±0.02
His+Ser	$[M+His+Ser+K]^+$	$[M+His+K]^+$	1.02±0.02

3.4 Conclusions

In this chapter, tandem mass spectrometry was utilized to investigate a possible mechanism of analysis of chiral drugs. Omeprazole was studied as an example, by introducing one amino acid, combinations of two amino acids, and dipeptides as chiral selectors, each with and without copper-bound. It was observed that a limited number of amino acids as one selector could lead to enantioselectivity of *R/S*-omeprazole, regardless of copper binding. Only Trp was found to be an ideal selector toward *R/S*-omeprazole, forming copper-bound diastereomeric complexes $[2M+2Trp+Cu+K-H]^{2+}$. In contrast, when two amino acids were used as selectors, there were multiple combinations possible. Combining different kinds of amino acids may create a totally different chiral environment, resulting in enhanced chiral effects. Among the combinations studied, four sets of amino acids (His+Ala, His+Leu, His+Thr and Phe+Trp) were able to discriminate omeprazole chirality, with relative CR values ranging from 1.17 ± 0.01 to 1.53 ± 0.07. Peptides, which are short chains of amino acids linked by peptide bonds, may utilize the chiral environment caused by amino acids while providing more stable and tightly bound structures. The results demonstrated that chiral recognition was achieved with all dipeptides applied, and numerous diastereomeric complexes were observed. The most chiral discrimination was obtained with $[M+2His\text{-}Ser+K]^+$ dissociated into $[2His\text{-}Ser+K]^+$ (CR = 0.75 ± 0.02), $[M+2His\text{-}Phe+K]^+$ dissociated into $[2His\text{-}Ser+K]^+$ (CR = 1.32 ± 0.08), and $[M+His\text{-}Ala+Na]^+$ dissociated into $[His\text{-}Ala+Na]^+$ (CR = 1.46 ± 0.05), respectively. The exceptional performance of dipeptides over two separated amino acids may be attributed to specific bindings within complex ions, enabling a large chiral effect when the chirality of omeprazole changes. In addition, some interesting findings regarding the binding affinity within complexes were also observed, which have a great impact on the

dissociation order.

To explore the versatility of peptides in chiral discrimination, another chiral drug, clopidogrel, was investigated as well, which demonstrated the superiority of peptides as chiral selectors. In addition, orbitrap-MS was applied for the chiral analysis of omeprazole using peptides as chiral selectors, proving the universality of this method. As only *L*-type dipeptides were studied, an in-depth study of those containing *D*-amino acid residues as well as those with different orders of residues will be done to conclude a general rule. To gain a better understanding of the basic molecular principle involved, the structures of these complexes will be further investigated in detail by density functional theory simulations.

Chapter 4. General Conclusions and Prospects

Rapid authentication methods for red wine were developed using MALDI-MS and DART-MS. Compared with conventional LC-MS and GC-MS, MALDI-MS and DART-MS require less sample preparation and enable high throughput analysis. Furthermore, direct mass spectrometry may retain more compound information, making it ideal for multivariate analysis. Extensive optimization of experimental conditions was performed, and the use of optimized automatic or semi-automatic acquisition modes allowed to obtain high-quality spectra. Though the equipment of MALDI-MS is not common in the laboratory because of its high cost, considering the overall time and labor, it is a worthwhile investment. As for DART, it is a very convenient ion source that can be easily connected to various types of mass spectrometry instruments. Both techniques make the authentication of wine in the real market easy and possible.

In this study, MALDI-MS was found to detect anthocyanin-related compounds mainly, and DART-MS enabled analysis of aromatic compounds, because of their specific ionization mechanisms. The two techniques were found to work complementarily for wine analysis. The approach of combining MALDI-MS and DART-MS was then proposed for the first time, and it was proven to be powerful in the discrimination of red wine in terms of origins, vintages and varieties, as it could combine advantages but minimized disadvantages of both techniques. The correct classification rates were improved significantly as well as fitting and predictive abilities, compared to using a single technology. Untargeted analysis was employed to acquire as much information as possible, and by coupling with OPLS-DA, useful information was well utilized and unrelated one was dismissed. Multivariate calibration models were established by using

OPLS-DA, and by following these models step by step, the origins of wine samples could be well classified, with correct rates even up to 100%. To better understand the compound information that contributed to the differentiation of red wine, characteristic markers were found by applying several criteria and identified by referring to literature or databases. However, the intensity of some markers was too low to conduct MS/MS, the identification of these markers needs further optimization.

Overall, a rapid and high throughput approach was developed by combining MALDI-MS and DART-MS in data analysis for the first time. The high correct rates obtained verified the reliability of the approach. It was also attempted to distinguish other features such as vintage years and grape varieties, with satisfactory classification results, indicating the robustness of the approach. Except for origin, vintage year and grape variety identification, it can also be extended to the differentiation of blended wines or the quantification analysis of wine components in the future. Considering the overall time and workload demanded, it is expected to be an alternative to traditional GC-MS or LC-MS, not only for the analysis of red wine but also for other samples. What's more, the thought of combining different types of mass spectrometric techniques and even other analytical techniques can also be extended to other fields for various applications.

Tandem mass spectrometry has been applied for the recognition of chiral drugs by ion trap mass spectrometry in this study. Several important chiral drugs with different structures were investigated for their differentiation, including ofloxacin, clopidogrel, bupivacaine and omeprazole. Chiral selectors were introduced to form diastereomeric complexes, which may show different dissociation patterns under the same CID energy, and metal ions were applied to provide a coordination site that may enhance the

intermolecular binding. With simple sample preparation and the optimized experimental conditions, various diastereomeric complexes were observed and dissociated in MS/MS. The chiral recognition ratio was employed to evaluate the degree of chiral recognition, comparing the intensity ration of product ion to precursor ion. Significant chiral recognition was observed with all chiral drugs investigated. The difference in structures and chiral effect were compared and discussed.

For ofloxacin, clopidogrel, omeprazole and bupivacaine, the major goal was to achieve chiral recognition by means of tandem mass spectrometry through systematic investigation, proving the feasibility of our method in chiral analysis. Several amino acids and cyclodextrins were applied as chiral selectors. Complex ions [*R/S*-ofloxacin +2Pro+Cu−H]$^{+}$, [*R/S*-clopidogrel+Cu+Trp−H]$^{+}$, [*R/S*-omeprazole+2Trp+K+H]$^{2+}$and [3(*R/S*-bupivacaine)+H]$^{+}$ showed the most chiral discrimination of chiral drugs, respectively. The selection of chiral selectors and metal ions for these three candidates was different, indicating the structure of the analyte would have a significant role in forming complex ions and in intermolecular binding. This study provides an approach to determine the absolute configuration of ofloxacin, clopidogrel, omeprazole and bupivacaine, and may provide insight into how these chiral drugs work in the biological environment.

To further explore how different structures of chiral selectors impact the chiral recognition of chiral drugs, omeprazole was studied as an example. Systematical analysis was performed by using one amino acid, two amino acids, and dipeptides as chiral selectors. Preliminary results showed the chirality of omeprazole could be recognized by these three groups of selectors, however, the selection of one amino acid

was very limited, mainly due to its simple structure, which could only provide a simple chiral environment. Two amino acids as selectors that provided a more complicated environment did perform better, with four sets of amino acids (His+Ala, His+Leu, His+Thr and Phe+Trp) resulting in good CR values. The most interesting observation was that dipeptides outperformed amino acids, as all dipeptides investigated here led to significant chiral discrimination of omeprazole. Compared with two amino acids, the structure of dipeptides is more stable, utilizing the chiral environment caused by amino acids but providing more stable and tight-binding structures. The MS/MS-based method using peptides as chiral selectors further was applicable to another chiral drug, clopidogrel, as well as to another mass spectrometry, orbitrap-MS. The fundamental molecular principle needs further study to have a deep insight into the structural information and draw some general rules for chiral analysis. In addition, the application of dipeptides in chiral analysis has been hardly reported, it is full of potential in this area. Considering the outstanding performance of peptides, they can be applied to chiral recognition of other chiral compounds, e.g., amino acids, sugars, nucleosides, proteins, polysaccharides and enzymes, and to other analytical techniques, such as HPLC, the column of which could be easily designed with peptides.

References

(1) Liu, A.; Song, H. Analysis and Forecasts of the Demand for Imported Wine in China. *Cornell Hosp Q* **2021**, *62* (3), 371-385.

(2) Alonso Ugaglia, A.; Cardebat, J.-M.; Jiao, L. The French wine industry. In *The Palgrave handbook of wine industry economics*, Palgrave Macmillan, Cham, 2019; pp 17-46.

(3) Dimson, E.; Rousseau, P. L.; Spaenjers, C. The price of wine. *J. Financ. Econ.* **2015**, *118* (2), 431-449.

(4) Snopek, L.; Mlcek, J.; Sochorova, L.; Baron, M.; Hlavacova, I.; Jurikova, T.; Kizek, R.; Sedlackova, E.; Sochor, J. Contribution of Red Wine Consumption to Human Health Protection. *Molecules* **2018**, *23* (7), 1684.

(5) Cordova, A. C.; Jackson, L. S.; Berke-Schlessel, D. W.; Sumpio, B. E. The cardiovascular protective effect of red wine. *J. Am. Coll. Surg.* **2005**, *200* (3), 428-439.

(6) Haseeb, S.; Alexander, B.; Baranchuk, A. Wine and Cardiovascular Health: A Comprehensive Review. *Circulation* **2017**, *136* (15), 1434-1448.

(7) Castaldo, L.; Narvaez, A.; Izzo, L.; Graziani, G.; Gaspari, A.; Minno, G. D.; Ritieni, A. Red Wine Consumption and Cardiovascular Health. *Molecules* **2019**, *24* (19), 3626.

(8) Fremont, L. Biological effects of resveratrol. *Life Sci.* **2000**, *66* (8), 663-673.

(9) Bertelli, A. A.; Giovannini, L.; Giannessi, D.; Migliori, M.; Bernini, W.; Fregoni, M.; Bertelli, A. Antiplatelet activity of synthetic and natural resveratrol in red wine. *Int. J. Tissue React.* **1995**, *17* (1), 1-3.

(10) Mazza, G. J. Anthocyanins and heart health. *Ann. Ist. Super. Sanita* **2007**, *43* (4), 369-374.

(11) Bitsch, R.; Netzel, M.; Frank, T.; Strass, G.; Bitsch, I. Bioavailability and Biokinetics of Anthocyanins From Red Grape Juice and Red Wine. *J. Biotechnol.*

Biomed. **2004**, *2004* (5), 293-298.

(12) Herrero-Latorre, C.; Barciela-Garcia, J.; Garcia-Martin, S.; Pena-Crecente, R. M. Detection and quantification of adulterations in aged wine using RGB digital images combined with multivariate chemometric techniques. *Food Chem. X* **2019**, *3*, 100046.

(13) Meloni, G.; Swinnen, J. The political economy of European wine regulations. *J. Wine Econ.* **2013**, *8* (3), 244-284.

(14) Meloni, G.; Anderson, K.; Deconinck, K.; Swinnen, J. Wine Regulations. *Appl. Econ. Perspect. Policy* **2019**, *41* (4), 620-649.

(15) Wajsman, N.; Arias Burgos, C.; Davies, C. The economic cost of IPR infringement in spirits and wine. *European Union Intellectual Property Office: Alicante, Spain* **2016**.

(16) Shen, A. 'Being Affluent, One Drinks Wine': Wine Counterfeiting in Mainland China. *Int. J. Crime Justice Soc. Democr.* **2018**, *7* (4), 16-32.

(17) Arapitsas, P.; Speri, G.; Angeli, A.; Perenzoni, D.; Mattivi, F. The influence of storage on the "chemical age" of red wines. *Metabolomics* **2014**, *10*, 816-832.

(18) Kreitman, G. Y.; Elias, R. J.; Jeffery, D. W.; Sacks, G. L. Loss and formation of malodorous volatile sulfhydryl compounds during wine storage. *Crit. Rev. Food Sci. Nutr.* **2019**, *59* (11), 1728-1752.

(19) Swami, S. B.; Thakor, N.; Divate, A. Fruit wine production: a review. *J. Food Technol. Res.* **2014**, *2* (3), 93-100.

(20) Kunkee, R. E. Some roles of malic acid in the malolactic fermentation in wine making. *FEMS Microbiology Letters* **1991**, *88* (1), 55-71.

(21) Ruiz, J.; Kiene, F.; Belda, I.; Fracassetti, D.; Marquina, D.; Navascues, E.; Calderon, F.; Benito, A.; Rauhut, D.; Santos, A.; et al. Effects on varietal aromas during wine making: a review of the impact of varietal aromas on the flavor of wine. *Appl. Microbiol. Biotechnol.* **2019**, *103* (18), 7425-7450.

(22) Garde-Cerdán, T.; Ancín-Azpilicueta, C. Review of quality factors on wine ageing in oak barrels. *Trends Food Sci. Technol.* **2006**, *17* (8), 438-447.

(23) Villano, C.; Lisanti, M. T.; Gambuti, A.; Vecchio, R.; Moio, L.; Frusciante, L.; Aversano, R.; Carputo, D. Wine varietal authentication based on phenolics, volatiles and DNA markers: State of the art, perspectives and drawbacks. *Food Control* **2017**, *80*, 1-10.

(24) Catalano, V.; Moreno-Sanz, P.; Lorenzi, S.; Grando, M. S. Experimental Review of DNA-Based Methods for Wine Traceability and Development of a Single-Nucleotide Polymorphism (SNP) Genotyping Assay for Quantitative Varietal Authentication. *J. Agric. Food Chem.* **2016**, *64* (37), 6969-6984.

(25) Almeida, C. M.; Vasconcelos, M. T. S. D. ICP-MS determination of strontium isotope ratio in wine in order to be used as a fingerprint of its regional origin. *J. Anal. At. Spectrom.* **2001**, *16* (6), 607-611.

(26) Angus, N. S.; O'Keeffe, T. J.; Stuart, K. R.; Miskelly, G. M. Regional classification of New Zealand red wines using inductively-coupled plasma-mass spectrometry (ICP-MS). *Aust. J. Grape Wine Res.* **2006**, *12* (2), 170-176.

(27) Son, H. S.; Kim, K. M.; van den Berg, F.; Hwang, G. S.; Park, W. M.; Lee, C. H.; Hong, Y. S. 1H nuclear magnetic resonance-based metabolomic characterization of wines by grape varieties and production areas. *J. Agric. Food Chem.* **2008**, *56* (17), 8007-8016.

(28) Geana, E. I.; Ciucure, C. T.; Apetrei, C.; Artem, V. Application of Spectroscopic UV-Vis and FT-IR Screening Techniques Coupled with Multivariate Statistical Analysis for Red Wine Authentication: Varietal and Vintage Year Discrimination. *Molecules* **2019**, *24* (22), 4166.

(29) Riovanto, R.; Cynkar, W. U.; Berzaghi, P.; Cozzolino, D. Discrimination between

Shiraz wines from different Australian regions: the role of spectroscopy and chemometrics. *J. Agric. Food Chem.* **2011**, *59* (18), 10356-10360.

(30) Ziolkowska, A.; Wasowicz, E.; Jelen, H. H. Differentiation of wines according to grape variety and geographical origin based on volatiles profiling using SPME-MS and SPME-GC/MS methods. *Food Chem.* **2016**, *213*, 714-720.

(31) Wu, H.; Tian, L.; Chen, B.; Jin, B.; Tian, B.; Xie, L.; Rogers, K. M.; Lin, G. Verification of imported red wine origin into China using multi isotope and elemental analyses. *Food Chem.* **2019**, *301*, 125137.

(32) Kammerer, D.; Claus, A.; Carle, R.; Schieber, A. Polyphenol screening of pomace from red and white grape varieties (Vitis vinifera L.) by HPLC-DAD-MS/MS. *J. Agric. Food Chem.* **2004**, *52* (14), 4360-4367.

(33) Karas, M.; Hillenkamp, F. Laser desorption ionization of proteins with molecular masses exceeding 10,000 daltons. *Anal. Chem.* **1988**, *60* (20), 2299-2301.

(34) Hillenkamp, F.; Peter-Katalinic, J. *MALDI MS: a practical guide to instrumentation, methods and applications*; John Wiley & Sons, 2013.

(35) Ng, T. T.; So, P. K.; Zheng, B.; Yao, Z. P. Rapid screening of mixed edible oils and gutter oils by matrix-assisted laser desorption/ionization mass spectrometry. *Anal. Chim. Acta* **2015**, *884*, 70-76.

(36) Lai, Y.-H.; Wu, Q.; So, P.-K.; Mok, D. K.-W.; Che, C.-T.; Yao, Z.-P. Rapid differentiation of Schisandra sphenanthera and Schisandra chinensis by matrix-assisted laser desorption/ionization mass spectrometry. *Int. J. Mass Spectrom.* **2018**, *434*, 258-263.

(37) Cody, R. B.; Laramee, J. A.; Durst, H. D. Versatile new ion source for the analysis of materials in open air under ambient conditions. *Anal. Chem.* **2005**, *77* (8), 2297-2302.

(38) Gross, J. H. Direct analysis in real time--a critical review on DART-MS. *Anal.*

Bioanal. Chem. **2014**, *406* (1), 63-80.

(39) Hajslova, J.; Cajka, T.; Vaclavik, L. Challenging applications offered by direct analysis in real time (DART) in food-quality and safety analysis. *Trends Anal. Chem.* **2011**, *30* (2), 204-218.

(40) Guo, T.; Yong, W.; Jin, Y.; Zhang, L.; Liu, J.; Wang, S.; Chen, Q.; Dong, Y.; Su, H.; Tan, T. Applications of DART-MS for food quality and safety assurance in food supply chain. *Mass Spectrom. Rev.* **2017**, *36* (2), 161-187.

(41) Pavlovich, M. J.; Musselman, B.; Hall, A. B. Direct analysis in real time-Mass spectrometry (DART-MS) in forensic and security applications. *Mass Spectrom. Rev.* **2018**, *37* (2), 171-187.

(42) Cajka, T.; Riddellova, K.; Tomaniova, M.; Hajslova, J. Recognition of beer brand based on multivariate analysis of volatile fingerprint. *J. Chromatogr A.* **2010**, *1217* (25), 4195-4203.

(43) Alecu, A.; Albu, C.; Litescu, S. C.; Eremia, S. A. V.; Radu, G. L. Phenolic and Anthocyanin Profile of Valea Calugareasca Red Wines by HPLC-PDA-MS and MALDI-TOF Analysis. *Food Anal. Methods* **2015**, *9* (2), 300-310.

(44) Rubert, J.; Lacina, O.; Fauhl-Hassek, C.; Hajslova, J. Metabolic fingerprinting based on high-resolution tandem mass spectrometry: a reliable tool for wine authentication? *Ana.l Bioanal. Chem.* **2014**, *406* (27), 6791-6803.

(45) Pesavento, I. C.; Bertazzo, A.; Flamini, R.; Vedova, A. D.; De Rosso, M.; Seraglia, R.; Traldi, P. Differentiation of Vitis vinifera varieties by MALDI-MS analysis of the grape seed proteins. *J. Mass Spectrom.* **2008**, *43* (2), 234-241.

(46) Chambery, A.; del Monaco, G.; Di Maro, A.; Parente, A. Peptide fingerprint of high quality Campania white wines by MALDI-TOF mass spectrometry. *Food Chem.* **2009**, *113* (4), 1283-1289.

(47) Guo, T.; Fang, P.; Jiang, J.; Zhang, F.; Yong, W.; Liu, J.; Dong, Y. Rapid screening and quantification of residual pesticides and illegal adulterants in red wine by direct analysis in real time mass spectrometry. *J. Chromatogr. A* **2016**, *1471*, 27-33.

(48) Jastrzembski, J. A.; Sacks, G. L. Solid Phase Mesh Enhanced Sorption from Headspace (SPMESH) Coupled to DART-MS for Rapid Quantification of Trace-Level Volatiles. *Anal. Chem.* **2016**, *88* (17), 8617-8623.

(49) Jastrzembski, J. A.; Bee, M. Y.; Sacks, G. L. Trace-Level Volatile Quantitation by Direct Analysis in Real Time Mass Spectrometry following Headspace Extraction: Optimization and Validation in Grapes. *J. Agric. Food Chem.* **2017**, *65* (42), 9353-9359.

(50) Liu, F. J.; Jiang, Y.; Li, P.; Liu, Y. D.; Yao, Z. P.; Xin, G. Z.; Li, H. J. Untargeted metabolomics coupled with chemometric analysis reveals species-specific steroidal alkaloids for the authentication of medicinal Fritillariae Bulbus and relevant products. *J. Chromatogr. A* **2020**, *1612*, 460630.

(51) Salvatore, E.; Cocchi, M.; Marchetti, A.; Marini, F.; de Juan, A. Determination of phenolic compounds and authentication of PDO Lambrusco wines by HPLC-DAD and chemometric techniques. *Anal. Chim. Acta* **2013**, *761*, 34-45.

(52) Perez-Enciso, M.; Tenenhaus, M. Prediction of clinical outcome with microarray data: a partial least squares discriminant analysis (PLS-DA) approach. *Hum Genet* **2003**, *112* (5-6), 581-592.

(53) Boccard, J.; Rutledge, D. N. A consensus orthogonal partial least squares discriminant analysis (OPLS-DA) strategy for multiblock Omics data fusion. *Anal. Chim. Acta* **2013**, *769*, 30-39.

(54) Monforte, A. R.; Martins, S.; Silva Ferreira, A. C. Discrimination of white wine ageing based on untarget peak picking approach with multi-class target coupled with machine learning algorithms. *Food Chem.* **2021**, *352*, 129288.

(55) Gu, S.; Chen, W.; Wang, Z.; Wang, J. Rapid determination of potential aflatoxigenic fungi contamination on peanut kernels during storage by data fusion of HS-GC-IMS and fluorescence spectroscopy. *Postharvest Biol. Technol.* **2021**, *171*.

(56) Chung, I. M.; Kim, J. K.; Han, J. G.; Kong, W. S.; Kim, S. Y.; Yang, Y. J.; An, Y. J.; Kwon, C.; Chi, H. Y.; Yhung Jung, M.; et al. Potential geo-discriminative tools to trace the origins of the dried slices of shiitake (Lentinula edodes) using stable isotope ratios and OPLS-DA. *Food Chem.* **2019**, *295*, 505-513.

(57) Song, H. H.; Kim, D. Y.; Woo, S.; Lee, H. K.; Oh, S. R. An approach for simultaneous determination for geographical origins of Korean Panax ginseng by UPLC-QTOF/MS coupled with OPLS-DA models. *J. Ginseng Res.* **2013**, *37* (3), 341-348.

(58) Springer, A. E. Wine authentication: a fingerprinting multiclass strategy to classify red varietals through profound chemometric analysis of volatiles. *Eur. Food Res. Technol.* **2018**, *245* (1), 179-190.

(59) Pan, Y.; Gu, H. W.; Lv, Y.; Yin, X. L.; Chen, Y.; Long, W.; Fu, H.; She, Y. Untargeted metabolomic analysis of Chinese red wines for geographical origin traceability by UPLC-QTOF-MS coupled with chemometrics. *Food Chem.* **2022**, *394*, 133473.

(60) Hu, X. Z.; Liu, S. Q.; Li, X. H.; Wang, C. X.; Ni, X. L.; Liu, X.; Wang, Y.; Liu, Y.; Xu, C. H. Geographical origin traceability of Cabernet Sauvignon wines based on Infrared fingerprint technology combined with chemometrics. *Sci. Rep.* **2019**, *9* (1), 8256.

(61) López-Aguilar, R.; Zuleta-Prada, H.; Hernández-Montes, A.; Herbert-Pucheta, J. E. Comparative NMR metabolomics profiling between Mexican ancestral & artisanal mezcals and industrialized wines to discriminate geographical origins, agave species or

grape varieties and manufacturing processes as a function of their quality attributes. *Foods* **2021**, *10* (1), 157.

(62) Cody, R. B. Observation of molecular ions and analysis of nonpolar compounds with the direct analysis in real time ion source. *Anal. Chem.* **2009**, *81* (3), 1101-1107.

(63) van den Berg, R. A.; Hoefsloot, H. C.; Westerhuis, J. A.; Smilde, A. K.; van der Werf, M. J. Centering, scaling, and transformations: improving the biological information content of metabolomics data. *BMC Genomics* **2006**, *7*, 142.

(64) Eriksson, L.; Johansson, E.; Kettaneh-Wold, N.; Wold, S. Multi-and megavariate data analysis. *Umetrics Academy, Umeå* **2001**, 43.

(65) Saito, T.; Rehmsmeier, M. The precision-recall plot is more informative than the ROC plot when evaluating binary classifiers on imbalanced datasets. *Plos One* **2015**, *10* (3), e0118432.

(66) Flamini, R. Recent Applications of Mass Spectrometry in the Study of Grape and Wine Polyphenols. *ISRN Spectroscopy* **2013**, *2013*, 1-45.

(67) Rothwell, J. A.; Perez-Jimenez, J.; Neveu, V.; Medina-Remon, A.; M'Hiri, N.; Garcia-Lobato, P.; Manach, C.; Knox, C.; Eisner, R.; Wishart, D. S.; et al. Phenol-Explorer 3.0: a major update of the Phenol-Explorer database to incorporate data on the effects of food processing on polyphenol content. *Database (Oxford)* **2013**, *2013*, bat070.

(68) Oliveira, J.; Alhinho da Silva, M.; Teixeira, N.; De Freitas, V.; Salas, E. Screening of Anthocyanins and Anthocyanin-Derived Pigments in Red Wine Grape Pomace Using LC-DAD/MS and MALDI-TOF Techniques. *J. Agric. Food Chem.* **2015**, *63* (35), 7636-7644.

(69) Carpentieri, A.; Marino, G.; Amoresano, A. Rapid fingerprinting of red wines by MALDI mass spectrometry. *Anal. Bioanal. Chem.* **2007**, *389* (3), 969-982.

(70) Gonzalez-San Jose, M. L.; Santa-Maria, G.; Diez, C. Anthocyanins as parameters for differentiating wines by grape variety, wine-growing region, and wine-making methods. *J. Food Compos. Anal.* **1990**, *3* (1), 54-66.

(71) Jones, G. V.; White, M. A.; Cooper, O. R.; Storchmann, K. Climate Change and Global Wine Quality. *Climatic Change* **2005**, *73* (3), 319-343.

(72) van Leeuwen, C. Terroir: The effect of the physical environment on vine growth, grape ripening, and wine sensory attributes. In *Managing Wine Quality*, Elsevier, 2022; pp 341-393.

(73) Stój, A.; Czernecki, T.; Domagała, D.; Targoński, Z. Comparative characterization of volatile profiles of French, Italian, Spanish, and Polish red wines using headspace solid-phase microextraction/gas chromatography-mass spectrometry. *Int. J. Food Prop.* **2017**, *20* (sup1), S830-S845.

(74) Sikuten, I.; Stambuk, P.; Tomaz, I.; Marchal, C.; Kontic, J. K.; Lacombe, T.; Maletic, E.; Preiner, D. Discrimination of genetic and geographical groups of grape varieties (Vitis vinifera L.) based on their polyphenolic profiles. *J. Food Compos. Anal.* **2021**, *102*, 104062.

(75) Farre, M.; Pico, Y.; Barcelo, D. Direct peel monitoring of xenobiotics in fruit by direct analysis in real time coupled to a linear quadrupole ion trap-orbitrap mass spectrometer. *Anal. Chem.* **2013**, *85* (5), 2638-2644.

(76) Qie, M.; Li, T.; Liu, C. C.; Zhao, Y. Direct analysis in real time high-resolution mass spectrometry for authenticity assessment of lamb. *Food Chem.* **2022**, *390*, 133143.

(77) Guo, T.; Li, Y.; Yong, W.; Fang, P.; Qin, Z.; Yan, A.; Dong, Y. Non-target geographic region discrimination of Cabernet Sauvignon wine by direct analysis in real time mass spectrometry with chemometrics methods. *Int. J. Mass Spectrom.* **2021**, *464*, 116577.

(78) Godelmann, R.; Fang, F.; Humpfer, E.; Schutz, B.; Bansbach, M.; Schafer, H.; Spraul, M. Targeted and nontargeted wine analysis by (1)h NMR spectroscopy combined with multivariate statistical analysis. Differentiation of important parameters: grape variety, geographical origin, year of vintage. *J. Agric. Food Chem.* **2013**, *61* (23), 5610-5619.

(79) Crook, A. A.; Zamora-Olivares, D.; Bhinderwala, F.; Woods, J.; Winkler, M.; Rivera, S.; Shannon, C. E.; Wagner, H. R.; Zhuang, D. L.; Lynch, J. E.; et al. Combination of two analytical techniques improves wine classification by Vineyard, Region, and vintage. *Food Chem.* **2021**, *354*, 129531.

(80) Xu, R.; Chen, L.; Zhang, H.; Crowder, M. W.; Zhu, J. Characterizing bourbon whiskey via the combination of LC-MS and GC–MS based molecular fingerprinting. *Food Chem.* **2023**, *423*, 136311.

(81) Green, J.; Parr, W.; Breitmeyer, J.; Valentin, D.; Sherlock, R. Sensory and chemical characterisation of Sauvignon blanc wine: Influence of source of origin. *Food Res. Int.* **2011**, *44* (9), 2788-2797.

(82) Berna, A. Z.; Trowell, S.; Clifford, D.; Cynkar, W.; Cozzolino, D. Geographical origin of Sauvignon Blanc wines predicted by mass spectrometry and metal oxide based electronic nose. *Anal. Chim. Acta* **2009**, *648* (2), 146-152.

(83) Gougeon, L.; da Costa, G.; Guyon, F.; Richard, T. (1)H NMR metabolomics applied to Bordeaux red wines. *Food Chem.* **2019**, *301*, 125257.

(84) Bentley, R. Role of sulfur chirality in the chemical processes of biology. *Chem. Soc. Rev.* **2005**, *34* (7), 609-624.

(85) Tang, W.; Zhang, X. New chiral phosphorus ligands for enantioselective hydrogenation. *Chem. Rev.* **2003**, *103* (8), 3029-3070.

(86) Tan, Q.; Higashibayashi, S.; Karanjit, S.; Sakurai, H. Enantioselective synthesis of

a chiral nitrogen-doped buckybowl. *Nat. Commun.* **2012**, *3* (1), 891.

(87) Nguyen, L. A.; He, H.; Pham-Huy, C. Chiral drugs: an overview. *Int. J. Biomed. Sci.* **2006**, *2* (2), 85-100.

(88) Noyori, R. Asymmetric catalysis: science and opportunities (Nobel lecture). *Angew Chem. Int. Ed. Engl.* **2002**, *41* (12), 2008-2022.

(89) Kaza, M.; Karazniewicz-Lada, M.; Kosicka, K.; Siemiatkowska, A.; Rudzki, P. J. Bioanalytical method validation: new FDA guidance vs. EMA guideline. Better or worse? *J. Pharm. Biomed. Anal.* **2019**, *165*, 381-385.

(90) Oppolzer, W. Asymmetric Diels-Alder and Ene Reactions in Organic Synthesis. New Synthetic Methods (48). *Angew Chem. Int. Ed. Engl.* **1984**, *23* (11), 876-889.

(91) Glueck, D. S. Catalytic asymmetric synthesis of chiral phosphanes. *Chem. Eur. J.* **2008**, *14* (24), 7108-7117.

(92) Ager, D. J.; East, M. B. *Asymmetric synthetic methodology*; CRC Press, 2020.

(93) Drayer, D. E. Pharmacodynamic and pharmacokinetic differences between drug enantiomers in humans: an overview. *Clin. Pharmacol. Ther.* **1986**, *40* (2), 125-133.

(94) Jamali, F.; Mehvar, R.; Pasutto, F. M. Enantioselective aspects of drug action and disposition: therapeutic pitfalls. *J. Pharm. Sci.* **1989**, *78* (9), 695-715.

(95) Davies, N. M. Clinical pharmacokinetics of ibuprofen. The first 30 years. *Clin. Pharmacokinet* **1998**, *34* (2), 101-154.

(96) Kaminker, R.; de Hatten, X.; Lahav, M.; Lupo, F.; Gulino, A.; Evmenenko, G.; Dutta, P.; Browne, C.; Nitschke, J. R.; van der Boom, M. E. Assembly of surface-confined homochiral helicates: chiral discrimination of DOPA and unidirectional charge transfer. *J. Am. Chem. Soc.* **2013**, *135* (45), 17052-17059.

(97) Francotte, E.; Davatz, A.; Richert, P. Development and validation of chiral high-performance liquid chromatographic methods for the quantitation of valsartan and of

the tosylate of valinebenzyl ester. *J. Chromatogr. B Biomed. Appl.* **1996**, *686* (1), 77-83.

(98) Chu, Y. Q.; Wainer, I. W. Determination of the enantiomers of verapamil and norverapamil in serum using coupled achiral-chiral high-performance liquid chromatography. *J. Chromatogr. A* **1989**, *497*, 191-200.

(99) Shiina, I.; Nakata, K.; Onda, Y. s. Kinetic Resolution of Racemic Carboxylic Acids Using Achiral Alcohols by the Promotion of Benzoic Anhydrides and Tetramisole Derivatives: Production of Chiral Nonsteroidal Anti-Inflammatory Drugs and Their Esters. Wiley Online Library: 2008.

(100) Ali, I.; Alam, S. D.; Al-Othman, Z. A.; Farooqi, J. A. Recent advances in SPE-chiral-HPLC methods for enantiomeric separation of chiral drugs in biological samples. *J. Chromatogr. Sci.* **2013**, *51* (7), 645-654.

(101) Tang, Y. Significance of mobile phase composition in enantioseparation of chiral drugs by HPLC on a cellulose-based chiral stationary phase. *Chirality* **1996**, *8* (1), 136-142.

(102) Mohr, S.; Weiss, J. A.; Spreitz, J.; Schmid, M. G. Chiral separation of new cathinone- and amphetamine-related designer drugs by gas chromatography-mass spectrometry using trifluoroacetyl-l-prolyl chloride as chiral derivatization reagent. *J .Chromatogr. A* **2012**, *1269*, 352-359.

(103) Wang, S. M.; Lewis, R. J.; Canfield, D.; Li, T. L.; Chen, C. Y.; Liu, R. H. Enantiomeric determination of ephedrines and norephedrines by chiral derivatization gas chromatography-mass spectrometry approaches. *J. Chromatogr. B: Anal. Technol. Biomed. Life Sci.* **2005**, *825* (1), 88-95.

(104) Bernal, J.; Toribio, L.; Del Nozal, M.; Nieto, E.; Montequi, M. Separation of antifungal chiral drugs by SFC and HPLC a comparative study. *J. Biochem. Biophys.*

Methods **2002**, *54* (1-3), 245-254.

(105) Coe, R. A.; Rathe, J. O.; Lee, J. W. Supercritical fluid chromatography-tandem mass spectrometry for fast bioanalysis of R/S-warfarin in human plasma. *J. Pharm. Biomed. Anal.* **2006**, *42* (5), 573-580.

(106) Bang, E.; Jung, J.-W.; Lee, W.; Lee, D. W.; Lee, W. Chiral recognition of (18-crown-6)-tetracarboxylic acid as a chiral selector determined by NMR spectroscopy. *J. Chem. Soc. Perkin Trans.* **2001**, (9), 1685-1692.

(107) Chankvetadze, B.; Burjanadze, N.; Pintore, G.; Strickmann, D.; Bergenthal, D.; Blaschke, G. Chiral recognition of verapamil by cyclodextrins studied with capillary electrophoresis, NMR spectroscopy, and electrospray ionization mass spectrometry. *Chirality: The Pharmacological, Biological, and Chemical Consequences of Molecular Asymmetry* **1999**, *11* (8), 635-644.

(108) Desiderio, C.; Fanali, S. J. J. o. C. A. Chiral analysis by capillary electrophoresis using antibiotics as chiral selector. *J. Chromatogr. A* **1998**, *807* (1), 37-56.

(109) Hancu, G.; Papp, L. A.; Rusu, A. Chiral Separation of the Enantiomers of Omeprazole and Pantoprazole by Capillary Electrophoresis. *Chromatographia* **2014**, *78* (3-4), 279-284.

(110) Sheppard, R. L.; Tong, X.; Cai, J.; Henion, J. D. Chiral separation and detection of terbutaline and ephedrine by capillary electrophoresis coupled with ion spray mass spectrometry. *Anal. Chem.* **1995**, *67* (13), 2054-2058.

(111) Chen, L.; Dean, B.; La, H.; Chen, Y.; Liang, X. Stereoselective supercritical fluidic chromatography –mass spectrometry (SFC-MS) as a fast bioanalytical tool to assess chiral inversion in vivo and in vitro. *Int. J. Mass Spectrom.* **2019**, *444*.

(112) Weisskopf, E.; Panchaud, A.; Nguyen, K. A.; Grosjean, D.; Hascoet, J. M.; Csajka, C.; Eap, C. B.; Ansermot, N. Stereoselective determination of citalopram and

desmethylcitalopram in human plasma and breast milk by liquid chromatography tandem mass spectrometry. *J. Pharm. Biomed. Anal.* **2016**, *131*, 233-245.

(113) Yu, X.; Chau, M. C.; Tang, W. K.; Siu, C. K.; Yao, Z. P. Self-Assembled Binuclear Cu(II)-Histidine Complex for Absolute Configuration and Enantiomeric Excess Determination of Naproxen by Tandem Mass Spectrometry. *Anal. Chem.* **2018**, *90* (6), 4089-4097.

(114) Berthod, A. Chiral recognition mechanisms. **2006**.

(115) Han, D.-Q.; Yao, Z.-P. Chiral mass spectrometry: An overview. *Trends Anal. Chem.* **2020**, *123*.

(116) Cooks, R. G.; Wong, P. S. H. Kinetic Method of Making Thermochemical Determinations: Advances and Applications. *Acc. Chem. Res.* **1998**, *31* (7), 379-386.

(117) Yao, Z. P.; Wan, T. S.; Kwong, K. P.; Che, C. T. Chiral analysis by electrospray ionization mass spectrometry/mass spectrometry. 1. Chiral recognition of 19 common amino acids. *Anal. Chem.* **2000**, *72* (21), 5383-5393.

(118) Brar, R. K.; Jyoti, U.; Patil, R. K.; Patil, H. C. Fluoroquinolone antibiotics: An overview. *Adesh Univ. J. Med. Sci. Res.* **2020**, *2* (1), 26-30.

(119) Hayakawa, I.; Atarashi, S.; Yokohama, S.; Imamura, M.; Sakano, K.-l.; Furukawa, M. Synthesis and antibacterial activities of optically active ofloxacin. *Antimicrob. Agents Chemother* **1986**, *29* (1), 163-164.

(120) Jung, K.; Kim, J. S.; Kim, T. H.; Kim, J. A Facile Solid-Phase Synthesis of (+)-(S)-Clopidogrel. *Helv. Chim. Acta* **2013**, *96* (2), 326-329.

(121) Saeed, A.; Shahzad, D.; Faisal, M.; Larik, F. A.; El-Seedi, H. R.; Channar, P. A. Developments in the synthesis of the antiplatelet and antithrombotic drug (S)-clopidogrel. *Chirality* **2017**, *29* (11), 684-707.

(122) El-Kimary, E. I.; Ragab, M. A. Recent Analytical Methodologies for the

Determination of Omeprazole and/or Its Active Isomer Esomeprazole in Different Matrices: A Critical Review. *Crit Rev Anal Chem.* **2022**, *52* (1), 106-130.

(123) Richter, J. E.; Kahrilas, P. J.; Johanson, J.; Maton, P.; Breiter, J. R.; Hwang, C.; Marino, V.; Hamelin, B.; Levine, J. G.; Investigators, E. S. Efficacy and safety of esomeprazole compared with omeprazole in GERD patients with erosive esophagitis: a randomized controlled trial. *Am. J. Gastroenterol.* **2001**, *96* (3), 656-665.

(124) Babst, C. R.; Gilling, B. N. Bupivacaine: a review. *Anesthesia progress* **1978**, *25* (3), 87.

(125) Cox, C. R.; Faccenda, K. A.; Gilhooly, C.; Bannister, J.; Scott, N. B.; Morrison, L. M. Extradural S(-)-bupivacaine: comparison with racemic RS-bupivacaine. *Br. J. Anaesth.* **1998**, *80* (3), 289-293.

(126) Ali, I.; Sekkoum, K.; Belboukhari, N.; Rebizi, M. N.; Zaid, M. E. A.; Yusuf, K.; Alothman, A. A.; AlJumah, B. A.; Ouladsmane, M. Determination of enantio-separation, absolute configuration and chiral recognition mechanism of ofloxacin and flumequine by HPLC and modeling studies. *J. Chem. Technol. Biotechnol.* **2021**, *96* (10), 2901-2908.

(127) Ferretti, R.; Zanitti, L.; Cirilli, R. Development of a high-performance liquid chromatography method for the simultaneous determination of chiral impurities and assay of (S)-clopidogrel using a cellulose-based chiral stationary phase in methanol/water mode. *J. Sep. Sci.* **2018**, *41* (6), 1208-1215.

(128) Zhu, G.; Kingsford, O. J.; Yi, Y.; Wong, K.-y. Recent advances in electrochemical chiral recognition. *J. Electrochem. Soc.* **2019**, *166* (6), H205.

(129) Suliman, F. O.; Elbashir, A. A.; Schmitz, O. J. Study on the separation of ofloxacin enantiomers by hydroxyl-propyl-β-cyclodextrin as a chiral selector in capillary electrophoresis: a computational approach. *J. Incl. Phenom. Macrocycl. Chem.* **2015**,

83 (1-2), 119-129.

(130) Soini, H.; Riekkola, M.-L.; Novotny, M. V. Chiral separations of basic drugs and quantitation of bupivacaine enantiomers in serum by capillary electrophoresis with modified cyclodextrin buffers. *J. Chromatogr. A* **1992**, *608* (1-2), 265-274.

(131) Bhavyasri, K.; Rambabu, D.; Prasad, P.; Balaram, V. M. Separation of enantiomers of clopidogrel on chiral stationary phases by packed column supercritical fluid chromatography. **2013**.

(132) Salama, N. Validated densitometric TLC method for analysis of (R)-and (S)-bupivacaine, using cyclodextrin derivatives as chiral selectors. *J. Planar Chromatogr. - Mod. TLC.* **2008**, *21* (6), 441-446.

(133) Tao, W.; Zhang, D.; Nikolaev, E. N.; Cooks, R. G. Copper (II)-assisted enantiomeric analysis of D, L-amino acids using the kinetic method: chiral recognition and quantification in the gas phase. *J. Am. Chem. Soc.* **2000**, *122* (43), 10598-10609.

(134) Wu, L.; Tao, A. W.; Cooks, R. Ligand and metal-ion effects in metal-ion clusters used for chiral analysis of α-hydroxy acids by the kinetic method. *Anal. Bioanal. Chem.* **2002**, *373*, 618-627.

(135) Steill, J.; Zhao, J.; Siu, C. K.; Ke, Y.; Verkerk, U. H.; Oomens, J.; Dunbar, R. C.; Hopkinson, A. C.; Siu, K. M. Structure of the observable histidine radical cation in the gas phase: a captodative α-radical ion. *Angew. Chem.* **2008**, *120* (50), 9812-9814.

(136) Yang, S.; Wu, F.; Yu, F.; Gu, L.; Wang, H.; Liu, Y.; Chu, Y.; Wang, F.; Fang, X.; Ding, C.-F. Distinction of chiral penicillamine using metal-ion coupled cyclodextrin complex as chiral selector by trapped ion mobility-mass spectrometry and a structure investigation of the complexes. *Anal. Chim. Acta* **2021**, *1184*, 339017.

(137) Cerda, B. A.; Wesdemiotis, C. The Relative Copper(I) Ion Affinities of Amino Acids in the Gas Phase. *J. Am. Chem. Soc.* **1995**, *117* (38), 9734-9739.

(138) Boix, C.; Ibanez, M.; Sancho, J. V.; Niessen, W. M.; Hernandez, F. Investigating the presence of omeprazole in waters by liquid chromatography coupled to low and high resolution mass spectrometry: degradation experiments. *J. Mass Spectrom.* **2013**, *48* (10), 1091-1100.

(139) Ieritano, C.; Yves Le Blanc, J. C.; Schneider, B. B.; Bissonnette, J. R.; Haack, A.; Hopkins, W. S. Protonation-Induced Chirality Drives Separation by Differential Ion Mobility Spectrometry. *Angew Chem. Int. Ed. Engl.* **2022**, *61* (9), e202116794.